UNIVERSITY OF SOUTHAMPTON

FACULTY OF NATURAL AND ENVIRONMENTAL SCIENCES

CHEMISTRY

RAPID CHARACTERISATION OF QUINAZOLINE DRUG IMPURITIES USING ELECTROSPRAY MASS SPECTROMETRY-MASS SPECTROMETRY AND COMPUTATIONAL CHEMISTRY APPROACHES

by

Angelika Galezowska, M.Sc.

Thesis for the degree of Doctor of Philosophy

December 2011

UNIVERSITY OF SOUTHAMPTON

ABSTRACT

FACULTY OF NATURAL AND ENVIRONMENTAL SCIENCIES

CHEMISTRY

Doctor of Philosophy

RAPID CHARACTERISATION OF QUINAZOLINE DRUG IMPURITIES USING ELECTROSPRAY MASS SPECTROMETRY-MASS SPECTROMETRY AND COMPUTATIONAL CHEMISTRY APPROACHES

by Angelika Galezowska

Structural characterisation of impurities from synthetic pathways of drugs is an important process in pharmaceutical development. Dissociation pathways of the impurities can vary between different classes of compounds, often resulting in a challenging and a time-consuming process of data interpretation. A detailed understanding of the specific structural features of the fragmentation behaviour of impurity gas-phase ions affords faster characterisation of the unknown sub-structures. Establishing electrospray ionisation-tandem mass spectrometry (ESI-MS/MS) fragmentation rules, based on structure specific and common fragmentation patterns, can improve the process as a screening method in the R&D of new drugs.

This project is focused on understanding dissociation pathways of protonated quinazolines using tandem mass spectrometry. Different ionisation techniques and mass analysers were used to allow comparison studies, which may help to define characteristic fragmentation processes of protonated quinazolines. It was found that the choice of mass spectrometer influences the dissociation pathways of

protonated quinazolines to some extent, but it is the structure of the molecule that predominantly controls the fragmentation behaviour.

Additionally, Density Functional Theory (DFT) calculations have been performed to investigate stabilities of protonated molecules and their product ions to improve the prediction of MS/MS data. It was found that specific forms of product ions and their probability of formation correlate to experimental data acquired using quadrupole-ion trap mass spectrometry (QIT MS) within 10 % difference in intensity. The approach of DFT-MS/MS may help interpretation of MS/MS data by indicating the favoured protonation sites and proposing most probable forms of product ions. It is suggested that the product ion mass spectrum is most probably a combination of individual product ion mass spectra formed from the heterogeneous population of singly protonated molecules; *i.e.* protonation does not have to occur on the most basic atom in the molecule, but it can be distributed on a number of most probable sites of protonation. In addition, the position of the charge does not have to be fixed and may transfer to a different heteroatom in the molecule prior the fragmentation.

These observations offer the possibility to partially assign structures to isomeric molecules using MS/MS and improve structural identification of quinazoline ions.

Ciociu, dziękuję Ci zaTwoją wiarę i miłość.
Jesteś najlepszą Matką Chrzestną jaką mogłam mieć. Kocham Cię.

Table of Contents

Table of Figures

Table of Tables

Table of Schemes

Declaration of Authorship

I, Angelika Galezowska, declare that the thesis entitled

"Rapid characterisation of quinazoline drug impurities using electrospray mass spectrometry-mass spectrometry and computational chemistry approaches."

and the work presented in the thesis are both my own, and have been generated by me as the result of my own original research. I confirm that:

- this work was done wholly or mainly while in candidature for a research degree at this University;
- where any part of this thesis has previously been submitted for a degree of any other qualification at this university or any other institution, this has been clearly stated;
- where I have consulted the published work of others, this is always clearly attributed;
- where I have quoted from the work of others, the source is always given. With the exception of such quotations, this thesis is entirely is my own work;
- I have acknowledged all main sources of help;
- where the thesis is based on work done by myself jointly with others, I have made clear exactly what was done by others and what I have contributed myself;
    - All work has been conducted wholly by myself with the exception of the following experiments;
        - Analyses of three compounds (2171003, 2171005, and 2171006) using APCI-QIT mass spectrometer with exact given protocol were acquired by Dr Mark W. Harrison from AstraZeneca
        - Data dependent analysis experiments for two compounds (2171007 and 2171023) using Finnigan FT LTQ mass

spectrometer were acquired by Paul R. J. Davey from AstraZeneca

- parts of this work have been published as
    - A. Galezowska, M. W. Harrison, G. J. Langley "Investigation of fragmentation patterns of quinazolines. A useful tool for structural characterisation in Pharmaceutical Development", AZtech 12 (2), 2010, 101-102
    - at many scientific conferences; please see Appendix 3, page 185.

Signed:

Date: 8th December 2011

Acknowledgments

The contribution of many people has made this thesis possible. Their kindness, time and expertise in English and mass spectrometry resulted in the success of this project.

I owe a special debt to my supervisor, Doctor G. John Langley, whose trust and given flexibility to work independently help me to succeed in this project. I also thank my industrial supervisor, Doctor Mark W. Harrison, whose advice regarding daily practice with mass spectrometers, experiments, and future choices made my life so much easier. Additionally, I want to thank my advisor, Doctor Mark E. Light, for his priceless quarter-report feedbacks that helped me focus on the workplan of the project. I am sending my warm gratitude to Doctor Chris-Kriton Skylaris who devoted plenty of his time to teach me the basics of Linux and computational chemistry.

With the oversight of my main supervisor, editorial advice has been sought. No changes of intellectual content were made as a result of this advice. My whole-hearted acknowledgements go to my editor – Julie Herniman, without her help with my miswording and countless misplacements of ‘the’ with ‘a’, or ‘an’, this thesis would not flow. Thank you!

I was invited for a 3-month placement in Pharmaceutical Development in AstraZeneca (Macclesfield, UK). I am sending my particular thanks to Doctor Anthony T. W. Bristow, who mentored me during the placement and shared knowledge and experience that taught me many different aspects of mass spectrometry. I was able to use a Finnigan FT LTQ mass spectrometer in the Structural Purity Group at the Alderley Site of AstraZeneca with the kind agreement and help of Paul R. J. Davey and Madeleine F. Vickers. Thank you! I am grateful that I have met some exceptionally intelligent and friendly people: Alison Coyle, Paula Chaili, Doctor Amjad Khan, and Ryan Greenwood who made my time in the Peak District area the most enjoyable part of my PhD course!

I want to thank my work family group Louisa, Stephen, Chrissie, and Jo, whose countless amount of tea and/or beer drunk with discussions from mass spectrometry to shoe picking made my three years of work in Southampton very pleasant. Additionally, exceptional thanks to Jacky, Emilia, Charlotte, Ola, Ala, Konrad, and Marco, whose support and friendship is beyond description. I am very lucky that I have met you guys!

I would be unable to survive these three years without my best friends – Agata, Kasia, Asia, Karolina, and Dani. Their visits, Skype talks and countless emails kept me strong. Such friendships, rescuing from sorrow and celebrating success, give a power to enjoy the present moments and follow the dreamed path of life.

Least, but not last – my family. A PhD is a tricky part of life, especially abroad. I want to thank my Godmother and grandparents that give me lots of support despite sometimes being the overwhelming distance of thousands of kilometres apart. Thank you.

List of Abbreviations

Ω	Angular frequency of the RF potential
α	Geometry ICR cell factor
ΔG	Change of total free Gibbs energy
ΔH	Change of enthalpy (change of heat of formation)
ΔS	Change of entropy
ADC	Analog-to-digital converter
ADME	Absorption, Distribution, Metabolism, and Excretion
AGC	Automatic Gain Control
AM1	Austin method
AMM	Accurate mass measurement
APCI	Atmospheric pressure chemical ionisation
API	Atmospheric pressure ionisation
APPI	Atmospheric pressure photoionisation
AZD1839	Batch code of Gefitinib (Iressa)
AZD2171	Batch code of Cediranib (Recentin)
AZD6474	Batch code of Vandetanib (Zactima)
B	Strength of the magnetic field
B3LYP	Becke, three-parameter, Lee-Yang-Parr functional
BAR rule	Bond-activation reinforcement rule
BO	Born-Oppenheimer approximation
CAD	Collisionally activated decomposition
cc-pVTZ	Correlation-consistent polarised triple-zeta basis set
CE	Collision energy
CGTO	Contracted Gaussian-type orbital
CHP	Curtin-Hammett principle
CID	Collision-induced dissociation
CRM	Charge residue model
CW	Continuous wave
DBE	Double bond equivalents
DC	Direct potential

DFT	Density Functional Theory
D_{R-X}	Dissociation energy
DU	Degree of unsaturation
E	Electronic charge (1.602×10^{-19} C)
ECD	Electron capture dissociation
E_{CM}	Centre-of-mass collision energy
E_e	Excitation energy
EE^+	Even-electron ion
EI	Electron ionisation
E_{ion}	energy of the ion
$E_{kin.}$	Kinetic energy
EPIC	Elucidation of Product Ion Connectivity
$E_{pot.}$	Potential energy
ES	Electrospray
ESI	Electrospray ionisation
f_c	Cyclotron frequency
FDA	Food and Drug Administration
FiD	Fragment iDentificator
FID	Free induction decay
f_m	Magnetron frequency
FPI	Forms of product ions
FPM	Forms of protonated molecule
GB	Gas-phase basicity
GC	Gas chromatography
HDX	Hydrogen/deuterium exchange
HF	Hartree-Fock method
HMW	High molecular weight
HR MS	High-resolution mass spectrometry
ICC	Ion Charge Control
ICR	Ion cyclotron resonance
IE	Ionisation energy
IEM	Ion evaporation model

IP	Ionisation potential
IRMPD	Infrared multiphoton dissociation
ISCID	In-source CID
IUPAC	International Union of Pure and Applied Chemistry
IW	Isolation width
k	Boltzmann constant (1.381×10^{-23} J K^{-1})
K	Reaction equilibrium constant
k_1 or k_2	Reaction rates
l	Length of the tube
LC	Liquid chromatography
LCMO	Low-mass cut-off
LC-MS	Liquid chromatography-mass spectrometry
LIT	Linear ion trap
LMW	Low molecular weight
m	Mass of the ion
MALDI	Matrix-assisted laser desorption/ionisation
m_{gas}	Mass of a collision gas atom
MM	Molecular mechanics
MMFF	Merck Molecular Force Field
MS/MS	Tandem mass spectrometry
MS^n	Multistage mass spectrometry
NCE	Normalised collision energy
N_{ion}	number of molecules in the sample of N molecules
NIST	National Institute of Standards and Technology
NL	Neutral loss
oaTOF	Orthogonal-acceleration TOF
$OE^{+\bullet}$	Odd-electron radical cation
PA	Proton affinity
PL4	Corr sweep attenuation
PL8	Ion activation attenuation
PRI	Process related intermediates
QET	Quasi-equilibrium theory

QIT	Quadrupole-ion trap
QM	Quantum mechanics
QqQ	Triple quadrupole
QTOF	Quadrupole time-of-flight
R	Gas constant (8.314 J mol^{-1} K^{-1})
R	Radius
R	Resolving power
RF	Radio frequency
RHF	Restricted Hartree-Fock
$RL^{\bullet}$	Radical loss
SE	Semi-empirical calculations
SORI/CID	Sustained-off resonance irradiation/CID
STEP	Statistical Test of Equivalent Pathways
SZ	Single-zeta basis set
T	Temperature
t	Time
TDC	Time-to-digital converter
TOF	Time-of-flight
U	Amplitude of DC
UHF	Unrestricted Hartree-Fock
V	Amplitude of RF (electric potential)
v	Velocity of the ion
XC	Exchange-correlation functional
z	Number of charges

Chapter 1 Instrumentation of Mass Spectrometry

"Mass spectrometry is the art of measuring atoms and molecules to determine their molecular weight."

John Bennett Fenn

Mass spectrometry is an analytical technique based on measuring the mass-to-charge ratio (*m/z* units) of analysed compounds. High accuracy mass measurement helps to deduce the molecular formula of an analyte and the relative peak abundance provides information regarding the favourability of the ion formation. The main advantages of mass spectrometry are: high sensitivity, low detection limit, and diverse applications.[1]

Many different types of mass spectrometers are available today, however all of them comprise main instrumental parts, including: an inlet, an ionisation source, a mass analyser, a detector, and a vacuum system, Figure 1.1. The sample can be introduced to a mass spectrometer by direct insertion probe, infusion, desorption from a surface of a sample or a matrix, or *via* an interface that couples the mass spectrometer to a separation instrument, *e.g.* a liquid chromatograph. The three instrumental parts (an ion source, a mass analyser, and a detector) of a mass spectrometer are under vacuum, unless an atmospheric pressure ionisation source is used then only two parts are under vacuum (shown by a dashed line in Figure 1.1).

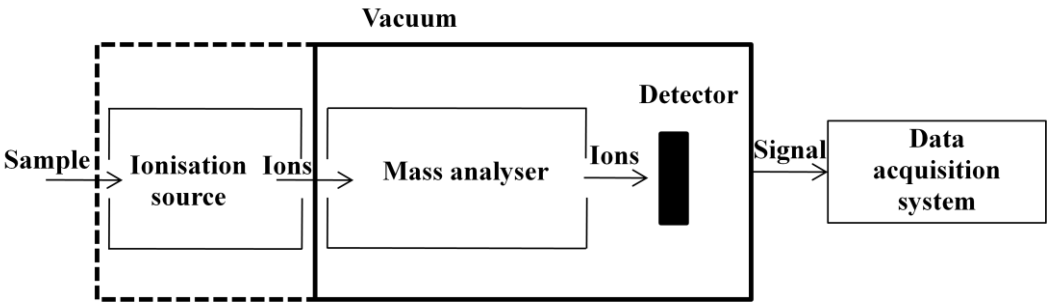

Figure 1.1 Schematic diagram of a mass spectrometer.

1.1 Ion sources

Different ionisation methods are used in mass spectrometry and the choice of the appropriate method can be determined according to the chemical properties of the analyte. Thermally stable and volatile compounds can be analysed using an electron ionisation (EI) source. This is high energetic ionisation process that requires a gas-phase sample and produces a spectrum with a high degree of fragmentation of the analyte.[1] If compounds do not possess these particular properties then they may be ionised using different types of ion sources. These energetically lower processes of ionisation, for example atmospheric pressure ionisation, require a type of sample that is introduced to the mass spectrometer in either the liquid or the solid phase.[1,2] To correctly establish the most appropriate method of ionisation (or narrow the list of possible methods), some partial structural information, such as the functional groups, may be of help.[3] The ideal scenario would be the analysis of a compound with a known structure. For example, a compound soluble in organic solvent substituted with an amine group, which is an easily ionisable group, could be analysed using an ion source requiring a liquid-phase type of sample, *e.g.* positive ion electrospray (ES).

Atmospheric pressure ionisation sources are widely used since they allow the transfer of a liquid sample to the gas-phase.[2] This has been rapidly recognised and applied to mass spectrometers with the liquid chromatography (LC).[2,4] Currently, many API methods are used, but the most common are: i) electrospray ionisation (ESI), ii) atmospheric pressure chemical ionisation (APCI), and iii) atmospheric pressure photoionisation (APPI).[2]

One of the hypotheses of these studies is focused on understanding whether the choice of an ionisation technique influences the fragmentation behaviour of small molecules. It is important to understand the basic differences between the chosen ionisation methods to understand and interpret correctly the collected data.

1.1.1 Electrospray Ionisation

ESI is widely used ionisation technique in mass spectrometry to analyse involatile, highly polar and thermally unstable compounds.[2,5] Depending on the experimental conditions used (*e.g.* positive/negative ion, spiked solvent), singly and/or multiply charged gaseous ions are formed through protonation $[M + nH]^{n+}$, cationisation processes $[M + nX]^{n+}$, where X is Na^+, K^+ or NH_4^+, and/or deprotonation $[M - nH]^{n-}$.[3,6] The basic interface of an electrospray ion source of a mass spectrometer is shown in Figure 1.2. This particular electrospray ion source comprises a heated capillary, a chamber, where desolvation process takes place, and a set of skimmers.

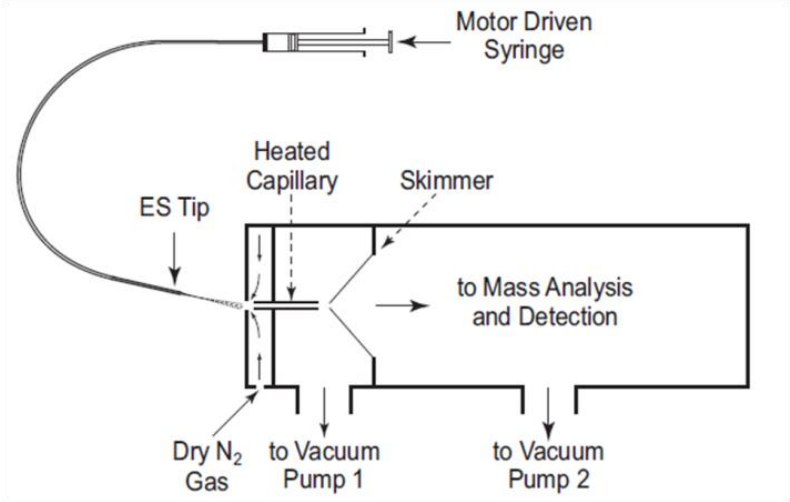

Figure 1.2 Schematic representations of one of ESI-MS,[7] reprinted with a kind permission from John Wiley & Sons, Ltd.

Essentially, it is an electrochemical process of charging the liquid at atmospheric pressure, which results in the formation of protonated molecules in the gas-phase, Figure 1.3.[2,5] In order to achieve this, the ESI source requires a high electric field applied to the capillary resulting in an accumulation of a charge on the liquid surface at the exit of the capillary that is followed by the formation of the ions. In positive ionisation, a high positive potential applied to the capillary causes anions to move towards the inner wall of the capillary and cations to move away from it,

to the counter electrode, where a lower potential is applied. Negative ions can be produced by reversing the polarity of the voltages on the capillary and the counter electrode.[8] The accumulation of the ions carrying the same charge at the end of the capillary results in a liquid tension that causes the solution to form a specific shape called the 'Taylor cone'.[9] The fine stream of the solution at the tip of the Taylor cone has an increasing number of charges. The excess of charges breaks the liquid tension by exploding and forming droplets. This results in a decrease of the density of a charge at the Taylor cone and the process is then repeated.[5,10] A drying gas, most commonly nitrogen, flows against the charged droplets and accelerates the desolvation process resulting in the formation of gas-phase ions, which migrate to a mass analyser.[11]

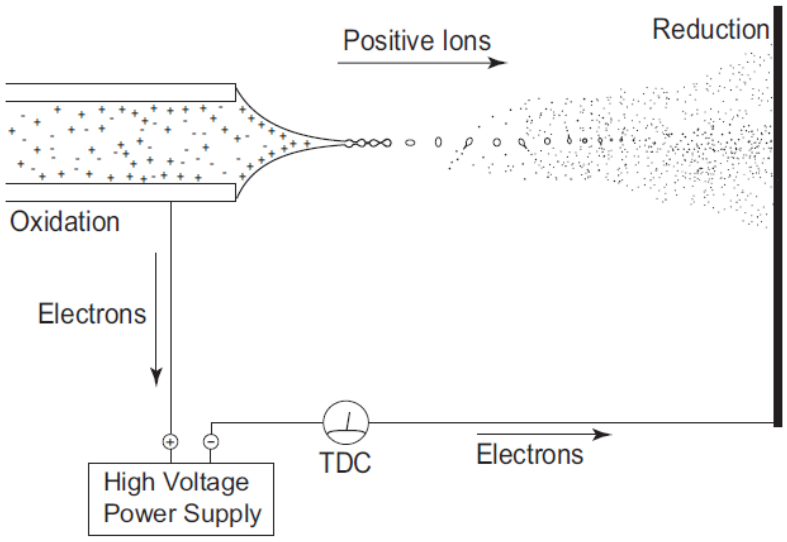

Figure 1.3 Schematic description of electrochemical process of positive ion electrospray;[7] reprinted with a kind permission from John Wiley & Sons, Ltd.

Two desolvation theories are most commonly discussed in the literature, Figure 1.4. They both share the same process of: i) production of the charged droplets at the ES capillary tip, ii) shrinkage of the charged droplets by solvent evaporation and repeated droplet disintegrations leading to very small highly charged droplets, and iii) production of gas-phase ions from very small charged droplets.[12] The charge residue model (CRM), proposed by Dole, is based on solvent evaporation

and coulombic repulsion.[13] A very small droplet, formed after many droplet explosions, can contain only one charged analyte molecule. The evaporation of the remaining solvent results in formation of the gas-phase ion. The CRM is believed to be specific for large molecular weight biomolecules.[14] According to the theory of the ion evaporation model (IEM), proposed by Iribarne and Thomson, ions are formed by their direct emission from the droplets with respect to the theory of Rayleigh instability.[15] Droplets shrink to the size where repulsive coulombic forces are equal to surface tension forces, *i.e.* until the charge at the droplet surface is sufficient for ion evaporation.[11] If charges are closer than 10 nm apart, this results in droplet instability and the direct emission of the ion.[7,8] The difference between these two models diminishes when the radius (R) of the droplets is below 10 nm and when R < 1 nm, it become indistinguishable – the difference between Coulomb fission in the droplet and an ion emission from the droplet is impossible to prove. Very small droplets, R < 10 nm, evaporate rapidly within a few microseconds. There is no experimental method to observe this process and determine whether a Rayleigh fission continues, as expected on the basis of Dole's charge residue model theory,[13] or direct emission of gas-phase ions occurs, as predicted by the Iribarne and Thomson theory.[15]

The formation of ions in ESI is possible in the liquid and gas-phase. Charged droplets may be formed in a solution, as described above, and during a droplet desolvation process.[11] The ions, which interact weakly with the solvent, will preferentially become the gas-phase ions by ion/molecule reactions.[5,12]

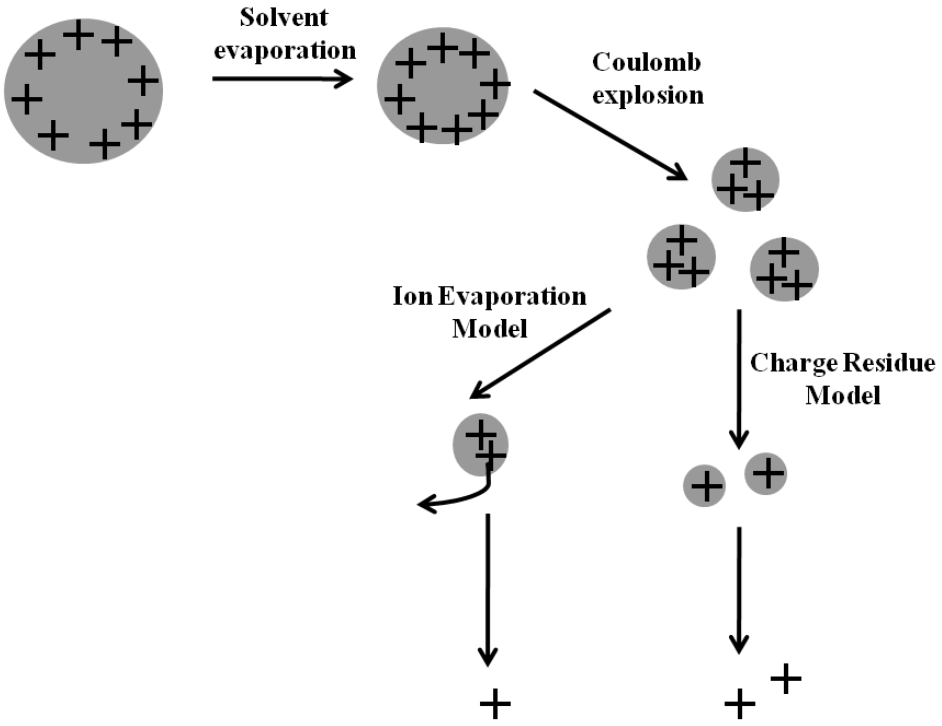

Figure 1.4 Schematic representation of a gas-phase ion formation by Ion Evaporation and Charge Residue Models in positive ion electrospray ionisation.

Electrospray ionisation is widely used in conjunction with separation techniques and with mass analysers that allow tandem mass spectrometry experiments (MS/MS), *e.g.* quadrupole-ion traps. The generation of product ion spectra using ESI-MS/MS produces detailed information to examine the gas-phase chemistry of an analyte, elucidate its structure, and compare differences in the fragmentation pathways of analysed compounds.[16] ESI-MS/MS has been used to produce general fragmentation rules for selected classes of compounds that could be applied to automated data interpretation software.[17] The applications of ESI-MS are focused among medium and high polarity small to large molecular weight molecules, such as small organic compounds containing N, S, and/or O atoms, peptides, oligonucleotides, and others. The disadvantage of the electrospray technique is a low tolerance for salts (sulphates, phosphates) because they affect the desolvation process and distract the potential gradient applied between capillary and the skimmer.[18] Thus, preparation of a sample, its purity and

the choice of a solvent are important to retain good sensitivity.[19] ESI protonation depends on pH and the ionic strength of a liquid phase, which if incorrectly selected, may cause ion suppression, *i.e.* a decrease of the analyte signal.[20] The solvent flow rate and concentration of the analyte are also responsible for the signal quality.[7,18]

1.1.2 Atmospheric Pressure Chemical Ionisation

APCI is an older technique than electrospray ionisation, however it has become popular in the last two decades, with the development of specific applications for liquid chromatography-mass spectrometry (LC-MS) methods.[2] Atmospheric pressure chemical ionisation is known to analyse low to medium-polar compounds with molecular weight up to approximately 1500 Da,[1,2,19] thus is often used with LC-MS where ESI is not applicable.[21] In contrast to ESI, it is a gas-phase ionisation technique that only forms singly charged species, including: protonated molecules $[M + H]^+$, deprotonated molecules $[M - H]^-$ or adduct (mostly with solvent) formation $[M + Solvent + H]^+$, which formation depends on an experimental conditions (*i.e.* positive or negative ion).[2] The schematic diagram of an APCI source is presented in Figure 1.5.

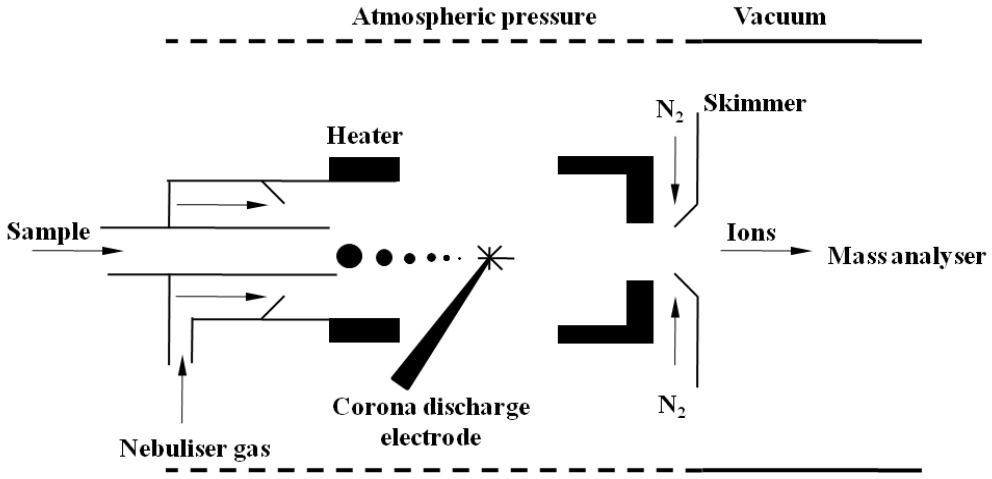

Figure 1.5 Schematic diagram of APCI source; reproduced from de Hoffman and Stroobant,[1] p.45, with a kind permission from John Wiley & Sons, Ltd.

The APCI source contains a heated vaporiser to improve the desolvation process, and thus improve the droplet formation. However, the efficient and quick heat transfer may cause thermal degradation of the analyte, therefore the temperature of the vaporiser needs to be carefully controlled.[2] Ions are transferred to a mass analyser by the same vacuum interface as in an electrospray ion source, thus switching between these two ionisation methods can be relatively easy.[21] Importantly, the electric field in APCI and APPI (described later) is not as high as in an ESI source.[22] The injected solution passes through the nebuliser where it is converted to a fine cloud of droplets and heated in a vaporisation chamber where solvent evaporates. After the desolvation process, gas-phase molecules migrate to the region of the corona discharge electrode where they are ionised and transferred to the mass analyser.

The ionisation process is initiated by low-energy electrons from a corona discharge electrode that ionise the gas molecules in a chamber (for example: nitrogen, oxygen, water or solvent molecules).[22] The ionisation process depends on the gas-phase basicity and proton affinity (PA), *i.e.* efficacy of proton extraction or donation, of all molecules in a chamber.[2,22,23] For example, a water molecule has one of the highest PA values of possible gases present in an APCI source, thus it captures any free protons. The protonated water molecules act as secondary reactant ions protonating molecules that are more basic (have a higher PA). These ion/molecule reactions result in the formation of gas-phase ions.

APCI is commonly used for the quantitative analyses of drugs and biological samples. In addition, it does not suffer from such extensive ion suppression effects as ESI, however purity and sample preparation is also essential.[2] The most successful systems of API mass spectrometers comprise a combined ESI/APCI ion source.[22]

1.1.3 Atmospheric Pressure Photoionisation

Photoionisation is a technique developed initially to be used as a detector in gas chromatography (GC).[24] For atmospheric pressure ionisation mass spectrometers, it was developed to overcome the problem that is the main disadvantage of ESI and APCI, *i.e.* a lack of ability to analyse non-polar compounds.[25] Covey *et al.* described APPI as "one of the variants of APCI source", because APPI was developed from limitations of the APCI source.[2] It is an excellent ionisation technique to analyse compounds regardless of their polarity.[25] It can ionise liquid and gas-phase type molecules and the formed gas-phase ions may comprise of two possible species: a protonated molecule $[M + H]^+$ and/or a molecular ion $M^{+\bullet}$.[26] The process of their formation will be described later.

A schematic description of an APPI source is presented in Figure 1.6. The similarities of the APPI source to the previously described APCI ion source can be noted with the main difference of UV lamp replacing a corona discharge electrode.

The injected sample passes through the heated nebuliser and the desolvation and ionisation process of the fine droplets takes place in the region of the UV lamp. The UV radiation produces a stream of photons, which can be absorbed directly and/or indirectly – through the charge carriers, following the ionisation of the molecules. The fill gas in an UV lamp is generally a rare gas, mostly krypton, which has emission energy in the range of 8-12 eV. This range guarantees sample ionisation, which is mostly achieved by an irradiation of 10 eV.[25]

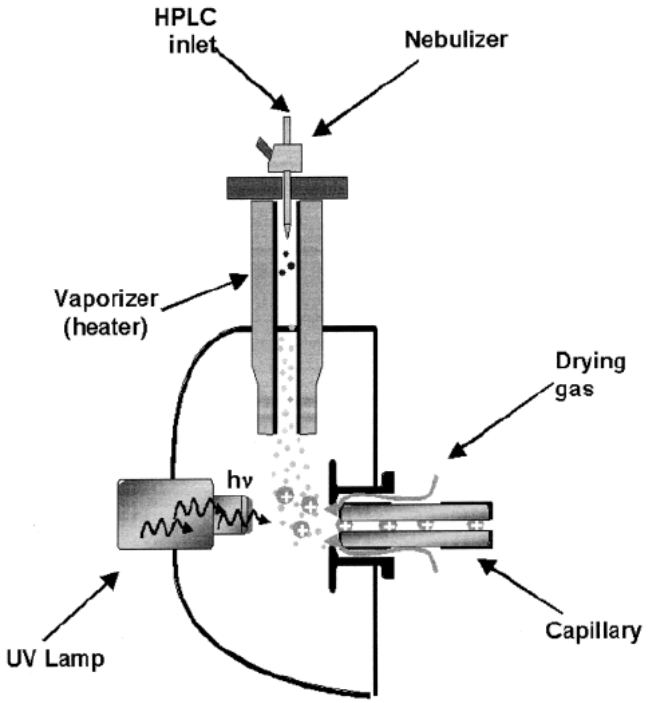

Figure 1.6 Schematic diagram of APPI source;[25] reprinted with a kind permission from ACS.

The mechanism of APPI is a competitive process between the formation of a molecular ion $M^{+\bullet}$ and a protonated molecule $[M + H]^+$.[24,25] The photons are emitted with a higher ionisation energy (IE) than the IE of the target molecule, therefore the excess energy is absorbed followed by formation of the excited molecule that emits the electron resulting in the formation of the molecular ion.[24] This process is mostly observed when ionising aromatic compounds because of their large number of free electrons from the conjugated aromatic pairs. The IE value of the solvent is generally higher (IE > 12 eV) than the energy emitted from the UV lamp, thus avoiding all possible interferences by ionising the solvent molecules.[22] It was found that a small amount of a dopant in the solution, such as toluene or acetone, aids the preferential formation of protonated molecules. The dopant is a charge carrier and when ionised it transfers a proton to the analyte resulting in a formation of a $[M + H]^+$.[24] Negative ion APPI is not as widely used as positive ionisation since the mechanism of anion formation is not fully understood. However hypotheses include electron capture and a charge exchange

as two main reactions resulting in the formation of anion $M^{-\bullet}$ and deprotonated molecule $[M - H]^-$, respectively.[24]

APPI is an ionisation source that can be coupled with LC systems and it has often been found to be more sensitive than APCI and ESI techniques when a low flow is applied.[25] APPI is applicable to smaller molecular weight molecules than APCI as it is used to ionise compounds up to approximately 1200 Da. Applications vary widely from the analyses of mixture samples and individual compounds, such as clinical samples, pharmaceuticals, lipids, and pesticides.[24,27] Its incorporation into multiple function ion sources such as APPI/APCI or APPI/ESI increased the ease and number of experiments that could be performed and easily allows comparison studies between different ionisation techniques.[24,25]

1.2 Mass Analysers

Once ions have been formed, they are transferred to a mass analyser where they are separated according to their mass-to-charge ratios. The selection of mass analyser depends on the sample type and the information required from the analysis.

Three features of the mass analyser determine the choice of appropriate mass analyser for a specific analysis: i) the upper mass limit, ii) the ion transmission, and iii) the mass resolving power. The first feature describes the mass range of a mass analyser and the second, the transmission of the ions, is the ratio of ions formed during the ionisation process to ions transmitted to the detector; higher ion transmission characterises with a lower signal loss. Resolving power (R) is a number describing the performance of the mass analyser; it is "a number that determines the capacity of the instrument to separate ions at different points on the *m/z* scale.", Equation 1.1 and Equation 1.2.[22,28] The mass resolution is the ability to distinguish and separate two neighbouring signals; a higher mass resolution means an improved separation of the signals.[1]

Equation 1.1 $\boldsymbol{R = \frac{m}{\Delta m}}$, where

Equation 1.2 $\boldsymbol{\Delta m = \frac{m_1}{m_1 - m_2}}$

Δm – unit mass resolution, m_1 and m_2 – *m/z* ions that require separation.[3]

Most of the time-of-flight (TOF) mass analysers operate at a constant value of resolving power R, hence the increasing *m/z* value increases resolution unit Δm. The mass resolving power of the ion cyclotron resonance (ICR) cell is an inverse linear function of the *m/z* value; thus the mass resolving power decreases with an increase of *m/z* value.[29] A quadrupole-ion trap (QIT) has a constant mass resolution throughout the *m/z* scale.[22]

This sub-chapter describes the operation principles of four mass analysers, *i.e.* the quadrupole ion trap, the ion cyclotron resonance (ICR) cell, the quadrupole time-of-flight (QTOF), and the triple quadrupole (QqQ) that were used to perform the tandem mass spectrometry experiments conducted in this research. Tandem mass spectrometry or multistage mass spectrometry (MS^n) is an unequivocal relationship between precursor and product ions, where a precursor ion is selected, activated, dissociated, and its fragments analysed.[30] Tandem-in-time mass spectrometry is the ability of a mass analyser to perform these operations in the same place. Tandem-in-space mass spectrometry happens in instruments where more than one mass analyser in a sequence is required to perform these processes.[1,22] MS/MS experiments became a structural elucidation solution to the widely used soft ionisation techniques, which give little or no structural information.[31]

Differences and similarities between product ion mass spectra acquired using different mass analysers were compared to understand whether a mass analyser and choice of ion dissociation technique influence the fragmentation behaviour of gas-phase ions. Most of the experiments were performed using collision-induced dissociation (CID); the experiments in the ICR cells were performed using sustained-off resonance irradiation/CID (SORI/CID) and infrared multiphoton dissociation (IRMPD). The choice of mass analyser and activation method may

influence the fragmentation behaviour of analysed compounds, therefore the understanding of their principles is crucial.

1.2.1 Quadrupole Ion Trap

The ion trap, often called Paul trap, is a mass analyser where ions are held in a three-dimensional space defined by metal surfaces.[32] In 1984, Stafford and co-workers modified the mass analyser, invented by Paul and Steinwedel, and described it as ion trap.[33,34] The QIT comprises the ring and two end-caps electrodes to which RF and DC potentials are applied forming the quadrupole field, which affects ions in three-dimensional directions, Figure 1.7.[21] The RF potential is applied with a fixed frequency but variable amplitude.[22] The ring electrode has a radius r_0 and is aligned to the centre of the end-cap electrode, which is described by a dimension z, Figure 1.7.[35]

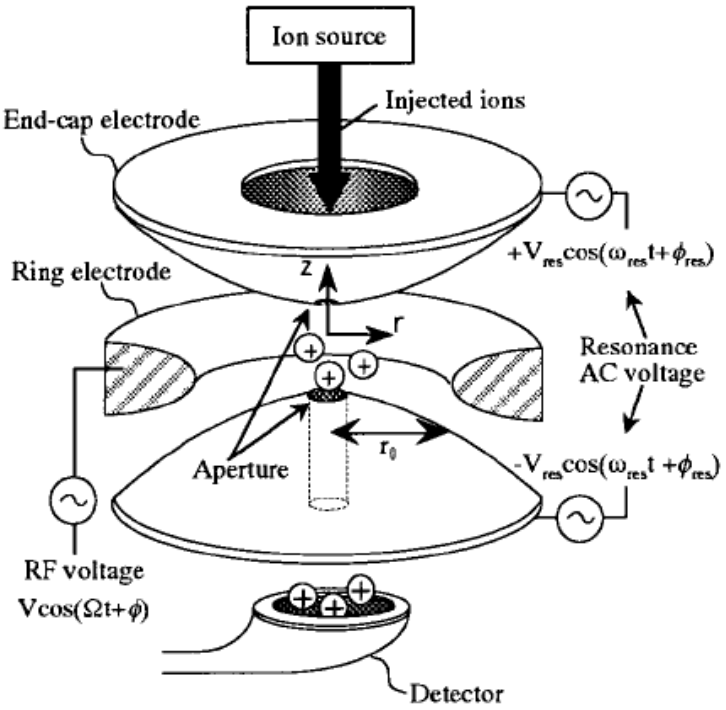

Figure 1.7 Schematic quadrupole ion trap mass analyser;[36] reprinted with a kind permission from John Wiley & Sons, Ltd.

The Finnigan LCQ Classic from Thermo Scientific and LC/MSD XCT trap from Agilent Technologies are the ion trap mass spectrometers used in these studies. The process of measuring the ions in the QIT mass spectrometer is as follows. Ions are produced in an external ESI source and are transferred to the mass analyser through a skimmer and two octapoles that focus the ion beam. The ions pass through the gating lens, which limits the number of ions that can enter the ion trap thus minimising the space charge effect.[37] This process is called Automatic Gain Control (AGC) and it ensures that the same amount of ions enter the trap. (The equivalent process in Agilent Technologies LC/MS XCT Trap is called Ion Charge Control (ICC)). When ions (for example, positive ions) enter the ion trap, the potential on the first end-cap electrode is at ground or negative.[1] When the fixed by AGC number of ions have entered the trap, the voltage increases and the trap closes (the positive potential is applied to the end-cap electrode).[37] Following this injection, ions are stored and analysed according to their masses. In 2002, Stafford and co-workers showed that trapping process can take a long time; stable ions were kept in the quadrupole-ion trap for over 15 minutes.[38] The aim of QIT operation is to create stable trajectories for the ions of interest and eject unwanted ions.[21,34] The homogenous field affects the ions and keeps them in a certain motion that resembles a "roller coaster ride" and a trajectory similar to a number 8.[39] The ejection of the ions from the trap is controlled by adjusting the potentials on the electrodes, hence disturbing stable ion trajectories. The mathematical analysis using Mathieu equations is helpful to understand and locate areas where *m/z* ions have a stable trajectory.[1,40] The stability diagram, consisting of an expression of frequencies of various amplitudes, is presented in Figure 1.8.

All ions can be represented on a stability diagram, which allows analysts to predict whether the ions will be stable and trapped or unstable and ejected.[38] The ion is stable if its trajectory is stable in z_0 and r_0 dimensions of the trap, Figure 1.7, in the region where these stability areas overlap, Figure 1.8. If the ion exceeds these values its stability is disturbed and its trajectory increases until is ejected from the ion trap. The Mathieu equations describe the trapping parameters, q_z

and a_z, as the functions of trapping efficiency of ions injected into the trap, Equation 1.3 and Equation 1.4.[1]

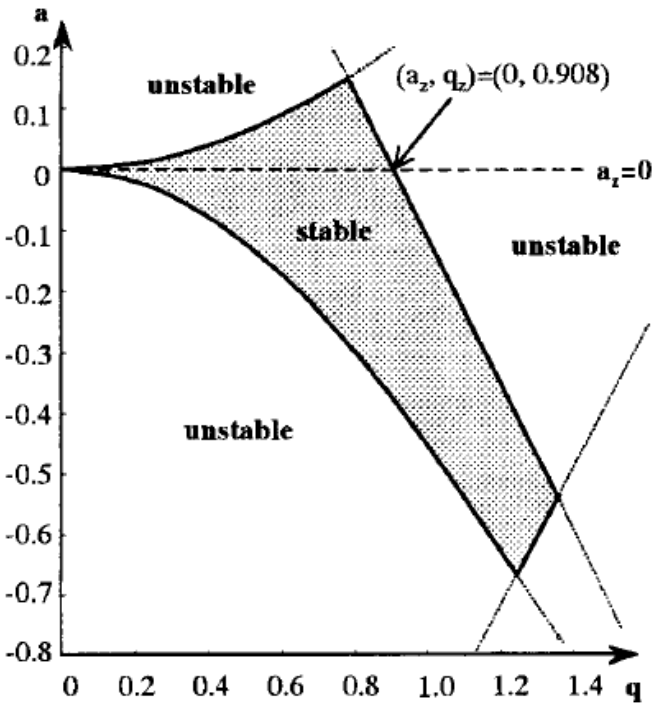

Figure 1.8 Stability diagram for a quadrupole ion trap;[36] reprinted with a kind permission from John Wiley and Sons, Ltd.

Equation 1.3 $$q_z = \frac{8eV}{m(r_o^2+2z_o^2)\Omega^2}$$

Equation 1.4 $$a_z = \frac{-16eU}{m(r_0^2+2z_0^2)\Omega^2}$$

e – electronic charge (1.602×10^{-19} C), V – amplitude of RF storing potential applied to the ring electrode, U – amplitude of DC applied to end-cap electrodes, m – mass, r_0 and z_0 – radial and axial dimensions of the ion trap (in LCQ: 0.707 and 0.785 cm, respectively), Ω – angular frequency of the RF potential

Ions can have stable trajectories only in the a_z and q_z regions that overlap. One of the overlapping stability regions go across the a_z axis at zero value, which allows to avoid one variable (a_z) from describing a stability of ions trajectories in QIT, Figure 1.8 and Equation 1.4. The a_z and q_z variables have a fixed relationship to V (radio frequency (RF)) and U (direct potential (DC)), respectively. If a DC

voltage is not applied (a_z is zero), the ion trap can work using RF (across q_z values) only. The RF potential, applied to the ring electrode, causes all ions to be trapped in a selected *m/z* units range. This means that ions will be stable only at q_z values of the stability diagram. All constant values, *i.e.* Ω, e, z_0 and r_0 simplify the Equation 1.3. The q_z value increases with an increase of amplitude V and decreases with an increase of the mass of the ion. In other words, an increase of the V value increases the q_z value; the ions of higher *m/z* units are moved to the edge of the stability diagram and, if the q_z value reaches 0.908, they become unstable and are ejected from the trap, Figure 1.8. The value 0.908 characterises the point of the lowest *m/z* ion that can be stored in the trap, called a low-mass cut-off (LCMO) point in the mass-selective instability mode.[21] In the LCQ, the q_z value is decreased to 0.83 because of the introduction of an additional RF potential applied to the end-cap electrodes (half the frequency applied to the ring electrode), called axial modulation, which is a sub-type of resonance ejection mode.[22,41] It helps eject ions successively and perform a selective storage of ions at certain *m/z* units values by performing the scanning process from low to high (and conversely) *m/z* units values.[21] Also, by decreasing the q_z value at a chosen point of the stability diagram called an "instability hole", which excludes a particular *m/z* units value from scanning, the resonant ejection can manipulate the mass range of QIT.[40] Hence, the ion selection and ejection can be controlled. Additionally, the particular selected *m/z* ion can be moved, by applying the RF and DC, towards the beginning of the stability diagram and the ion activation experiment can be performed.

All ions kept in the ion trap have an excess amount of rotational and vibrational energies, which often caused the ions to spread in the region of the trap. The excess of these energies is reduced by ion/neutral collisions with a "cooling gas", which is most commonly helium (or argon) under relatively high pressure, *e.g.* 1 mTorr. This helps to focus the ions towards the centre of the ion trap.[1,22,42] Stafford and co-workers discovered that the presence of this cooling gas in the ion trap improves peak shape, and hence increases mass resolution.[33,43]

As well as being a "cooling gas" and an aid to focus the ions in the centre of the trap, helium atoms also collide with the ions transferring excess energy to the ions resulting in their fragmentation. This process is known as collisionally activated decomposition (CAD) or collision-induced dissociation.[44] The fragmentation is a time-dependent process as all operations take place inside the ion trap. Four basic steps that explain the operation of the ion trap, including: trapping, isolating, exciting, and ejecting the ions, can be repeated many times for a selected *m/z* ion. Louris *et al*. achieved MS^7 stage involving six stages of CID.[45] Obviously, the number of possible MS stages depends on the abundance of the precursor ion and its fragmentation behaviour.[21]

One requirement of the CID process is that ions have a high kinetic energy thus cooling and focusing them in the centre of the trap needs to be accelerated by the external signal of an AC voltage applied for a short time.[40,46,47] The process, known as a resonance excitation, induces multiple collisions of the ions with helium molecules (up to 10^6 ion/helium collisions).[48] Thus, the fragmentation of the ions and a formation of the product ions is affected by the increase of their kinetic energy, which is converted in to the internal energy.[43,47] The degree of the excitation and thus ion fragmentation, can be controlled by varying the amplitude of the excitation voltage or the length of time of activation,[46] which causes some limitations to possible experiments. The manual optimisation of the applied energy resulting in the ion fragmentation was a disadvantage of the experiments. The solution, proposed by Lopez and co-workers, was to adjust the applied energy by applying the normalised collision energy during the ion activation process to the scanned mass range.[49] Larger *m/z* precursor ions require higher collision energy (CE) for effective fragmentation thus when using the normalised collision energy the relationship of the particular *m/z* ion and collision energy applied can be automatic.

Another limitation that improved automatic MS/MS experiments was focused on a number of experiments needed to achieve a sufficient number of product ion spectra from which the structure could be elucidated. Many compounds lose

a water molecule, which is often the only product ion formed, $[M + H - H_2O]^+$ and is therefore structurally not very informative. Such fragmentation behaviour requires another stage of CID to generate second generation product ions that would allow structural characterisation. The problem was solved by substituting the standard resonance excitation with wideband excitation.[49] The standard resonance excitation used a narrow isolation width for analysis of a precursor ion, yet opening of the isolation window, *i.e.* up to 20 *m/z* units, allows fragmentation of the $[M + H - H_2O]^+$ ion with the second stage of CID within one experiment, Figure 1.9. The first generation product ion spectrum acquired with wideband excitation mode on resembles a spectrum of two separately performed experiments with wideband activation off. However, as a wider *m/z* range needs to be excited, more energy (higher RF voltage) is required to achieve a sufficient fragmentation of the precursor ion using wideband excitation. The comparison of spectra acquired using the wideband excitation mode on and off is often crucial in mechanistic studies.[49]

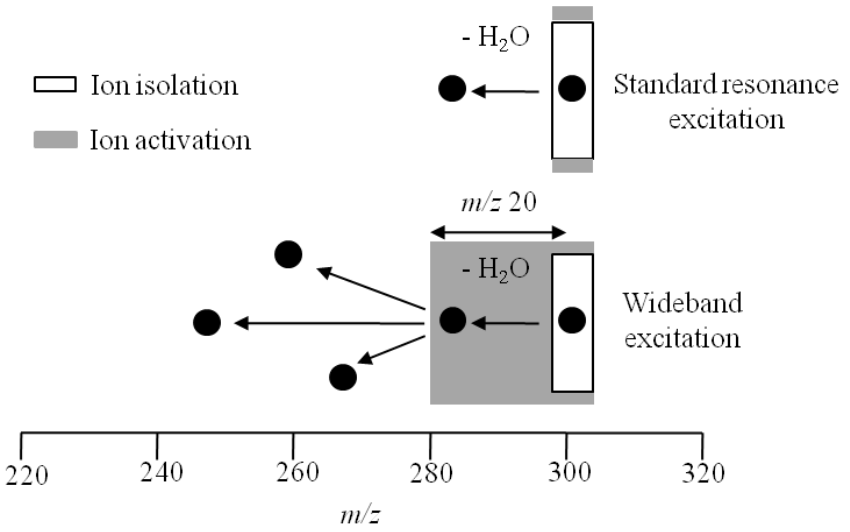

Figure 1.9 Schematic representation of wideband excitation mode in CID experiment; reproduced from Lopez *et al.*[49] with a kind permission from John Wiley & Sons, Ltd.

The ability of the QIT to store ions "in-time" rather "in-space" offers unique advantages for possible experiments.[40] The QIT is one of the most common mass

analysers used for structural elucidation studies, because all product ions formed due to the fragmentation originate from the precursor ion. Papac and Shahrokh stated that MS based methods in many areas of pharmaceutical industry are focused on ion trapping methods.[50] Different applications of QITs are mainly focused on the identification of metabolites, degradation products and proteomics studies and most are coupled to ESI. The ion trap covers a medium *m/z* range (up to *m/z* 6000) compared with other mass analysers and with low mass resolution and accuracy, it still has a very high sensitivity and specificity.[22] The low cost of the QIT mass analyser, its ability to coupled to many ionisation techniques and to undertake multistage mass spectrometry experiments (MS^n) in the same analyser, makes it one of the most successful mass spectrometers.[47]

1.2.2 Ion Cyclotron Resonance cell

The ion cyclotron resonance cell is the mass analyser of the FT-ICR mass spectrometer, which was introduced in 1974 by Comisarov and Marshall who showed that the analysis of a CH_4^+ ion is possible within a resolution of 0.005 mDa using the magnetic field of a 0.32 T magnet.[51]

The principles of ICR cell operations are based on charged molecules affected by a magnetic field at a frequency related to the *m/z* value of the ion.[22] In other words, a specific *m/z* value is calculated from a path of frequency and its trajectory when affected by the electric and magnetic field.[44] In a time domain, the *m/z*-dependent frequencies are represented as a waveform, which is composed of many individual frequencies and their amplitudes determine the abundance of the ions with a specific frequency. The complex waveform is converted to a mass spectrum by the mathematical Fourier transform function. The high accuracy of the experiments and a resolving power of the mass analyser results from an acquired frequency, which is a physical parameter that can be easily measured.[29]

Two FT-ICR mass spectrometers were used in this project, *i.e.* the Apex III from Bruker Daltonics and the Finnigan LTQ FT from Thermo Scientific. The main differences between the Apex III and the Finnigan LTQ FT instruments are as follows: i) the type of ion activation method – SORI/CID and IRMPD and ii) the strength of the magnet – 4.7 and 7 T, respectively. Both instruments contain an atmospheric pressure ion source followed by an ion guide and an actively shielded magnet with an ICR cell. The Finnigan LTQ FT additionally contains a linear ion trap (LIT) that operates in a similar way to the LCQ QIT mass analyser although the extended size of the trap and two detectors on the side of the mass analyser improves sensitivity of the experiments.

The heart of the FT-ICR mass spectrometer is a cylindrical cell called a Penning trap, which traps and stores the selected ions. It is built of three pairs of trapping, exciting and detecting electrodes, Figure 1.10. Similar to the quadrupole ion trap, the ICR cell operates using an axial trapping mode, which involves applying a DC voltage to the trapping plates to control the opening and closing of the cell. The exciting plates focus on applying the RF potential to increase the kinetic energy of the ion with a specific frequency whilst the detecting electrodes register the signal of the ion frequencies. To ensure that ions are kept in the centre of the trap, a static electric and magnetic field B is applied. The magnetic field and electric potential affect cyclotron, trapping and magnetron motions of the ions.[52]

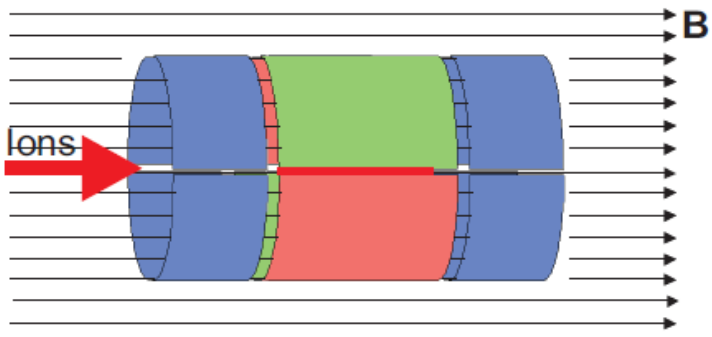

Figure 1.10 Schematic representation of a cylindrical ICR cell with three pairs of trapping (blue), exciting (green) and detecting (red) electrodes reprinted with a kind permission from Thermo Scientific.[53]

The cyclotron motion is formed from the interaction of the ion velocity and its direction with a perpendicular direction to the magnetic field axis, Figure 1.10.[53] The force, called a Lorenz force, causes ions to travel in circular paths that can be expressed by cyclotron frequency,[52] which depends on the strength of the magnetic field B and the charge and a mass of the ion *z*, Equation 1.5. Each *m/z* ion has a characteristic cyclotron frequency, f_c,[1] which is proportionally to the strength of a magnetic field; for a fixed *m/z* ion, a stronger magnetic field provides a higher frequency. Consequently, higher values of cyclotron frequencies of measured *m/z* ions generate more data points thus the measurements are more accurate.[22,44]

Equation 1.5 $$f_c = \frac{zB}{2\pi m}$$

f_c – cyclotron frequency, z – number of charges, m – mass of the ion, B – strength of the magnetic field

The radius of the cyclotron motion of the ion depends on its kinetic energy.[52] The trapping motion of the ions is affected by the low positive potential (if positive ions are stored) applied to the trapping plates mounted perpendicular to the magnetic field direction. A simple harmonic oscillation of ions between plates characterises the motion. The magnetron motion is affected by the three-dimensional field formed from an electric potential V and strength of the magnetic field B. It also depends on the distance between the trapping plates and the geometry of the ICR cell, which is described with the specific geometry factor α.[52] This motion is independent of the *m/z* of ions, Equation 1.6.[52]

Equation 1.6 $$f_m = \frac{\alpha V}{\pi a^2 B}$$

f_m – magnetron frequency, V – electric potential, a – distance between trapping plates, α – geometry cell factor

Thus, when the *m/z* ion absorbs energy when RF potential is applied to the exciting plates it starts to move according to the described motions. The overall ion motion is similar to a spiral.[21] The detecting plates register the trajectory of ion motions, described in frequencies.[52] As a result, the time-domain frequency spectrum is formed and it can be easily converted into a mass spectrum. The cyclotron motion of ions is represented by a signal that, when processed, gives an image current. This is a unique, non-destructive detection feature of FT MS.[52] Unselected *m/z* ions are expelled from the cell.[1] Ions are detected in non-destructive way causing that theirs frequency can be repeatedly measured, which increases the sensitivity and resolution of the experiment.[54]

The benefit of using the ICR cell for *m/z* measurements is the high resolution, accuracy and dynamic mass range of the experiment.[53] The resolution of the LTQ FT is "100 000 at *m/z* 400 with a scan repetition rate of 1 second, while acquiring a mass range from *m/z* 200 to 2000."[53] The mass range of the FT-ICR mass spectrometer is up to 4000 *m/z* units with a 7 T magnet. An ICR mass analyser offers tandem-in-time mass spectrometry with multiple stages of fragmentation. The principles of operations are similar to a QIT mass analyser. The tandem mass spectrometry experiments inside the ICR cell are not advantageous compared with possible ion activation experiments performed outside the ICR cell, which would increase the duty cycle and maintain the ultra high vacuum inside the cell.[19] In the Apex III, ion dissociation is achieved by the introduction of a collision gas into the ICR cell, excitation of the precursor ion to perform SORI/CID followed by the ejection of the collision gas and an acquisition of the product ion spectrum. The IRMPD MS/MS experiment in the Finnigan LTQ FT excludes the stage of introducing and ejecting the gas into the cell; here the CO_2 laser activates the selected precursor ion.

For optimum performance of the ICR cell a high vacuum is essential. It must be 2-3 orders of magnitude higher than the vacuum of low resolution mass analysers (10^{-6} Torr) to avoid interferences (ionised air molecules) and achieve high resolution and accuracy.[21,22] ICR mass analyser applications are focused on the

investigation of ion/molecule reactions, identification of individual components in complex samples, impurities and proteins that require confident elemental formulae determination.

1.2.3 Triple Quadrupole

The triple quadrupole is a tandem mass spectrometer consisting typically of three quadrupoles, built from stainless steel rods. Each quadrupole is responsible for a specific role within the mass analyser.[22] The first and third quadrupoles are mass filters and the Q2 is a collision cell where the CID process takes place, Figure 1.11. The 6410 Triple Quad LC/MS from Agilent Technologies was the QqQ mass analyser used in this project.

In positive ion, the protonated molecules enter the mass analyser through the octapole, which focuses the ion beam, followed by a set of skimmers. The Q1 and Q3 within triple quadrupole mass analysers are mass filters operating in RF and DC potentials and have the ability to select a specific *m/z* ion.[55] The quadratic electric field is created when the RF and DC voltages are applied to an opposite pair of rods. As long as RF is higher than DC potential, ions are pushed through the space between the quadrupole rods.[56] The stability of ions is determined by Mathieu equations that explain the relationship between RF and DC potentials. RF focuses the ions whilst DC potential supports that process by de-focussing ions (attracting them to the rods) in one dimension and focussing (repulsing them from the rods) in the other.[57] Unselected ions strike the rods of the mass analyser.

The Q2 (often presented as ‘q’) operates in RF potential only and, in 6410 Triple Quad LC/MS from Agilent Technologies, is actually a hexapole partially filled with nitrogen gas that is present in order to cool the ions and collide with them by multiple ion/neutral collisions.[22,58] When RF potential is applied to the three pair of rods, the hexapole keeps the ions focused in the centre line of rods. However, RF gives an inhomogeneous field, which pushes ions up and down or back

and forth as in an oscillating electric field.[59] The velocities of the ions reduce and if the RF potential is strong enough, the ions can be deflected to the opposite rods. This process is called an effective potential or pseudopotential.[59] The initial energy of the ions is transferred into RF oscillations and back as a translation motion. Consequently, the motions of the ions act as a potential barrier for the field. RF pushes ions towards the ion guide axis by creation of the harmonic oscillations frequency, which depends on the mass of the ions, RF frequency and amplitude. Lack of DC voltage allows to focus the ions in the centre of a quadrupole field where ion activation experiments are performed.[60] The values of voltage applied to the Q2 must be however different from RF applied to Q3 to enhance the ion attraction to the last quadrupole where the acquisition of the product ions takes place.[58]

Yost and Enke have described the QqQ mass analyser as "a simple and efficient approach for selected ion fragmentation."[61] The main advantage of a QqQ mass analyser is its selectivity and sensitivity based on the use of an efficient low-energy CID and a high transmission of ions along the ion path.[61] The QqQ is a simple to operate, robust mass analyser able to perform many different types of CID. In contrast to the QIT, it is a tandem-in-space mass spectrometer; the mass spectrum acquired using a QqQ is mostly a combination of many generations of product ions therefore it is often found to be less advantageous for structural elucidation studies. The main applications of the QqQ mass analyser are focused on quantitation and trace analysis of organic compounds in the fields of food science, environmental, pharmaceuticals and toxicology studies.[58]

1.2.4 Quadrupole Time-of-Flight

The first quadrupole-time-of-flight instrument was launched over 15 years ago and essentially the mass analyser is a hybrid mass analyser consisted of QqQ where the Q3 was replaced by a TOF analyser.[56] The TOF analyser is a beam-type mass spectrometer[22] that detects ions within few microseconds after their

formation.[56] QTOF is a robust mass analyser that combines the strength of both mass analysers to a level that could not be obtained using either a QqQ or TOF alone. It is characterised with high sensitivity (from the QqQ), mass resolution and mass accuracy for precursor and product ions (from the TOF).[22] The tandem-in-space experiments performed on a QTOF are similar to QqQ, Figure 1.11. Not all type of MS/MS experiments are possible, but they are improved with the benefit of a high mass accuracy and hence easier identification of gas-phase ions.[56] The comparison of "in-space" CID between QqQ and QTOF may show key insights of differences and similarities in the fragmentation behaviour of gas-phase ions.

QTOF has an additional Q-zero 'Q0' thus the instrument comprises Q0, Q1, Q2 (q) followed by a reflecting TOF (mostly orthogonal-acceleration TOF (oaTOF)).[62] In some QTOF instruments, Q0 and Q2 are substituted with hexapoles;[60] different QTOF instruments have different sets. Quadrupoles focus the ions to the axis of the ion guide but hexapoles and octapoles have a more homogenous field close to the rods thus they are better at keeping the ion beam in control and away from rods, *i.e.* better ion transmission.[59]

In this project analyses were performed using a MicrOTOF-Q from Bruker Daltonics, which has an additional hexapole Q0. The quadrupole part of the mass analyser is already explained in the previous sub-chapter. It can scan all ions, select a chosen *m/z* units range, isolate a precursor ion and direct it to the Q2 where the ion activation experiment takes place. During the acquisition of a mass spectrum across the whole *m/z* range of interest, the Q0, Q1 and Q2 operate in RF only mode and serve the role of the transmission element whilst the TOF analyser measures the times of flight of ions, which are converted to *m/z* units. In an MS/MS experiment, the ions formed for example in ESI, pass through the set of funnels and Q0, which is responsible for the collisional cooling of ions (allows better ion transmission) that improves the focus of the ion beam. Q0 and Q2 work in RF potential only and they provide axial and radial damping of the ions by ion/molecule collisions with a neutral gas (argon or nitrogen mostly).[56] The Q1

operates as a mass filter and transmits the selected *m/z* ions. Ions are accelerated to energies between 20 to 200 eV before entering the Q2 where the CID process is performed. Following the ion decomposition, the product ions are cooled, focused to a fine ion beam and transferred to a field free region called a modular gap. Once this extraction region is populated, ions are pushed in the direction of the TOF through the accelerating columns by an applied pulse of electric field.[60] For example, the positive ions are accelerated from ground to a high negative potential in TOF. The separation of ions takes place in a field free region of a TOF tube and the precise time of crossing the chamber is measured. The ions are accelerated with the same kinetic energy that is dependent on the mass and the velocity of the ions, Equation 1.7.[3]

Equation 1.7 $$E_{kin.} = \frac{mv^2}{2}$$

m – mass of the ion, v – velocity of the ion

Ion velocity depends upon the inverse square root of *m/z* unit so the smaller ions will have higher velocities hence will have shorter time of flight through the TOF tube, Equation 1.8.

Equation 1.8 $$v = \sqrt{\frac{2E_{kin.}}{m}}$$

The kinetic energy of the ion equals the potential energy of the ion at the starting point of the flight, Equation 1.9.

Equation 1.9 $$E_{kin.} = E_{pot.} = zU$$

$E_{pot.}$ – potential energy, *z* – number of charges of the ion, U – local potential at starting point

The velocity of the ion in the drift tube can be determined from its length and time of flight, Equation 1.10. Consequently, the mass of the ions can be deduced from the measured time of the flight of the ion, Equation 1.11.

Equation 1.10 $$v = \frac{l}{t}$$

l – length of the tube, t – time of the flight of the ion

Equation 1.11 $$t = \frac{l}{\sqrt{2U}} \sqrt{\frac{m}{z}}$$

However, a small difference in the position of each *m/z* ion in a modular gap will slightly change the energy, thus the velocities of each ion will cause different time of flight of ions getting into the detector. An unfocused ion beam of the same *m/z* ions causes poor mass resolution. A reflector helps to prevent this problem by normalising the differences in energy between the same *m/z* units ions and hence improve the mass resolution. The same *m/z* ions but with different velocities will penetrate the reflector field to different depths enabling the same *m/z* ions to be focused into a beam. Additionally, a reflector extends the length of the tube, which means that a better ion separation is achieved. When ions hit a detector the precisely measured time is converted to readable value of *m/z* units by an analog-to-digital converter (ADC) or a time-to-digital converter (TDC) forming a mass spectrum.

A QTOF can analyse a large mass range of ions; there is no sharp cut-off point as in the QIT (explained in details in following sub-chapter); however the wider *m/z* range is achieved by extending the length of duty cycles. A high RF potential causes a loss of smaller *m/z* ions, but a low value of RF potential results in the poor focus of heavier ions thus a poor mass resolution. Many QTOF mass spectrometers are coupled to liquid chromatographs and are mostly used in the analyses of qualitative and quantitative biological samples where high mass accuracy and robustness is crucial.[56] Additionally, matrix-assisted laser desorption/ionisation (MALDI) coupled to QTOF expanded biological research to samples that are unable to ionise from a liquid phase.

1.3 Ion activation processes in tandem mass spectrometry

Three ion activation methods were used to perform MS/MS studies, *i.e.* CID, SORI/CID and IRMPD. CID is the most widely used ion activation method in tandem mass spectrometry.[22] The CID-MS/MS experiments performed in this project are low-energy CID (< 500 eV) therefore only this CID energy-type is discussed.

The applications of tandem mass spectrometry are countless, including: ion/molecule reaction and structural elucidation studies, such as sequencing proteins, identifying metabolites and pharmaceuticals, and characterising sugars and oligonucleotides.[19,61,63] In this project, MS/MS experiments were conducted to acquire first generation product ion spectra of analysed compounds to compare differences in their fragmentation behaviour using different ion activation methods.

1.3.1 Collision-Induced Dissociation

Jennings compared CID with the 50 eV EI process.[64] He believed that the processes are principally identical; the transfer of energy to the compound affects its fragmentation. In CID, the collision of ions with neutral molecules causes the conversion of translation energy into internal energy and consequently, fragmentation of the ions; the process takes 10^{-15} second,[21] which is identical to the time of the electron ionisation process.[65] The difference lies in the distribution of the internal energy and its randomisation resulting in specific fragmentation behaviour. One example is the number of reaction steps needed to form the analogous product ions. It is assumed that most CID experiments are two step processes comprising the activation of the ion by collisions with the gas molecules and a unimolecular dissociation of the activated ion.[48] Another proposed mechanism involves a one-step process, called “a stripping mechanism”, which theoretically should be a very fast process if the time for possible structure

rearrangement is excluded. The stripping mechanism became difficult to prove as CID data often involve many structure rearrangement reactions.[48] EI can form a product ion due to the loss of a large neutral molecule in one step, but in CID that product ion can mostly be only formed due to the several smaller losses,[64] which, if overlooked, can often lead to incorrect elucidation of the structure.[66] The internal energy of an activated protonated molecule is composed of an internal energy of the molecule held before the activation and the energy transferred during the collision process. Generally, the latter energy is higher than the internal energy of non-activated ion, however it has a limit described by a centre-of-mass collision energy, E_{CM}, Equation 1.12.

Equation 1.12 $$\boldsymbol{E_{CM} = E_{lab} \frac{m_{gas}}{m_{gas} + m_{[M+H]^+}}}$$, where

m_{gas} – mass of a collision gas atom, $m_{[M+H]^+}$ – mass of the protonated molecule, and E_{lab} – kinetic energy of the ion

The centre-of-mass collision energy is described for a perfect "head-on" collision, however many collisions happen at an angle, which broadens the range of the amount of energy transferred to the ion. Also, the amount of energy being transferred depends on the mass of the analysed ion; the higher the mass of the ion the less energy is transferred to it.[21] Thus, multiple collisions transfer more energy to the ions, resulting in a higher fragmentation ratio. This process can be controlled by varying the collision gas pressure; a higher pressure gives the rise to a higher probability of multiple collisions and higher degrees of fragmentation. In addition, the degree of fragmentation depends on the number of charges carried by the ion; the higher the charge state of the ion, the probability to dissociate is increased, because an increase of electric field increases the kinetic energy of the ion.[22]

In 1978, Yost and Enke presented the first tandem mass spectrometer based on the CID ion activation method.[63] The triple quadrupole mass spectrometer, the first tandem-in-space mass analyser, performs low-energy CID characterised by a lower number of product ions formed than formed by high-energy CID.[31] QqQ-

CID-MS is one of the most widely used tandem mass spectrometry techniques. The main advantage of the QqQ mass spectrometer is its ability to perform many scan types on a particular precursor ion, Figure 1.11.

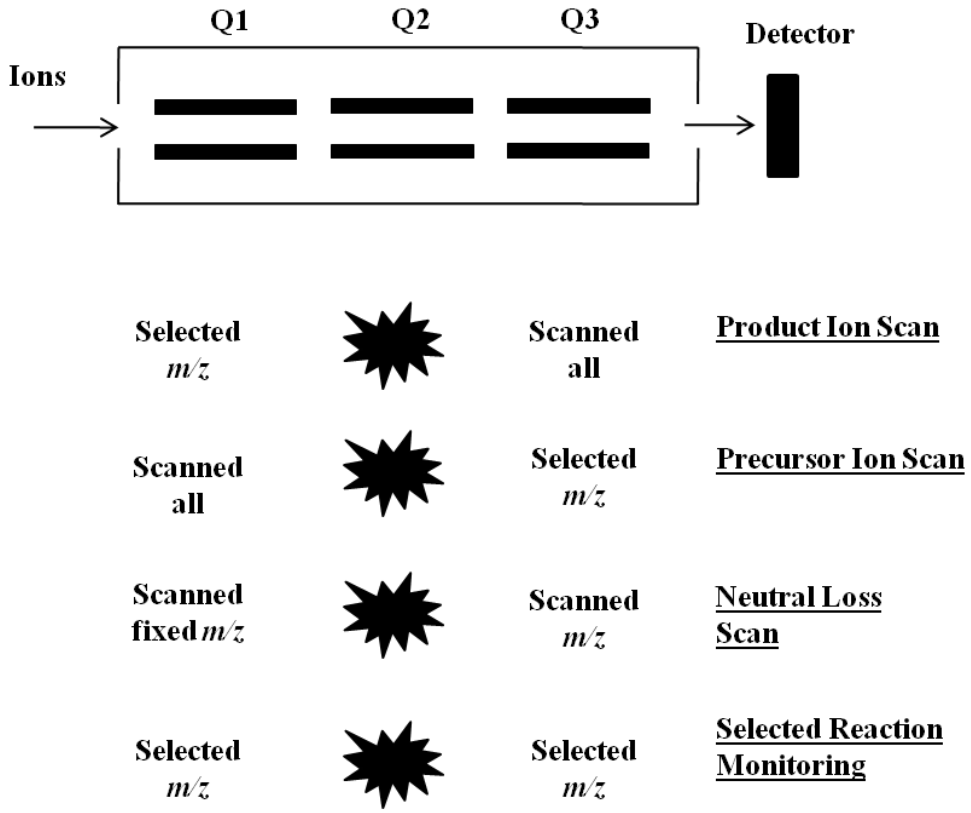

Figure 1.11 Schematic description of scan modes available in tandem-in-space MS on example of QqQ MS.

The product ion scan in in-space CID analyses is used in this project. Here, a precursor ion (mostly a protonated molecule) is selected, followed by its activation and fragmentation in the collision cell and finally, the analysis of the fragment ions. The precursor ion scan is the opposite type of analysis. In this case, all precursor ions that give a selected product ion are determined. The neutral loss scan selects a specific loss of *m/z* units and scans precursor and product ions that lead to the chosen loss. A selected reaction monitoring type of scan is based on a selection of a precursor and a product ion therefore, there is actually no scan. The chosen precursor ion is detected only if it fragments to a selected product ion.[1] The only scan possible in tandem-in-time mass spectrometers is a product ion

scan, because all operations (precursor-ion isolation, activation, and dissociation as well as product ion *m/z* analysis) happen in the same space, but different times.[22]

1.3.2 Sustained-Off Resonance Irradiation/Collision-Induced Dissociation

SORI/CID is a sub-type of CID ion activation method for the FT-ICR mass spectrometer[54] that mainly differs from CID by application of an RF pulse slightly above or below the resonant frequency value of the precursor ion.[67] SORI/CID is an ion/neutral interaction where ions low of kinetic energy (<10 eV) are activated by multiple dissociations with helium or argon resulting in the transfer of a small amount of internal energy to the ion and hence the formation of first generation fragment ions.[42,68] Ion translation energy in SORI/CID is smaller, 1-300 eV, than in CID therefore longer activation times occur. Sustained excitation of ions at the resonance frequency results in large radii of cyclotron motions causing ions to undergo multiple acceleration/deceleration cycles as they repeatedly increase/decrease their orbits before fragmentation.[68] Ions excited by the off-resonance frequency RF pulse can be sustained in the ICR cell for up to 1 s without ejection (especially observed when performing the fragmentation of high-mass compounds that need a longer RF pulse for the activation stage).[21] However, a long activation time favours the structure rearrangement of ions that often complicates the mass spectral data interpretation.[54,69] A magnetic field in FT-ICR mass spectrometer does not have a focusing property so after some time, an off-axis displacement of ions known as magnetron radial expansion is reduced by applying the RF potential pulse, which focuses ions back to the centre of the trap.[1]

SORI/CID is one of the most commonly used ion activation methods for investigating the fragmentation of biomolecules in FT-ICR MS[70] and ion/molecule reactions.[71] The method is also used to differentiate the bond dissociation energies.[54] One of the disadvantages of SORI/CID is the need for

a collisional gas, when it is pulsed into the ICR cell it decreases the vacuum and thus the mass resolving power of the mass analyser.[21,22]

1.3.3 Infrared Multiphoton Dissociation

IRMPD is a MS/MS technique based on ion/photon interactions using the monochromatic radiation of a laser that by emitting photons excites the ions followed by their photodissociation. [68,72] A process of ion activation using photons is schematically presented in Reaction 1.1.[42,67]

Reaction 1.1 $[M + H]^+ + nh\nu \rightarrow [M + H]^{+*} \rightarrow$ product ions

n – number of absorbed photons, hν – photons energy

In this project experiments were performed using a low-power continuous wave (CW) infrared gas CO_2 laser of 10.6 μm wavelength with an output of 10^{22} photons where each photon has an energy of 0.117 eV.[21] Thus, the absorption of just one photon provides enough energy to initiate the dissociation of the ion[35,68] at the lowest energy decomposition pathway without the need to introduce the collision gas.[54] The amount of energy obtained by ions is controlled by the time (5-300 ms)[21] and amount of laser irradiation (normalised values of the laser energy). The IRMPD technique requires the absorption of the photon energy by the ion. All ions, with an ability to absorb a photon, undergo the IRMPD process and hence it is not a very selective method of activation and often results in the formation of second generation product ions.[21,68]

The IRMPD activation method often gives complementary information about fragmentation behaviour to other ion activation techniques.[21] For example, only when electron capture dissociation (ECD) and IRMPD are used together they do give more information about the fragmentation behaviour of glycosylated peptides.[73] One of the advantages of IRMPD beyond the CID technique is that the constant RF voltage can be used in the activation process (CID requires an altered

RF voltage). In addition, IRMPD does not need to pulse the gas into the ICR cell therefore it permits faster fragmentation (faster analysis) and a higher mass resolution than any multi-collisionally based ion/neutral dissociation method[73] yet it is an expensive technique.[21]

Chapter 2 Interpretation of mass spectral data

"...the most important part of learning how to interpret unknown mass spectra is actually to practice interpreting mass spectra."

Fred W. McLafferty

An interpretation of a mass spectrum gives information related to the chemical composition and structure of the analysed compound. Understanding the behaviour of gas-phase ions may help to define the interpretation rules for specific compounds or classes of compounds. In this project, the behaviour of gas-phase ions from pharmaceutical impurities and process related intermediates (PRI) was studied to develop a set of rules, which could help elucidate structures rapidly and with confidence. This complex task demands a detailed understanding of the theoretical approaches of gas-phase ion interactions, individual structure characteristics, and a correct method of data acquisition. Thus, the basics of interpreting mass spectral data involving differences between functional groups and atomic properties are discussed. Additionally, a protocol for mass spectrometry experiments that supports and aids data interpretation is presented. All compounds were protonated using API ion sources and hence, the precursor ion was always a protonated molecule, and fragmentation studies were restricted to the first generation product ion spectra.

2.1 The insights of a mass spectrum

One of the easiest ways to identify an unknown structure is to use mass spectral databases that contain reference data.[74,75] McLafferty prepared a table that contains over 15000 peaks from the fragmentation studies of over 4000 compounds using EI-MS.[74] The approach of mass spectral data correlation according to functional groups helped classify compounds and searched for

possible similar structural data.[74] Unfortunately, present-day databases, especially for API-MS techniques, are often strictly confidential and for internal use only. The number of public database libraries is greatly reduced and the cost of those that are available is high. Thus, it actually becomes necessary to identify a structure using the mass spectrum rather than referring to the reference data. Many possible structures can be deduced from a mass spectrum and additional information about the sample, *e.g.* its synthetic route, helps to propose a correct structure or narrow the list of possible structure hits that fit the mass spectrum.[44] The first step of the mass spectral interpretation process involves finding the peak corresponding to the protonated molecule. The peak's isotope pattern helps to estimate the number of specific atoms in a molecule[44,65] and specific characteristics of organic molecules aid structural identification. Two major rules apply to the characteristics of every organic molecule, including: i) the nitrogen rule: if a compound contains an odd number of nitrogen atoms, its nominal molecular mass will be an odd number and ii) the degree of unsaturation (DU), which defines the number of valence electrons in the ion (odd- or even-electron ion).[65,76-78] The abundance of ions in a mass spectrum reflect their stability in the gas-ion phase[65] thus, a series of comparable mass spectra indicates similarities and differences in product ion favourability. Summarising this approach of finding the peak corresponding to the protonated molecule, the information gained is: i) the estimated number of carbon atoms and characteristic substituents, ii) the amount of double bonds and rings within the structure, and iii) an odd or even number of nitrogen atoms. However, to ensure a correct structure identification and proper elucidation of mechanistic pathways of protonated compounds analysed using API-MS, the analysis should include experiments such as: tandem mass spectrometry, analyses of compounds in standard and deuterated solvent (HDX), and accurate mass measurement (AMM). The analysis of compounds using soft ionisation methods does not generally give much structural information, thus MS/MS experiments are required to resolve this problem by generating product ions. AMM experiments narrow the list of probable formulae and HDX experiments indicate the number of exchangeable hydrogen to deuterium atoms,

which become crucial for proposing the mechanistic pathways of dissociation reactions.

Many mass spectral data interpretation guides are available, with McLafferty and Turecek's "Interpretation of Mass Spectra" being one of the most respected.[78] The "Standard Interpretation Procedure" defines the step-by-step interpretation using a standard set of rules applied to organic molecules.[65,78,79] Despite the fact that the set of rules is written for EI-MS, it also applies to mass spectrometers that form even-electron ions. Mass spectral data interpretation rules are focused on defining observations for typical and specific functional groups as well as they need to account for the different types of mass spectrometers and the type of dissociation process. The identification of typical functional groups may not necessarily help a detailed structural characterisation however, identifying the functional group can often help to partially elucidate structure or narrow the search to specific scaffolds, *e.g.* loss of CO_2 is most likely formed from –COOH hence the structure may be a carboxylic acid. Recent publications focus on specific fragmentation behaviour with regards to the characteristic substituents present in the molecule.[80,81] However, these rules are often applicable to compounds with one functional group and they often fail for structural identification where there are multiple functional groups. Possibly the construction of new rules, focused on specific classes of compounds, and/or specific mass spectrometers used, may enhance the rapid characterisation of small molecules. The set of observations established from interpreting the fragmentation behaviour of quinazolines should aid the rapid characterisation of quinazoline impurities with an unknown structure, Chapter 10, page 157.

2.2 Understanding the fragmentation behaviour – a structure view

The fragmentation behaviour of protonated quinazolines is often difficult to interpret as many of them can fragment differently. The interpretation of mass spectral data of protonated quinazolines can be improved by finding and

understanding fragmentation trends and building them into the rules of interpretation. The fragmentation pathways may be thermodynamically and/or kinetically driven (Chapter 3, page 55). Essentially, the ion needs an excess of internal energy in order to fragment.[44] Many theories and rules have been stated to help understand the behaviour of small molecules ion in the gas-phase and elaborate upon the predictive approaches. For EI-MS, the determination of bonds that may cleave was used to explain fragmentation rates and predict mass spectra of small molecules (mainly alkenes), which is commonly known as Quasi-equilibrium theory (QET).[82] It uses the excess of energy to determine the possible bond cleavages. Another theory, known as the Hammond principle, states that fragmentation of a gas-phase ion is an endothermic process and is driven by the stabilities of the formed product ions.[83] Product ion stability is an important driving force in ion decomposition reactions and can be enhanced by resonance and kinetic effects of fragmentation processes.[78] However, it was also stated that charge localisation affects the fragmentation process ("a charge site triggers the ion fragmentation") and the presence of atoms with lone pairs of electrons (electron-donating substituents) induces electron delocalisation (the lone pair are not strictly fixed on free orbitals).[44] However, electron-donating substituents, such as $–OCH_3$, $–NH_2$, also increase the number of ions with insufficient internal energy and hence decrease the degree of fragmentation.[84] The joint picture of the ion stability and charge delocalisation processes helps to understand the fragmentation behaviour of gas-phase ions. Charge localisation stabilises the ion, resulting in production of a specific (and the most stable) form of the ion that affects which site of the molecule induces the fragmentation to the most stable product ion (not the path, but the stability of the product ion defines this).[85] Additionally, the most favoured reaction pathways are also driven by: i) formation of a new bond – a reaction may lead to a stable ion and ii) the steric factors of the ion structure, which define broad interactions of electron sharing, resonance and inductive effects.[65]

2.2.1 Protonation site

Molecules may have one, many or no obvious sites of protonation.[86] It is hypothesised that if many sites of protonation are possible, not only one type of ion is formed, but a population of ions are formed in a gas-phase ion cloud; different forms having different sites of protonation. In this project, the forms of ion with different sites of protonation are called: forms of protonated molecule (FPM) and forms of product ions (FPI).

The choice of protonation site affects the understanding of how the bonds cleave and predicts which ones will dissociate.[86] For example, a hydrocarbon analysed using EI-MS forms product ions due to the C-H and C-C bond cleavages. However, when one of the hydrogen atoms is substituted with an amine group, the most probable protonation site becomes the nitrogen atom. The product ions formed due to the loss of hydrocarbons would possibly be suppressed by the more favoured loss of an amine functional group. Thus, the localisation of the most probable protonation sites by literally placing a charge in the molecule helps the interpretation of the mass spectra and proposed mechanism pathways. To ensure that none of the possible species are omitted from investigation, every possible FPM and FPI is defined. The probability of protonation is defined by the strength of the hypothetical protonation bond in the gas phase, (H-N, H-S, *etc.*) and it is estimated that the highest probability of protonation site is at a nitrogen atom and the weakest at a chlorine atom – N > S > O > Cl.[86] Consequently, the most probable site of protonation emerges at the most basic atom and hence, it can be determined by calculating proton affinities values for each possible FPM.

The discussed rules and observations were mostly based upon initial observations of an extensive collection of mass spectral data acquired using EI-MS. Can these observations really apply to ESI-MS studies? Does the ESI process influence the site of protonation? Smith and co-workers stated that ESI affects the charge distribution in a molecule[11] and that the charge distribution is structurally dependent. The most probable sites of protonation in the ion in a solution and

a gas phase can differ[87] in the same way as the geometries of the ion in these two phases differ.[82] Thus, the PA values of the specific atoms in the molecule in a liquid and a gas phase must differ and hence the most probable indicated FPMs should be different. Additionally it was found that atoms with a high proton affinity in the gas phase are not always the ones that are protonated.[87] The stability of the ion structure itself, regardless of the presence of the solvent, affects the PA value, which is called (for a gas-phase ion PA) an "effective proton affinity".[87] Thus, the choice of the protonation site is also influenced by the stability of the ion structure. The protonation occurs on a less basic atom in the molecule if the final FPM is more stable that the FPM protonated on the most basic site.[3]

Additionally, the site of protonation can change during the ion activation and dissociation process, *i.e.* during the CID process. Ion interactions with neutral gas-phase molecules can cause a charge migration to alternative different sites of protonation.[88,89] The change of protonation site can take place according to the basicity of the atom, stability of the initial ion structure, and stability of the final protonated form.

2.2.2 Bond fission

The prediction of fragmentation behaviour is essentially the prediction of bond cleavage. Thus, predicting mass spectral data means understanding which bond in the molecule is most likely to break. Additionally, it is important to predict, which fragment will retain the charge and which will be discarded as a neutral loss.[90]

The relationship of PA and ion structure stability explained above does not just relate to the protonated molecule. It also explains the fragmentation behaviour of a molecule. Field's rule states that the formation of the product ions depends on the proton affinity of the fragments; the higher PA of one fragment of the structure enhances its tendency to retain a charge.[91] Stevenson's rule states that, in

the electron ionisation process, the decision of which fragment retains a charge is determined by an ionisation potential (IP) (it also known as the ionisation energy – IE). After the bond is cleaved, a positive charge is retained on the fragment with the lowest ionisation potential,[92] which can also be calculated kinetically.[93] The ionisation energy can only be applied to EI homolytic-bond cleavages, because it is the energy required to remove the weakest bound electron.[94,95] Thus, odd-electron ions can have a higher ionisation potential than even-electron ones and their product stability, regardless of IP value, also affects the fragmentation.[92] The stability of odd-electron ions increases with a conjugation or resonance of the free electron,[79] and hence its stability is structure dependent.

It is even more difficult to rationalise and predict rearrangement reactions. It was found that the transfer of a hydrogen atom always migrates towards the part of the molecule that is electron deficient. Odd-electron ions ($OE^{+\bullet}$) are known to be unstable species, however it was observed that those that have the possibility of the 6-membered transition state for transferring the hydrogen atom form a more stable radical cation (thus are observed with a higher ion abundance), Reaction 2.1.[96]

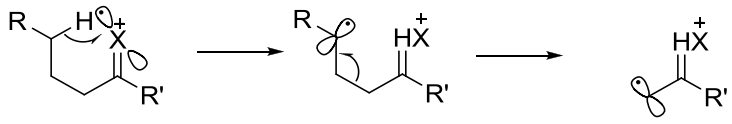

Reaction 2.1 Scheme of the 1,5-proton-shift reaction towards the part of molecule with deficient amount of electrons; reprinted with a kind permission of ACS. [86,96]

One of the ways to determine bond fission is to calculate the bond dissociation energy. It is more difficult to measure the bond dissociation energy for heterolytic than a homolytic bond cleavages.[93] The Reaction 2.2 presents the reaction defining the dissociation energy of the bond R-X in the molecule RX during the electron-ionisation process.[44] This definition can be applied to homolytic bond dissociation energies.

Reaction 2.2 $$\boldsymbol{RX_{gas} + e \rightarrow R^{+\cdot}_{gas} + X_{gas} + 2e}$$

The energies related to the heat of energy of the formed radical cation, Reaction 2.2, are related to the radical cation's appearance A and ionisation energy IE. The R-X bond dissociation energy can therefore be represented by the amount of the formed radical cation and hence, the appearance potential of the $R^{+\bullet}$, $A_R{}^{+\bullet}$, Equation 2.1.

Equation 2.1 $$\boldsymbol{D_{R-X} = A_{R^{+\cdot}} - IE_{R^{+\cdot}}}$$

$D_{R\text{-}X}$ – dissociation energy, $IE_R{}^{+\bullet}$ – ionisation energy, $A_R{}^{+\bullet}$ – appearance energy

However, even for EI-MS reactions, this argument did not agree entirely with mass spectral results.[44] It was found that the appearance energy also depends upon the kinetic energy $E_{kin.}$ and excitation energy (rotational, vibrational, and electronic energies) E_e of the Reaction 2.2 and Equation 2.2.[97] Thus, the dissociation bond energy should also be lowered by the kinetic and excitation energies of the species in Reaction 2.2.

Equation 2.2 $$\boldsymbol{A_{R^{+\cdot}} = D_{R-X} + IE_{R^{+\cdot}} + E_{kin.} + E_e}$$

$E_{kin.}$ – kinetic energy, E_e – excitation energy (rotational, vibrational, and electronic energies)

2.2.3 Specific atoms and functional groups

Extensive studies of EI-MS data have proven that the type of functional groups present in a molecule drives fragmentation behaviour. It is believed that the analyses of API-MS/MS data may also show a similar pattern.

For the typical atoms making up an organic molecule, the inductive effect of withdrawing an electron is the strongest for chlorine and weakest for a hydrogen

atom – Cl > Br, O, S > I >> N, C, H.[65] Fluorine is omitted from the estimated strength order, because it is an exceptionally specific atom affecting fragmentation for types of bond fission other than inductive cleavage. McLafferty states, a fluorine atom affects the fragmentation behaviour of the compound in a similar way to a nitrile group.[65] Fluorine-substituted compounds eliminate HF readily, but a loss of $F^{\bullet}$ is less common;[86] the C-F is a very strong bond (fluorine is a strong electron-donating atom, but is characterised with high electronegativity).[85] Other C-halogen bond strength decreases from C-F to the relatively weak C-I bond.[44] Its order is as follows: -F > -OH > -Cl > $-NH_2$ > $-SCH_3$ > -SH, -Br > -I.[44] The C-Cl, C-Br, and C-I are weak bonds with strong electron-withdrawing characteristics and hence their homolytic cleavage is common.[44] Additionally, Br and Cl can easily be recognised in a mass spectrum because of their characteristic isotope patterns. The difference in these three halogen bond strengths was presented by the comparison of three mass spectra showing formation of a radical cation due to the loss of halogen radical. The chloro-, bromo- and iodo-benzene molecules lose the halogen radical and form a product ion of 57, 37, and 8 % abundance, respectively.[79] Thus atoms, or more specifically the bond strengths binding them to other atoms, influence the specific fragmentation patterns.[44] Sometimes subtle differences in a structure can result in a totally different fragmentation behaviour.[86]

Beynon believed that the fragmentation behaviour of every compound is functional group specific.[90] Some functional groups often give characteristic fragment ions or losses independent of compound substitution, *e.g.* loss of CO_2 from –COOH.[98] Evaluation of the specific functional group trends in the gas-ion phase helps to partially elucidate the structure and propose dissociation mechanism pathways.[99] This is still the most common way of correlating mass spectra.[80,81] The dominative behaviour of the functional group proves that fragmentation behaviour can be functional group-specific and the influence of some functional groups can suppress the effect of others.[44] Product ions of the compounds analysed using EI-MS, containing groups such as carbonyl, nitro, nitryle, and/or sulfonyl are more abundant than hydrocarbons or compounds

containing functional groups such as amino, thiol, and/or hydroxyl.[79] However, it is risky to rely on the functional group recognition pattern only.[44] Specific functional groups do not always influence the mechanistic pathways and a false-positive functional group recognition may cause the wrong structural identification.[85] Additionally, structures with multiple functional group substitution show a hierarchy based on the dominative strength of functional groups.[80,81]

When considering a compound's different atoms and functional groups, its structure can be elucidated by identification of the characteristic ions and/or losses. Sometimes, even the general ions and/or losses give insights about the structure; for example: for *m/z* 91 the list of possible ions is limited to $C_7H_7^+$ within the error of 30 ppm (almost 2.9 mDa) or a loss of 28 *m/z* units can be a loss of C_2H_4, CO or N_2.[65] Additionally, the loss itself can also help to understand structure interactions; *e.g.* $[M + H - 1]^{+\bullet}$ represents a loss of product ions due to the loss of $H^\bullet$. This radical has to come from a labile hydrogen atom or correspond to a labile substituent. A product ion due to the loss of 15 *m/z* units, $[M + H - 15]^{+\bullet}$, indicates specific loss of $CH_3^\bullet$ radical that has to be bound to a weak, easily cleavable, bond.[65] As well as previous partial structural assignments, the possible losses should be specified carefully. Neutral losses are not always the simplest structures, often the losses consist of the concerted, smaller in mass, losses involving loss rearrangement.[82]

2.2.4 Even-electron rule

One of the most common rules in mass spectral data interpretation is the so-called "even-electron rule". This rule was defined from the observation of many EI data. Its definition is as follows. Odd-electron ($OE^{+\bullet}$) cations (molecular ions or radical cation product ions) may fragment to give an even-electron product ion (EE^+) and a radical loss ($RL^\bullet$) or a radical cation ($OE^{+\bullet}$) and a neutral loss (NL), Scheme 2.1, (a) and (b).[65] Even-electron ions (EE^+, protonated molecules or even-electron

product ions) will usually undergo a NL to form another EE^+, Scheme 2.1, (c). The reaction (d) in Scheme 2.1, which involves the loss of a radical to form an $OE^{+\bullet}$, "has a much lower probability" because it involves the formation of a usually less stable free radical loss.[79] An even-electron ion is highly dependent on stability, therefore its dissociation to a stable product ion often demands rearrangement of a structure and charge-remote fragmentation.[78]

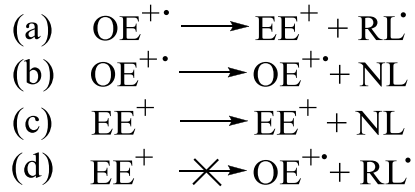

Scheme 2.1 A schematic description of even-electron rule.[65]

McLafferty's observations of gas-phase ion energetics and fragmentation behaviour were developed from studies originating in 1939.[100] The beginning of World War II was a time for mass spectrometrists to explore the potential of EI-MS. Delfosse and Bleakney discovered an unexpected formation of even-electron ions $C_2H_3^+$ and CH_3^+. They had been unable to explain the formation of these particular ions and they left readers with the conclusion that: "...the ions with an even number of electrons are more stable that those with an odd number."[100] Cummings and Bleakney followed this work and tried to explain the formation of specific ions.[101] Ion formation can be described in terms of three energies, *i.e.* the dissociation and ionisation energy of the formed ion, and the kinetic excitational energy of its product ions. They discovered that the charge of a gas-phase ion was able to be localised on an oxygen atom. This observation expanded studies of mechanism rearrangements and the involvement of nonbonding orbitals in dissociation energy values.[101] Later, it was concluded that a charge localisation; i) "triggers" the fragmentation resulting in the prediction of preferable modes of cleavage, ii) indicates bonds in a molecule that are most likely affected by ionisation, and iii) determines the direction of the fragmentation process.[85]

The hypothesis of even-electron ions being more stable than odd-electron ones,[100] as well as the conclusion that the dissociation energies are important to understand ion formation and fragmentation process,[101] was followed by the analyses of lactones by Friedman and Long in 1953.[102] They concluded that a structure can rearrange if it results in the formation of product ions with a high stability. Their experiments confirmed that the formation of a stable even-electron product ion from a lactone structure could be the result of the ring opening.

Following McLafferty's conclusions of the types of fragmentation reactions, Cooks investigated bond formation and discussed how the fragmentation reactions presented in Scheme 2.1 were energetically favoured.[103] He stated that the reactions (a), (b), and (c) represented in Scheme 2.1, are energetically favoured processes and, agree with the studies of Friedman and Long,[102] reaction (a) does not usually involve the formation of a bond, but most probably a structural rearrangement.[103]

The observations of ion formation in the gas-phase have become one of the most common mass spectral interpretation rules despite that the number of exceptions had already been discovered, *i.e.* Friedman and Long had observed differences between fragmentations of lactones.[102] The characteristic reaction types were finally named the "Even Electron rule" in a paper by Karmi and Madelbaum even though it only describes a large numbers of violations.[104] This demonstrated that the word "rule" is too strong attempt for the observations discussed and should be considered with caution.[104]

Many software packages still use this rule to evaluate mass spectral data acquired on instruments other than EI-MS; *e.g.* Data Analysis™ or Xcalibur™, both have the choice to limit possible product ions to "even", "odd" or "both" with respect to the number of valence electrons. However, the default choice is mostly configured for "even" product ions only. This restriction, used mostly to aid mass spectra assignment and limit the number of possible formulae candidates, may actually cause false-positive interpretation of data.

Chapter 7, page 105, contains the discussion of the actual use and meaning of the even-electron rule in present data interpretation models of protonated quinazolines.

2.3 Computerised methods to help mass spectral data interpretation

Mass spectral data processing, analysis, and interpretation can be time-consuming processes that require the use of computer-aided methods.[105] One of the first computerised methods for data interpretation was designed to enable the mass spectrometrist to correctly identify the structure of an unknown analyte.[106] Software automated structural elucidation has proven to be a challenge involving a countless number of variables from the knowledge and experience of a mass spectrometrist. Unfortunately, 40 years ago, computer technology was incapable of helping structural elucidation from any newly compiled interpretation software. Scientists however, believed that improvements in PC technology would succeed in building such software in order to substitute the routine data interpretation tasks of a mass spectrometrist.[106] In the 1970s, the subject of using computerised methods to aid mass spectral data interpretation of EI-MS was very popular (such as the use of EI libraries of National Institute of Standards and Technology (NIST) Standard Reference Database), however by the 1980s the amount of focus in this subject area decreased dramatically.[107] Today, the need for computational help to interpret soft ionisation MS/MS data is even greater than it was a few decades ago for EI-MS data. Electrospray ionisation (ESI) low energy fragmentations, *e.g.* CID MS/MS, although extensively utilised, have only recently been used to build library databases. However, these databases are still much smaller than commercially available EI libraries because the interpretation of ESI-MS/MS spectra of small molecules can be specific for an individual compound, sub-classes or structurally similar scaffolds. Computerised methods have been developed to help the mass spectrometrist with mass spectral data interpretation.[108] Many computational approaches are available, including

i) a library search method,[106] ii) a pattern recognition method,[108] or iii) new software to follow the steps of a mass spectral data interpretation.

One of the aims of this project is to aid the characterisation and understanding of the fragmentation behaviour of gas-phase ions using predictive software.[106,109,110] The use of new computational approaches targeted at understanding and predicting the fragmentation behaviour of gas-phase ions is described (Chapter 8.5, page 137). The recent evolution of a number of different computational methods that could help to achieve this goal are presented here.

2.3.1 Library searching

Library searching involves the automatic matching of unknown data to reference data.[106,108] It is one of the computationally least demanding methods for structural interpretation that only requires a data storage capability and time (of few seconds or minutes) to search the reference data. Different library searching options were established, for example instead of comparing a complete mass spectrum only a few specific ions were chosen. This process saves time by increasing the number of possible hits but the confidence of finding the correct data set is decreased. The improvement of this type of library searching is known as compound-type identification. Many library search files of EI-MS data were grouped according to their specific functional groups and thus, classes of compounds. The unknown analyte was compared across specific ions and losses for classes of compounds and if a class of compounds is positively identified, the detailed searching would only take place within data for that particular class of compounds. This process saves even more time as opposed to looking through all possible reference data and enables the determination of a large part of the structure.[106] It was known that the library would benefit from high-resolution mass spectrometry (HR MS) data input, which would increase the confidence in matching the correct data, but would increase the data storage and length of time for a library search.[106]

2.3.2 Pattern recognition

Pattern recognition is a challenging way to elucidate an unknown structure that gives the best results. The method involves the use of data interpretations of data from many similar, structurally known compounds to find and highlight a specific pattern for that particular group of compounds, *e.g.* compounds containing a phenyl group. The structurally unknown compounds can be matched against it by recognising specific product ions and their intensities.[108] In 1973, Ting and Lee presented a method of pattern recognition for pharmaceutical compounds.[111] Mapping the product ions of known compounds enabled them to decide which compounds fitted into that group. The pattern recognition studies for many small molecule organic compounds was stated to give at least 83 % correct structural assignments.[111] However, the high confidence score (*i.e.* > 83 %) was often limited to the compounds substituted with carbonyl, methyl, ethyl and S-containing functional groups.[112]

Structurally similar compounds may dissociate giving common patterns with common product ions or losses. Therefore the identification of the product ions would not necessarily improve their absolute identification since they may not be structure specific.[113] The identification of a product ion (or ions) that is (are) structure specific helps assign a spectrum (spectra) of a particular compound or class of compounds. The specific functional groups the compound is substituted with (or class of compounds it belongs to), can indicate specific fragmentation patterns and therefore, enhance the structural elucidation.

2.3.3 Heuristic methods

Heuristic methods consist of a structure generator, structure fragmenter, and a correlation of theoretical and experimental data.[108] Structures are generated using the specific parameters of functional group behaviour in the gas-ion phase and fragmentation based on "appropriate rules of mass spectral decomposition".[108]

The results and general observations for the fragmentation behaviour of gas-phase ions are assumed to form rules that ease the process of data interpretation, *e.g.* the even-electron rule[79] or Stevenson's rule.[92] The 'theoretical', generated fragment ions are compared with the real data and the output file presents a list of possible structure matches.

The DENDRAL project was one of the first projects to focus on the problem of structural elucidation of unknown molecules using heuristic approaches.[114] It resulted in extensive investigations of the fragmentation behaviour of small molecules based on analyses using EI-MS. Additionally, the input of the isotope pattern and HR MS data was used to increase the confidence of data hits.[115] A possible empirical formula, suggested from HR MS data, is the starting point for data interpretation. The data from DENDRAL would be scanned for possible structures of a given chemical composition and the mass spectrum would be correlated to fragment ions of possible structures with a given fit of confidence.[114] This project was a pioneer in structural elucidation matching software.[114,115] Further improvements in computer technology enhanced the capabilities of structure predictive software for EI mass spectrometry approaches leading to projects such as CHEMICS and MASSIMO.[116-118] These had similar aims; to build software that, given a structure, could predict mass spectral data. It was also understood that building larger databases with the addition of even more rules, *e.g.* a rule for isotope patterns, would give higher confidence for matching the structure to spectra of an unknown compound.[119,120] Finally, expanding databases with reference data ensured the success of libraries of EI-MS data[121] and the first publically available program (for peptide sequencing) was built by Biemann and co-workers in 1966.[122]

Mass Frontier™ is a commercially available, universal prediction software package based on the fundamental rules of fragmentation, such as: characteristic isotope pattern, the nitrogen rule and the even-electron rule.[123] It is software based on these rules together with information gathered from similar classes of compounds into a large database. However, it is known that the fragmentation

behaviour of some structurally similar compounds can differ, Chapter 2.2.3, page 42.[86] Structural elucidation using libraries becomes even more difficult if different mass analysers or ionisation methods are used. Mass Frontier includes the choice of ionisation method and the choice of types of bond fission in the search parameters and therefore the proposed product ions are based on the basic rules of ion formation and its fragmentation. As previously mentioned, such rules can often limit the number of possible scores causing false-positive identification. In addition, one of the main disadvantages of all currently available prediction software is that they all must be based on the knowledge of prior interpreted, structurally identified, compounds.[124]

2.3.4 Computational simulation approaches

In this study, different theoretical approaches were undertaken to attempt to understand the specific fragmentation behaviour of small molecules. Previous studies have presented data on the understanding of fragmentation behaviour with respect to kinetic and thermodynamic theories, although the majority have concentrated on the latter.[125-128] Moreover, the transition state calculations or molecular dynamics applied to gas-phase ion reactions often challenge the understanding of the mechanistic pathways of the fragmentation behaviour, because they involve a high computing power and advanced knowledge of physical-organic and computational chemistry, and physics (Chapter 3, page 55).[129,130]

Computational chemistry methods are based on advanced theoretical knowledge that requires specific computer skills. Analytical chemists often use the commercially available computational chemistry software, *e.g.* Gaussian, Jaguar or Spartan.[131,132] Density functional calculations, based on Density Functional Theory (DFT), Chapter 3.1.3.3, page 61, are used to help understand the specific fragmentation behaviour of small molecules.[109] Well-optimised simulations should improve the knowledge of atom interactions on a molecular level and help

to understand dissociation patterns of gas-phase ions for small molecules. Most of the *in silico* studies of small molecules are performed using B3LYP level of theory[109] that is commercially available in most DFT software packages.[131,132] Vessecchi's approach, including the transition state species, presents a coherent explanation of specific fragmentation mechanisms. The possible marriage of mass spectrometry with DFT calculations should facilitate the interpretation of the fragmentation behaviour of small molecules.[131] Alex *et al.* used a DFT-MS/MS approach to discuss the influence of a change of bond length when molecule has charge placed at different atoms. Their conclusion is that the site of protonation influences the elongation or contraction of bonds that may be several bonds away from it and these bonds could possibly cleave during the fragmentation process.[133] Thus, their conclusions follow the observations regarding protonation site and bond fission rules described in Chapter 2.2, page 37. Alcami and co-workers reviewed in details the bond shorthening/lengthening process, known as the bond-activation reinforcement rule (BAR rule).[109] The BAR rule relates to the charge density of the two possible atoms involved in protonation. In principle, the comparison of the electronegativity values of the two atoms indicates which one is more favoured to retain a charge[109] and excludes the rationale of measuring the dissociation energy of bonds that may also be relevant, although are not necessary length dependent.[134] The bond energies were implemented in a new prediction model based on *ab initio* approaches called Fragment iDentificator (FiD).[135] It involves the analysis of possible single-step and multistep fragmentation pathways as well as hydrogen rearrangement reactions.

Current computational approaches to build prediction software for small molecule fragmentation are focused on a deep understanding of the fragmentation behaviour of gas-phase ions. The establishment of a set of rules, based on structure specific and common fragmentation behaviour of sub-classes of compounds, would simplify the structural elucidation process. A combination of the optimum features from pre-existing models, with specific rules for classes of compounds may give promising results to build prediction software package without the need to upload reference data. However, the use of different mass

analysers and/or ion activation methods can cause method specific fragmentation behaviour. Whilst there may also be some generic, cross platform rules to consider, any fragmentation rules established will need to note mass analyser specific dissociations. Finally, it is important to stress that this could aid, not substitute the mass spectrometrist in the structural elucidation process by reducing the length of time spent on repetitive tasks that are a "must" when dealing with mass spectral interpretation. Hill and Mortishire-Smith's approach is considered to be a good example of the "big picture" view of prediction software.[136] The aim of their model called EPIC (Elucidation of Product Ion Connectivity), was focused on reducing the number of possible product ions by identifying the precursor ion using high-resolution mass spectrometry and incorporating the accurate mass measurement into the prediction software.

Chapter 3 Computational and theoretical approaches allied to mass spectrometry

"Computers don't solve problems, people do. Computers just generate numbers."

Frank Jensen

Mass spectrometry focuses on the behaviour of gas-phase ions and can be defined by four stages: ions formation, excitation, fragmentation, and detection. These stages can be characterised by different interactions, which depend upon the choice of the ionisation technique, the mass analyser, and the ion dissociation method.[42] Thus, a choice of a mass spectrometer defines the interactions that can occur and hence may influence gas-phase ion behaviour. For example, an interactions of ions in ESI-QIT mass spectrometer depend on specific processes, including: i) ESI; ions can be formed from a solution and a gas phase and ii) CID, which is based on ion/neutral interactions that specifically in a QIT are tandem-in-time type of reactions.[42] Consequently, understanding the principles and driving forces of mechanism pathways as well as knowing the structure of the analyte, may help predict specific gas-phase ion behaviour. These structural interactions, which are essentially explained by physical-organic properties, are impossible to predict without experimental or computational approaches. Physical-organic properties calculated using *in silico* methods help to obtain key insights of the gas-phase ions fragmentation behaviour compared to mass spectral data.

The choice of appropriate calculation models depends on the quality of desired results, the time needed for experiments, and size of molecules of interest.[137] This brief introduction to computational methods and specific models will help to understand how crucial is to choose the correct model as well as optimise specific calculations. The theoretical sub-chapter describes kinetic and thermodynamic

approaches of useful characteristics of a molecule that can be used to help to understand the fragmentation behaviour of gas-phase ions.

3.1 Introduction to computational chemistry – choice of a model

The raw results of generated, by computational chemistry models, data are rarely useful, but they often become crucial to understand the unknown if rationally interpreted and applied to specific problems.[138] Today, computer technology improves rapidly and hence computational chemistry starts to compete with a necessity to perform standard laboratory experiments. It is common to choose projects focused on the benefits of computational methods. The main use of computational methods allied to the mass spectrometric side of this project is to investigate the shapes of molecules, their protonation sites and internal energies. The behaviour of a molecule is described by its total energy, including i) energies, which determine the reactivity and its stability and ii) dynamical simulations (kinetic motions), including translation, vibration, and rotation dynamics.[129]

In computational chemistry, a molecule, defined as a number of electrons among nuclei, becomes the centre of attention and a starting point for every calculation. A negatively charged electron and positively charged nucleus interact resulting in the formation of measureable potential and a distance between defined particles. The classical description of the molecule system however omits its changes over time, *i.e.* motions (dynamics) of the molecule. Electrons are too small to be described by classical mechanics (*i.e.* Newton's Law) yet they can be defined by quantum chemistry wave function. The square of the wave function gives the probability of finding an electron at a given position and a fixed time. However, the dual function of time-dependent wave function is impossible to solve (neither position nor time can be exactly measured). Thus, the position of the electron can be measured by time-independent wave function. Nuclei are much heavier than electrons and hence, from the electron "point of view" nuclei do not move, which gives the ability to describe an electron wave function with the fixed position of a nucleus. This way a molecule is described as a number of electron wave

functions (a potential role) among nuclear wave functions (a fixed position). This specific molecule separation is known as the Born-Oppenheimer (BO) approximation, which defines electrons as one homogenous mass, dependent upon the position of the nucleus (nuclei can be excluded from the calculations).[138] In other words, all electrons are treated as one mass, which is the "glue" that holds the nuclei together. The Schrödinger equation is very hard to resolve because of many interactions that need to be included, such as: interactions of coulombic repulsion, attractions, and kinetic energies of nuclei and electrons.[139] Thus, the BO approximation keeps the nuclei in a fixed position and molecules can be treated as electronic structures only.

Based on the above description of a molecule, computational techniques investigate chemical problems including molecular geometry, energies of molecules, and their chemical reactivity. Three types of methods are defined, which are: molecular mechanics (MM), quantum mechanics (QM) including: i) *ab initio*, ii) semi-empirical (SE), and iii) density functional theory calculations (DFT), and molecular dynamics.[140]

MM are rough calculations based on classical mechanics approximations and an input of real data (in computational chemistry called a parametrisation function) to indicate possible shapes of the molecules. *Ab initio* and SE calculate the molecular wave function (Schrödinger equation), which is hard to measure to provide a single solution. Semi-empirical calculations additionally involve a parametrisation function. DFT calculations are based on electron density calculations and molecular dynamics involve motions of ion into simulations. The wave functions cannot be solved exactly thus, to apply them practically, all calculations are based on partial approximations.[141] In addition, the strict line between types of methods diminishes with the wide use of hybridised models that merge the advantages of a few methods into one model.

3.1.1 Computational cost

Computational simulations cost time and money. Very complicated model sets that require powerful computers and long simulation time often give the most accurate results. The choice of a simpler model reduces the amount of simulation time but also reduces the accuracy.[142] Thus, the trick is to know how to maximise the accuracy of results yet minimising the investment cost of computer power and time. The length of time needed for a calculation depends on the choice of hardware, software, and the structure of the molecule. From a hardware point, three components affect the computational cost: i) the simulation time, which depends on a hardware processor and mathematic operations of the model used, ii) the performance of PC, *i.e.* memory (more memory shortens the time of operation consequently improving the computational performance), and iii) the storage disk (bigger disk stores more data). From the software viewpoint, the computational cost depends on the choice of individual program performing the specific calculations, this may be a commercially available software or new written code.[141] The length of time for calculations decreases for smaller molecules. Each atomic orbital has to be described by the function called contracted Gaussian-type orbital (CGTO). Larger molecules have more orbitals, thus the basis set has to contain a larger number of CGTOs. Single-zeta (SZ) is a minimal basis set using only one CGTO per atomic orbital. Thus, larger basis sets need to be used for larger molecules to include functions describing their molecular orbitals. An increase of basis set increases the length of time for calculations and may be additionally increased when using basis sets containing polarisation functions.[143,144] A polarisation function allows the valence electrons be more flexible, which means that they can displace from their original, theoretical positions.[145] One of the most commonly used basis sets is the 6-31G*, which adds the polarisation function to all atoms and improves the modelling of valence electrons (increasing the accuracy of measurement).[145,146] The two asterisks placed in the name of the basis set, **, mean that the additional orbital is added to the atom, *e.g.* a hydrogen atom is 1s whereas in ** function will be

calculated as p-orbital. Larger basis sets including a polarisation function give high-accuracy results of 1-2 kcal/mol and better geometry of structures.

It is not possible to estimate computational cost precisely.[145] The time complexity scales differently for different methods. The theoretical, expected time of DFT calculations scales to N^3, where N is the number of orbitals in the calculations, which is proportional to the number of atoms.[145] Thus, the calculations depend on the number of atoms and type of basis set used; *i.e.* the calculations performed on a larger molecule mean there are more atoms, thus more orbitals to take into the account, which demands use of a larger basis set resulting in a longer time of calculation.[147] The size of the structure and amount of heavy atoms (a heavy atom in computational chemistry is an atom heavier than He) dramatically affects the simulation time, Scheme 3.1. For example, the time of DFT calculations based on the same parameters for 10 alkenes from CH_4 to $C_{10}H_{22}$ in linear conformation will increase with the increase of number of atoms in the molecule, for non-linear scaling DFT it increases exponentially (N^3), and for linear scaling DFT it increases proportionally to the number of atoms, Scheme 3.1.

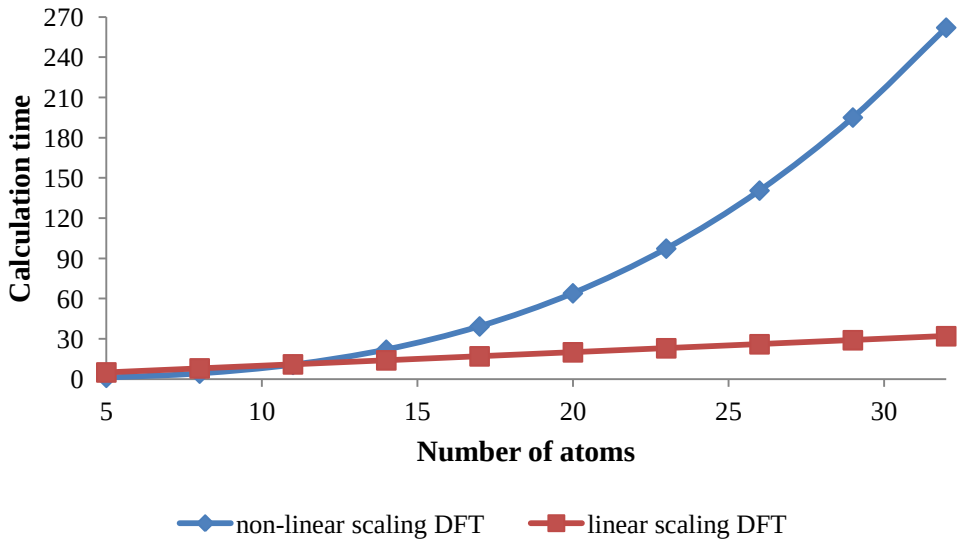

Scheme 3.1 Comparison of the length of time for calculations to the number of atoms in the molecule using linear (squares) and non-linear scaling DFT (diamonds).

3.1.2 Molecular Mechanics

Molecular geometries defining a probable shape of the small to medium-sized molecules are commonly calculated using molecular mechanics. A molecule is presented by spheres and connecting springs, thus the electronic properties of the molecule are impossible to calculate.[137] However, the balls and springs are based on parameters externally estimated (IR spectrum, X-Ray experiments), thus the method employs a partial parametrisation function. The Merck Molecular Force Field (MMFF) is a common model of MM for structure calculations and was used during this project to define the shapes of the molecules.[148] MMFF reveals all possible structure geometries and an inaccurate value of total minimum energy indicates the conformer stabilities.[145] The MM approach excludes the effect of bond breaking, charge, and spin changes that define structural behaviour, but it is widely available, stable, and very fast model that is applicable to very large molecules, because these calculations are approximately 1000 times faster than quantum mechanics.[141,145,149]

3.1.3 Quantum Mechanics

3.1.3.1 *Ab initio* calculations

Ab initio (*from first principle*) calculations are based on the behaviour of all electrons in the molecule thus on the full molecular wave function of the molecule (on the Schrödinger equation). Consequently, they calculate the energy of the molecule. The main disadvantage of *ab initio* calculations is that they are very slow methods involving huge computational power.[138,140] The newest computer technology allows the performance of *ab initio* calculations with less time, but increases the computational costs. The most common *ab initio* calculations are Hartree-Fock (HF) calculations applicable to calculate molecule geometries, thermodynamic properties, bond lengths, and angles. Two types of HF are

distinguished, *i.e.* restricted HF (RHF) and unrestricted HF (UHF). RHF treats molecular orbitals as being occupied by two electrons thus, can be used to analyse even-electron species only. UHF is more flexible, it treats electrons separately and hence it can analyse odd-electron compounds. However, the method neglects the electron correlation thus the calculations are not very accurate.[150] One of the first calculations of gas-phase ions was performed on hydrocarbons using HF calculations.[151] *Ab initio* calculations of gas-phase ions were a great breakthrough to estimate structure symmetry and bond lengths that became "more than just a guess."[152] However a few decades ago, computer technology was not so developed thus the compromise of computational cost and accuracy was an issue.

3.1.3.2 Semi-empirical calculations

Semi-empirical calculations, *"partially-experimental"* calculations, are based on the fundamental physical equation (as *ab initio*) and experimental values (parametrisation function).[138] One of the common SE methods is an Austin method (AM1), which was also used during this project. One of the main characteristics of this method is the input of hydrogen bonding, four-membered rings and activation energies into the model.

The SE calculations are slower than MM but faster than *ab initio* and DFT calculations, however the loss in accuracy is great. They are widely used to investigate the geometries of large molecules, such as proteins or nucleic acids, but they are approximate calculations.[140] It is expected that SE methods often underestimate the bond lengths and keep thermodynamic values in errors higher than 5 kcal/mol.[140]

3.1.3.3 Density functional calculations

Density functional calculations are based on electron probability density function (electron density), which interprets the probability of finding any electron within a

specified volume.[95,140] Density functional theory is not based on wave function, but on an electron density, which is observable and measureable using X-ray. According to the triangle scheme, if electron density is known a structure and its reactivity can also be understood, Figure 3.1.

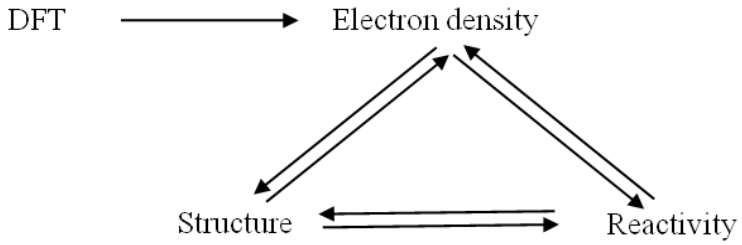

Figure 3.1 Schematic description of DFT use, reprinted with a kind permission from VUB Brussels University Press.[153]

The principle of DFT is based on the Hohenberg-Kohn theorem stating that the electron density determines a ground state electronic energy; in other words: that any ground state molecule property is a functional of the electron density at the known position, thus it can be calculated.[129,154] A wave function of an N-electron system contains 3N coordinates (three energies for each electron: a kinetic energy, nuclei-electron attraction, and electron-electron repulsion). Thus, an electron density is a square of the wave function dependent upon its coordinates. The complexity of the wave function increases with the addition of an electron, but the electron density will have the same variables regardless of the increasing size.

The exchange-correlation functional (XC) part of DFT is its weak point. The exchange correlation potential needs to include self-interactions, which are coulombic interactions of any orbital with itself (the electron-electron repulsion).[154] It is a relatively small percentage of the total energy of the molecule, however it is crucial for defining ionisation and atomisation energies.[155] It holds the unknown, approximated value and hence some interactions are not well-presented, *e.g.* van der Waals interactions, resonance effects, hydrogen bonds or geometries.[141] If the exact exchange-correlation energy were known then it would provide an exact total energy including electron correlation.[138] Today, most of the new model sets are focused on introducing an additional functional to solve

the exchange-correlation energies problem. One of the most common levels of theory is BLYP, which is a hybridised model of Becke's exchange and Lee, Yan, and Parr's correlation functionals.[141] Its improvement, a B3LYP, is coupled with a HF exchange functional,[156] which makes the hybrid functional, together with, for example 6-31G* basis set, one of the most widely sophisticated calculation model set for solid-state physics and chemistry applications.[145]

One of the main advantages of DFT properties, especially for this project, is its ability to calculate, with high precision and reasonable computational cost, the energies of odd-electron ions. Calculations of radical cations cannot be performed using any other methods except the UHF, however the density functional calculations are more reliable.[144]

The length of time for density functional calculations is comparable to HF methods; usually faster than *ab initio* but slower than SE. Greater accuracies can be achieved by *ab initio* calculations, but DFT can handle larger molecules (generally up to 200 heavy atoms).[138,157] The technique has improved rapidly; in 1999 the DFT approaches of computing total energy of a "large complexity molecules with at least ten atoms" was a success.[156] Lately, molecules of a thousand atoms or more can be analysed this way.[158]

3.1.4 Molecular dynamics

The last type of calculation method is molecular dynamics, which applies the function of molecular motions. This type of method can simulate all the motions during reaction time, for example: a change of the molecule's conformation and a formation/cleavage of the bonds. Consequently, they are very expensive calculations, which are performed only on supercomputers demanding advanced computational skills.[140]

3.2 Kinetic and thermodynamic approaches of gas-phase ions

The theoretical calculations of gas-phase ions help to understand and predict mass spectral data. Thermodynamic and kinetic approaches represent all types of reactions and can compete with each other.[93,159] A theoretical approach can help to answer questions about which product/form/species is more favoured as well as quantify its probability in population studies. Such answers, if correlated with experimental data, help to define and understand specific fragmentation behaviour as well as predict behaviour for "unknown" compounds.

From the thermodynamic point, the change of total free energy reaction (ΔG) describes the main characteristic of the reaction favourability, which is also known as negative gas-phase basicity (GB) value.[93] ΔG depends on change of heat of formation (ΔH), change of entropy (ΔS), and temperature T, Equation 3.1. The fragmentation of an isolated ion can be measured as a free Gibbs energy. The temperature inside the mass analyser is unknown. Johnstone stated that ions have a greater temperature than ambient, but estimated values were not stated.[160] The change of entropy for gas-phase ions is very small, even negligible and hence the change of a free Gibbs energy depends on a change of heat of formation energy only.[130,160] ΔH is the most useful thermodynamical characteristic of the molecule[161] that is also known as a negative proton affinity (PA).[93]

Equation 3.1 $\Delta G = \Delta H - T\Delta S$

ΔG – free Gibbs energy, ΔH – change of enthalpy (heat of formation), ΔS – change of entropy, T – temperature

A change of entropy connects the thermodynamic and kinetic properties of a reaction; it is proportional to the natural logarithm of a kinetic equilibrium constant K for a given reaction, Equation 3.2, and hence can describe the kinetic approach of the reaction pathway.[162]

Equation 3.2 $\Delta S = R \ln[K]$

R – gas constant (8.314 J mol^{-1} K^{-1}), K – reaction equilibrium constant

For example, Reaction 3.1, is a proton transfer reaction described by the equilibrium constant in Equation 3.3, *i.e.* the ratio of the amount of products, A and $[B + H]^+$, to a starting compounds, B and $[A + H]^+$.

Reaction 3.1 $[A + H]^+ + B \rightarrow A + [B + H]^+$

Equation 3.3 $$K = \frac{[A][B+H]^+}{[B][A+H]^+}$$

K – kinetic reaction equilibrium constant

Decomposition reactions are more of interest than proton transfer reactions in this project so kinetic and thermodynamic approaches of understanding the fragmentation reactions are discussed. In CID, a reaction mechanism is affected by the structure of a precursor ion, the activation energy for the fragmentation reaction, as well as a stability of a product ion. The ion activation reactions are characterised with rapid equilibriums between low-energy barrier species (any forms with similar energetic values are in equilibrium). Energy input in the CID process is higher that the isomerisation energy therefore the rearrangement processes, resulting in a formation of many product ions, intermediate tautomeric or transition state forms, are common.[66] The Boltzmann population distribution can express the equilibriums of these forms.[93,138,159] However, the ion activation and dissociation process using an IR laser results in a non-Boltzmann population distribution.[72] IRMPD, which activates ions quicker than CID and does not need a collisional gas, was a different ion activation method used in these studies, which may become fundamental to understand fragmentation behaviour between different MS/MS data. The dissociation of gas-phase ions depends initially on the ion activation stage and dissociation reactions, Reaction 3.2, which, from a kinetic point, is a pressure-dependent process.[72]

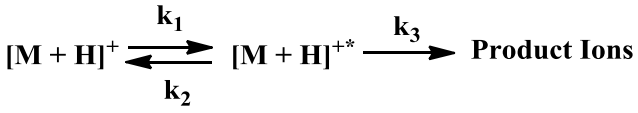

Reaction 3.2

$[M + H]^{+}$* – activated protonated molecule

The change between a protonated molecule $[M + H]^{+}$ and an activated protonated molecule, $[M + H]^{+*}$ is quick thus, the reaction rates, k_1 (activation) and k_2 (de-activation) must characterise with low-energy barriers. The fragmentation process represented by a reaction rate k_3 is believed to be much slower and less probable than the activation/de-activation process.[72] The product ions are formed when the pressure decreases, however is does not mean that the reaction rate k_3 becomes quicker, but that the activation/de-activation processes become slower (in lower pressure less de-activation processes occur). The activated molecule must possess energy that is at least equal to an activation energy barrier in order to dissociate. Thus, it is more probable that the ion will decompose if it possesses higher amount of the energy.[72]

Reaction 3.3 presents a typical fragmentation reaction that can be described with a kinetic rate constant k_3 (further called k_P). Often however, more than one product ion is formed from a precursor ion. Here, for simplicity of description and to understand the dissociation behaviour, only one additional product ion is added. Reaction 3.4 presents a formation of Product 2 with a kinetic rate constant k_{P2}.

Reaction 3.3 $[M + H]^{+} \xrightarrow{k_{P1}} P_1^{+} + Loss$

Reaction 3.4 $[M + H]^{+} \xrightarrow{k_{P2}} P_2^{+} + Loss$

The formation of product ions become competitive and depends on: i) their kinetic rate constants, k_{P1} and k_{P2}, ii) the time allowed for the reaction to occur, and iii) the initial amount of a protonated molecule. In a fixed moment of time, the amount of protonated molecule is described by its initial amount and the rate constants of the product ions, Equation 3.4.[162]

Equation 3.4

$$\frac{-d\{[M+H]^+\}}{dt} = \left(k_{P_1} + k_{P_2}\right)\{[M+H]^+\}$$

In a case when all of the protonated molecules are fragmented to form product ions, the products rate constants dictate the decomposition process, Equation 3.5. The ratio of Product 1 and Product 2 is defined by reaction equilibrium constant and products kinetic rate constants.

Equation 3.5

$$\frac{[P_1^+]}{[P_2^+]} = K\left(\frac{k_{P_1}}{k_{P_2}}\right)$$

The Curtin-Hammett principle (CHP) also describes the competitive reactions when more than one product is formed and it states that the activation energy barrier affects the favourability of product formation.[163] The Curtin-Hammett principle is one of the most important mechanistic chemistry theories.[130] The CHP cannot predict the reaction, but if presented with hypothetical reaction pathways, it can indicate which one is more favoured. It is commonly used in synthetic reactions but it is also applicable to gas-phase ion reactions.[130] Thus, the Curtin-Hammett principle is used to explain the formation of two product ions formed from a protonated molecule presented in Reaction 3.3 and Reaction 3.4. The product energies and their intermediates (for example tautomeric or transition state forms) are represented on the potential energy diagram, which is used to determine the minimum energy pathways of ions and decomposition reactions when competitive reactions occur, Figure 3.2.

The energy diagram shows the energy of ions and their energetical barriers. Figure 3.2 presents a formation of two products, P1 and P2, formed through their intermediates, I1 and I2. The intermediates can be in equilibrium, because the difference in their energy barriers is small, although it is noted that I2 is more stable than I1. The energy difference between P1 and P2 is bigger that between I1 and I2 thus they cannot be in equilibrium and their formation is competitive; yet P1 is more stable than P2. The less stable I1 results in the formation of P1 through a lower transition-state-energy barrier (activation-energy barrier) than the

transition state of a P2 reaction pathway. According to the Curtin-Hammett principle, energy barriers distinguish the favourability of product formation. Thus, the favoured product is P1, which comes from the I1 characterised with the lower energy barrier height despite its lower stability.[163]

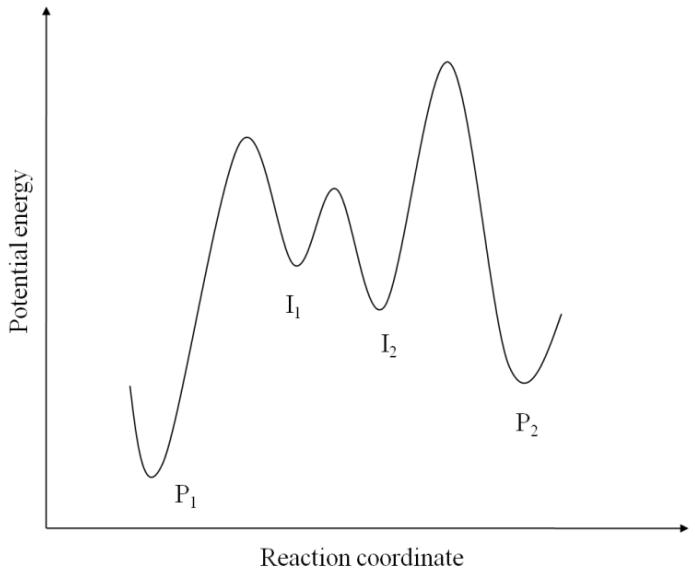

Figure 3.2 Schematic diagram representing the Curtin-Hammett principle redrawn with a kind permission of ACS;[130] product ratio is determined by the heights of the energy barriers and not stability of the intermediates.

The energy barriers of two products are often represented as the difference in a change of energies (if ΔG is calculated for each, then $\Delta\Delta G$ represents the difference between these energy barriers). As explained above, the free Gibbs energy of gas-phase ions depends mostly upon the change of enthalpies, thus a favoured product ion can be indicated by comparing the enthalpies of discussed species, *i.e.* $\Delta\Delta H$. The calculations of heat of protonation can therefore indicate which form of protonated species is more favourable. Changes of heat of formation energies are related to proton affinities, *i.e.* $PA = -\Delta H$,[93] *i.e.* in agreement with the Curtin-Hammett principle. Thus, the comparison of proton affinity values can indicate the forms of the most favoured molecule.[130]

3.3 The calculation model used for this project

According to the characteristics of computational methods and available time, hardware resources, and type of structures, a two-step process was chosen for calculations in this project. The first part indicates the most stable conformer with the second part focusing on the most favourable forms of protonated molecules and product ions.

Hehre stated that the most probable molecule conformer in a ground state is one represented with least geometrical tension.[145] Thus, geometry optimisation studies for different structure types were calculated using MMFF. They are quick, reliable calculations for geometry optimisation. The most stable conformer was chosen for more advanced calculations, which could help distinguish the reaction mechanisms in a mass spectrometer. Different kinetic features and thermodynamic properties describe the decomposition reactions. Unfortunately, the kinetic approach of understanding reactions is influenced by changes of temperature and pressure, which are difficult to measure in the centre of the collisional cell.

All computational methods calculate the energy of the molecule however, the choice of the method must be based on specifics of the molecular structure and the desired result. Here, the aim is to find a model with a balance between an acceptable computational cost and accuracy for the calculation of thermodynamical properties of the chosen molecules. The DFT method using B3LYP, the main hybrid model used in chemical applications,[95,138] was chosen to investigate thermochemical properties of the analysed compounds. It can also calculate the energies of even and odd-electron species. The accuracy levels are expected to be up to 3 kcal/mol depending on the basis set used. The accuracy of calculated heats of formation using B3LYP is comparable to many more complex and expensive, in computational cost, functionals,[164] *e.g.* TPSSh; (atomic and molecular proton affinities (PA) correspond to around 1.5 kcal/mol).[165] The accuracy increases with an increase of basis set until a plateau response where

a larger basis set does not increase the accuracy but still requires more computer power and time for calculations.[141] Thus, different basis sets were compared and the structural energetics were calculated using commercially available software called Spartan.[148] The choice of the software was based on the ease of usage and level of training required to use it.

In this project, DFT is used as an application tool for the computational prediction of molecule properties. Theoretical approaches are based on the structure of the molecule. The knowledge of how atoms are connected and what is the lowest energetic tension and geometry, are important for a correct structural optimisation and planned calculations.[141] However, a comparison of theoretical and experimental data is problematic. In a mass spectrometer, gas-phase ions are kept together, in a cloud of ions, that are in equilibrium. Their behaviour is affected by the specific properties of each method, molecule interactions, temperature, and pressure. Calculations discard the temperature and pressure dependence and are mostly performed for a single molecule.[141] Thus, the comparison of experimental and theoretical data is not straightforward. Well-constructed, optimised calculations that include many possible structure forms and different conditions improve the comparison of experimental and theoretical data.

Chapter 4 Mass spectrometry in pharmaceutical development

Mass spectrometry is one of the most important analytical methods in the pharmaceutical industry.[50,166] Figure 4.1 presents a flow-scheme of a pharmaceutical drug research pipeline,[167] which will be described in basics with the indication where mass spectrometry approaches are used.

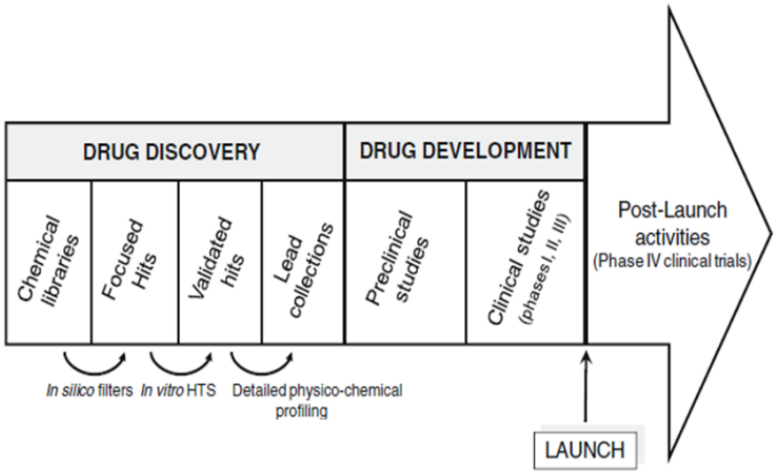

Figure 4.1 A flow scheme of a drug process[167] reprinted with a kind permission from Springer.

4.1 Principles of drug research process

The drug discovery process starts with the choice of a target disease. Finding a lead compound for a target disease is difficult and it is mostly achieved by screening databases of natural materials, existing drugs, or previously synthesised compounds.[137,168] Often, the drug discovery, design, and development processes are based on computational approaches to accelerate the drug-research flow and increase the confidence of finding the correct target compound.

In the discovery process, understanding the fundamentals of the disease-drug interactions helps a combinatorial search to find compounds that may be biologically active against the target disease, which results in the narrowed list of possible target compounds.[169] A combinatorial search process consequently helps to correctly select a possible lead compound and synthesise many of its related sub-structures.[37,137,169] LC-MS or GC-MS are the two mostly used techniques to confirm the synthesised products.[170] When structural information is required, tandem mass spectrometry experiments are used with support of the accurate mass measurements that aid to propose most probable formula of the compound.[171] The identified compounds are screened against their biological activity (*in vivo* and *in vitro* studies),[50] which improve the time of finding the positively active compound that can undergo further stages of the discovery process.[172,173] For example, it is crucial to obtain a drug with good solubility in a solvent that will be adjustable to human metabolism. Thus, an investigation of physicochemical properties (ionisation, lipophilicity, and solubility) reduces the number of candidates.[167] Absorption, Distribution, Metabolism, and Excretion, known as the ADME stage, follows the determination of physicochemical properties of the target compounds. This part of the process is often called pharmacokinetics and it involves the fast characterisation of thousands of synthesised compounds increasing the probability of the correct choice of a drug compound for the development stage.[174] It is a difficult and a time-consuming process, and hence well-established high-throughput methods are required to improve the speed of analyses. Selective and sensitive methods, such as mass spectrometry, play a pivotal role in this process.[50] Mass spectrometers coupled to separation instruments monitor the drugs, their impurities, and metabolites. Qualitative and quantitative analyses are performed using mostly QqQ and TOF mass spectrometers. Mass spectrometers with a QIT mass analyser can often be used to characterise the mechanism pathways of compounds using multiple stages of tandem mass spectrometry experiment if necessary. AMM experiments help to identify the possible formulae of drug impurities and metabolites using a TOF, a FT-ICR or an orbitrap mass spectrometer.

The QqQ, TOF, QIT, FT-ICR, and orbitrap mass spectrometers are also used in the drug development process. Drug development process involves transforming a compound from a drug candidate to a drug product approved for marketing.[175] There are two phases of the drug development process. Phase I evaluates additional information about the toxicity and pharmacokinetics of a drug, its impurities and metabolites; usually a drug synthesis is changed from mg to g scale.[168] The main objective stays the same: to achieve a very good drug disposition,[176] *i.e.* adsorption, distribution and elimination, in the human body. Phase II is a further stage of pharmacokinetics that essentially proves that the drug can actually work when produced in the kg scale. Additionally, its novel biochemistry mechanisms are proposed, as well as the long, difficult process involving the characterisation of every side impurity and metabolite. The compound must respond positively to these two phases before it can be transferred to clinical studies in the development process.[50] Mass spectrometry is used here to identify, characterise, and quantify the compounds, impurities, and metabolites. A great focus is put into metabolite identification and MS is used here to quantify and detect drugs and their metabolites in the human body.[177] The structural elucidation of drug impurities and metabolites is often difficult and consequently many methods have been proposed to develop a quick solution for the identification of small molecules.[168,176]

This project is focused on identification and evaluation of possible generic and specific rules of fragmentation behaviour for a rapid characterisation of drug impurities of protonated quinazolines. Understanding fragmentation behaviour of drug impurities helps the mass spectrometrist to propose their mechanism pathways and predict pathways for "unknown" compounds from the same class of structures. Bandu and Desaire proposed a STEP (Statistical Test of Equivalent Pathways) method for the prediction of fragmentation pathways of pharmaceutical compounds.[178] The acquisition is based on two consecutive, product ion spectra using high and low-energy ion activation methods. The statistical STEP analysis is used to distinguish first and second generation product ions by calculating the ratio of product ion peak area. If the STEP ratio is below or equal to one then the

product ion is defined as the first generation product ion; if the ratio is greater than one then the product ion is determined as the second generation product ion (Figure 6.5, page 101). The STEP process helps to speed up the characterisation of the fragmentation mechanisms of gas-phase ions by saving 50 % of experiment time.[178]

It needs to be noted that the compounds have to be formulated before the use, which means that a drug is combined into tablets, injections, or capsules with other substances.[179] The most crucial characteristics of this process are the physicochemical properties of the drug candidate. They are therefore determined right at the beginning of the drug discovery process. This phase of drug development is expensive and time-consuming mostly because many drugs fail safety regulations (none of the drugs are completely non-toxic and safe)[180] and hence are discarded from the drug research process.[50] Therefore, every new drug candidate is treated as dangerous, to ensure that it meets strict regulatory rights and safety issues during every stage of drug research. To limit the risks and drug withdrawal from the market, complex testing is essential. A successful drug is transferred to clinical trial steps, which are a legal requirement before the drug is sold.[180] The clinical trials involve four phases. Phase I is focused on a safety evaluation with a small number of healthy volunteers and phase II involves studies on a larger group of healthy volunteers whilst the dosage level of the drug is defined. If phase II is positive, it is followed by phase III of clinical studies, where a group of patients with the disease is treated and a final decision to move the drug to a registration point is taken.[175,181] Phase IV is focused on post-marketing safety monitoring. Here, mass spectrometry together with other analytical techniques is involved in monitoring and quality control studies. Additionally, mass spectrometry is an essential technique to investigate and control counterfeits of drugs already available in the market using quantitative and qualitative studies.

4.2 Quinazolines – impurities of Cediranib, Vandetanib, and Gefitinib

An impurity is "any component of the new drug product that is not the drug substance or an excipient in the drug product".[182] Impurities are characteristic of the synthetic route of a drug; different synthetic routes may form different impurities. Many variable synthesis factors affect the formation of an impurity, including incomplete reactions, over-reactions, side-reactions influenced by a solvent or impurities from a starting material.[183] Three groups of impurities are recognised including, organic, inorganic, and residual solvents impurities. Organic impurities relate to a drug substance, its synthetic pathway, starting materials, and intermediates. Inorganic impurities include reagents such as heavy metals, catalysts, and salts that are used in the synthesis process. Residual solvents are the remaining amounts of a liquid used in the synthesis of a drug substance.[184] Most safety regulations require less than 1-2 % of total organic impurities in a drug substance[184] therefore, the synthesis reactions of drugs are developed with an attention to reduce the amount of impurities.[184] All drug impurities above 0.05 % of high-dosage daily drugs must be defined by toxicity levels. These levels are one of the factors involved in safety drug therapy and are determined using techniques that can be rapidly developed.[184] The strategies for an investigation of drug impurities may differ between companies, but they all involve the use of separation techniques, MS, and NMR spectroscopy.[183] Mass spectrometry is often used because of its high specificity and sensitivity abilities, which are crucial for determination of impurities levels.[183]

This project is focused on the analyses of synthetic impurities of the anti-cancer drugs, AZD2171 (Cediranib, Recentin), Scheme 4.2, and The Food and Drug Administration (FDA) approved and market available drugs: AZD6474 (Vandetanib, Zactima), Scheme 4.3, and AZD1839 (Gefitinib, Iressa), Scheme 4.4, from AstraZeneca. The International Union of Pure and Applied Chemistry (IUPAC) recognises the nomenclature of quinazoline sub-structures, which the numbering system starts from the first nitrogen atom in the quinazoline ring, Scheme 4.1.[185]

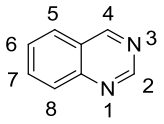

Scheme 4.1 Schematic description of the numeric system for the nomenclature of the quinazoline sub-structures.[185]

Cediranib is an inhibitor of kinase tyrosine enzyme that is crucial in angiogenesis, which is the formation of new blood vessels in tumours bigger than 1 mm. Recentin plays an important role in cancer biology, because an inhibition of kinase tyrosine enzyme in tumours may inhibit formation of the tumour blood vessels, and hence its growth. Thus, Cediranib was selected for chemotherapies of various cancer types[186] and it was specifically active in patients with glioblastomas (brain tumours)[187] and colorectal cancer.[188] Unfortunately, Recentin did not aid improvement in the survival of patients and the drug is now withdrawn from Phase III of clinical trials; its biological activity is now being examined against different types of cancer.[188]

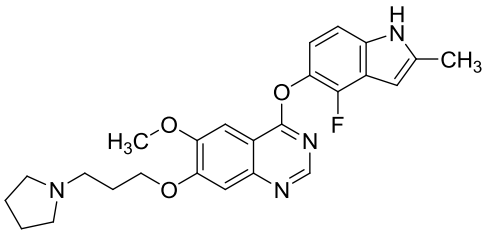

Scheme 4.2 A structure of AZD2171 Cediranib, 4-(4-fluoro-2-methyl-1H-indol-5-yloxy)-6-methoxy-7-[3-(1-pyrrolidinyl)propoxy]quinazoline, $C_{25}H_{27}FN_4O_3$, MW_{mono} = 450.20672.

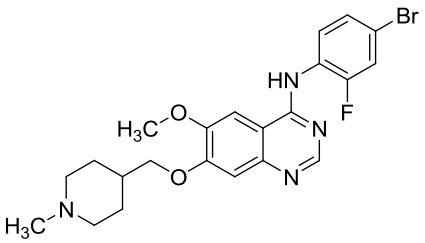

Scheme 4.3 A structure of AZD6474 Vandetanib, N-(4-bromo-2-fluorophenyl)-6-methoxy-7-(1-methylpiperidin-4-ylmethoxy)quinazoline-4-amine, $C_{22}H_{24}BrFN_4O_2$, MW_{mono} = 474.10667.

Vandetanib also inhibits the tyrosine kinase enzyme[189] and it was found that it inhibits the tumour angiogenesis of many solid type tumours except breast cancer cells.[190] The Food and Drug Administration approved Zactima as an oral, once a day drug to treat a thyroid cancer that cannot be removed by surgery or when it has already spread to other parts of the body.[191]

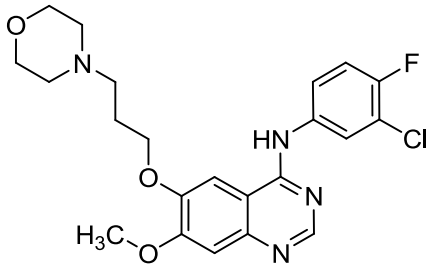

Scheme 4.4 A structure of AZD1839 Gefitinib, N-(3-chloro-2-fluorophenyl)-7-methoxy-6-(3-morpholin-4-ylpropoxy)quinazoline-4-amine, $C_{22}H_{24}ClFN_4O_3$, MW_{mono} = 446.15210.

Gefitinib, marketed as Iressa also reduces cancer cells growth by an inhibition of tyrosine kinase enzyme similarly to the two previously described drugs. FDA approved the drug as an oral tablet to treat "non-small cell lung cancer that has not responded to traditional treatment".[192,193] Lung cancer is the most typical cause of cancer death all over the world.[194]

Chapter 5 Experimental design

5.1 Mass spectrometry experiments

5.1.1 Materials

Often mass spectral data are classified according to the type of analysed compounds (pharmaceuticals, peptides, or sugars, *etc.*) or the functional groups in the molecule.[82] In this project, compounds are classified according to their lead compound project presented in Chapter 4.2, page 75 (Appendix 1, page 165).

Analyses using a Finnigan LCQ, LC/MS XCT Trap, and Apex III mass spectrometers were performed by direct infusion, for Finnigan FT LTQ a sample solution was injected *via* the HPLC column, and the remaining mass spectrometric analyses were based on a loop injection. Stock solutions at 1 mg mL^{-1} were prepared in MeOH (Table 5.1) for all experiments and stored in the fridge. Daily working solutions of 1 μg mL^{-1} were prepared for direct infusion. The sample concentrations for a loop injection and HPLC analysis were varied; Apex III – from 0.2 to 1 μg mL^{-1}, MicrOTOF-Q and 6410 Triple Quad LC/MS – 10 μg mL^{-1}, and Finnigan FT LTQ – 100 μg mL^{-1}. All sample solutions, except those prepared for Apex III, Finnigan FT LTQ, and APPI-QIT MS experiments, were spiked with a formic acid (MeOH: HCOOH, 99.9: 0.1 %, v/v). Hydrogen/deuterium exchange (HDX) experiments were performed using an LCQ Finnigan ESI-QIT mass spectrometer by preparing solutions of 1 μg mL^{-1} in deuterated methanol and spiking them with the fully deuterated formic acid, Table 5.1. The product ion mass spectra were acquired immediately after a control to show that all labile hydrogen atoms of the protonated molecule are exchanged to deuterium atoms.

Table 5.1 Information about solvents used for mass spectrometric analyses.

Mass spectrometer	Solvent
LCQ Finnigan ESI-QIT MS (Thermo Scientific)	• MeOH, HPLC grade from Fisher Scientific Ltd., Loughborough, UK • MeOD-4, >99.5 % from Apollo Scientific Ltd., Stockport, UK • Formic acid, Analytical reagent grade from Fisher Scientific Ltd., Loughborough, UK • Formic acid-D2, >99.0 % from Apollo Scientific Ltd., Stockport, UK
LC/MS XCT Trap API-QIT MS (Agilent Technologies)	• MeOH, HPLC grade from Fisher Scientific Ltd., Loughborough, UK • Acetone (APPI dopant), HPLC grade from Fisher Scientific Ltd, Loughborough, UK
Apex III ESI-FT-ICR MS (Bruker Daltonics)	• MeOH, HPLC grade from Fisher Scientific Ltd., Loughborough, UK
Finnigan FT LTQ ESI-LIT FT-ICR MS (Thermo Scientific)	• Methanol, HPLC grade from Fisher Scientific Ltd., Loughborough, UK • ACN, E Chromasolv for HPLC, for UV from Sigma Aldrich, Steinheim, Germany • Formic acid, Analytical reagent grade from Fisher Scientific Ltd., Loughborough, UK • Water, HPLC grade from Sigma-Aldrich Chromasolv., St. Louis, USA
MicrOTOF-Q ESI-QTOF MS (Bruker Daltonics)	• Methanol, HPLC grade from Fisher Scientific Ltd., Loughborough, UK • 0.25 mM HCOOH, Solution for HPLC from Fisher Scientific, Loughborough Ltd., UK
6410 Triple Quad LC/MS ESI-QqQ MS (Agilent Technologies)	• MeOH, LCMS Chromasolv. from Fluka Analytical, Sigma-Aldrich, Steinheim, Germany • 0.25 mM HCOOH, Solution for HPLC from Fisher Scientific, Loughborough Ltd., UK

The calibrants for accurate mass measurement experiments performed using Apex III and MicrOTOF-Q mass spectrometers included erythromycin (>95 %), gramicidinS hydrochloride from *Bacillus hrevis*, josamycin, piperazine

dihydrochloride hydrate, 4-dimethylaminopyridine, terfenadine, diphenhydramine hydrochloride, oxybutynin chloride and reserpine, which were all purchased from Sigma Aldrich Company Ltd, USA and used without further purification.

The linear calibration of Finnigan FT LTQ mass spectrometer was performed using MSCAL5 ProteoMass LTQ/FT-hybrid ESI Pos. calibration mixture purchased also from Sigma Aldrich Company Ltd, USA.

5.1.2 Methods

The product ion mass spectra of drug impurities and process related intermediates were acquired using different mass spectrometers, which allowed a cross-platform comparison of data. The product ion mass spectrum was acquired when the abundance of the precursor ion was diminished to a minimum (less than 3 %). Two mass spectra types were acquired for each sample, including: i) the *m/z* isolation window to 1 *m/z* unit to allow a fragmentation of the mono-isotopic ion only and ii) the isolation of 4, 6, 8, or 10 *m/z* units to obtain a mass spectrum with a full isotopic pattern distribution. The isolation width (IW) of 1 *m/z* unit ensures that the precursor ion is isolated from possible interference ions and it simplifies the assignments of the mass shifts when performing HDX experiments. The wider *m/z* units window is used for observation of a full isotope pattern of the ions.

5.1.2.1 ESI-QIT MS (Thermo Scientific)

MeOH and MeOD sample solutions were directly infused at a constant flow of 3 μL $min.^{-1}$. Nitrogen was used as sheath and auxiliary gas, and helium as collision gas. The source conditions were as follows: sheath gas 30 arbitrary units, auxiliary gas 1 arbitrary unit, spray voltage 3.7 kV, capillary temperature 200 °C, capillary voltage 31 V and tube lens offset 5 V. Normalised collision energy (NCE) was optimised for each analyte and was varied from 20 % to 60 % to allow a full dissociation of the precursor ion. Additionally, the spectra were acquired

using WideBand activation on or off. The averaged product ion spectrum was composed of 20 scans and it was interpreted using Xcalibur™ software, version 1.2.

The D-labelling experiments were performed using the analogous procedure.

5.1.2.2 API-QIT MS (Agilent Technologies)

The comparison of product ion spectra using different ionisation techniques, *i.e.* ESI, APCI, and APPI, was undertaken to understand whether the ion source influences the fragmentation behaviour of protonated quinazolines. Samples solutions were directly infused into the mass spectrometer at the flow of 16 µL $min.^{-1}$.

The product ion spectra were acquired with the precursor ion abundance adjusted to minimum value by varying the fragmentation amplitude (analogous value to NCE of Thermo Scientific) and different *m/z* units isolation widths. All data were evaluated using Data Analysis™ for LC/MSD Trap v.3.3 from Bruker Daltonics Inc., Bremen, Germany.

5.1.2.2.1 ESI-QIT MS

The source conditions were as follow: capillary -4500 V, end plate offset -500 V, nebuliser 50 psi, dry gas flow 7 L $min.^{-1}$, drying gas temperature 350 °C, skimmer 40 V, and capillary exit 158 V.

5.1.2.2.2 APPI-QIT MS

The APPI-QIT MS experiments involved spiking analyte samples with acetone (MeOH: acetone, 95: 5 %, v/v; Table 5.1) to enhance the formation of protonated

molecules. The source conditions were as follow: capillary -4200 V, end plate offset -500 V, nebuliser 60 psi, flow of dry gas 5 L $min.^{-1}$, drying gas temperature 350 °C, vaporiser temperature 400 °C, skimmer 20 V, and capillary exit 110 V.

The UV lamp operations were controlled by APPI Hyper Terminal v. 5.1 software from Bruker Daltonics Inc., Bremen, Germany.

5.1.2.2.3 APCI-QIT MS

The APCI source conditions were as follows: high-voltage capillary -4200 V, corona current 4000 μA, endplate offset -500 V, nebuliser 40 psi, dry gas flow 3 L $min.^{-1}$, drying gas temperature 250 °C, vaporiser temperature 250 °C, lens 2 -60 V, and capillary exit 110 V.

5.1.2.3 ESI-FT-ICR MS

Two FT-ICR mass spectrometers were used in these studies, *i.e.* an Apex III with SORI/CID ion activation method, and a Finnigan FT LTQ with IRMPD. The comparison of these ion activation techniques may help understand specific differences in mechanism pathways of protonated quinazolines.

5.1.2.3.1 Apex III

The accurate mass measurements were performed using Apex III FT-ICR mass spectrometer with a 4.7 Tesla actively shielded magnet (Bruker Daltonics Inc., Bremen, Germany) with the API 1600 control unit. The external Apollo ESI ion source was used and sample solutions were directly infused at the constant solvent flow of 3 μL $min.^{-1}$ using a syringe pump.

Two calibration mixtures for the acquisition of a full mass spectrum were prepared, one covering the low molecular weight (LMW) and the other for high molecular weight (HMW) mass range. The *m/z* units value in brackets represents the ion observed in a mass spectrum. The LMW calibration mixtures contains: diphenhydramine (*m/z* 167.0855, 256.1696), oxybutynin (*m/z* 358.2377), and terfenadine (*m/z* 472.3210). The HMW calibration mixture consisted of terfenadine (*m/z* 472.3210), doubly charged gramicidinS (*m/z* 571.3603), erythromycin (*m/z* 734.4685), and josamycin (*m/z* 828.4740). The accurate mass measurements MS/MS experiments were calibrated using a quadratic calibration curve for the product ions of reserpine (*m/z* 609.2807). The first generation product ion mass spectrum can contain the following ions: $C_{32}H_{37}N_2O_8^+$ (*m/z* 577.25444), $C_{23}H_{30}NO_8^+$ (*m/z* 448.19659), $C_{22}H_{30}NO_8^+$ (*m/z* 436.19659), $C_{22}H_{25}N_2O_3^+$ (*m/z* 356.18597), $C_{13}H_{18}NO_3^+$ (*m/z* 236.12812), $C_{10}H_{11}O_4^+$ (*m/z* 195.06519), $C_{11}H_{12}NO^+$ (*m/z* 174.09314), $C_9H_{11}O_3^+$ (*m/z* 167.07027), and $C_8H_{11}O_2$ (*m/z* 139.07536).

The mass range of experiments was set between 65 and 650 *m/z* units (80 to 2000 *m/z* units for analytes with a higher molecular weight than 649 g mol^{-1}) and data were acquired with a 512k FID (free induction decay) size. Nitrogen was used as a drying gas and argon as a collision gas. Source parameters for a positive ion ESI MS/MS were as follows: capillary -4.5 kV, spray shield -3.8 kV, capillary exit 80V, drying gas temperature 250 ºC, skimmer 1 12 V, and skimmer 2 6 V. ICR cell parameters were PV1 1.25 V, PV2 1.20 V and excite plate PL3 6 V. The values of corr sweep (PL4) and ion activation (PL8) attenuations, which are responsible for the isolation of selected *m/z* units and its fragmentation, were varied for each MS/MS experiments to ensure peak isolation from possible interfering ions and sufficient energy applied for the fragmentation of the isolated ion. The first generation product ion mass spectra were acquired when the peak corresponding to the protonated molecule was fully fragmented. The ESI FT-ICR MS/MS spectra were acquired using Xmass 7.0.8 and were evaluated using Data Analysis™ 3.4 software from Bruker Daltonics Inc., Bremen, Germany.

5.1.2.3.2 Finnigan FT LTQ

The Finnigan FT LTQ mass spectrometer was coupled to LC system thus, the samples were analysed using LC-MS.

The 1100 Agilent liquid chromatograph consisted of a quaternary pump, diode array detector, 1100 autosampler, and Hypersil Gold column (C18 95 µm, 50 x 2.1 mm) from Thermo Fisher Scientific. The solvent A was a 0.05 % aqueous solution of formic acid and solvent B was acetonitrile (Table 5.1) with a gradient elution starting from 5 % A in 0 min. to 90 % in 9.5 min. and 0 % in 10 min. at a flow rate 1 mL $min.^{-1}$. The autosampler was used to inject 5 µL of sample solutions.

The Finnigan FT LTQ FT-ICR mass spectrometer with a 7 Tesla actively shielded magnet was used to perform the IRMPD experiments. The mass spectrometer was linearly calibrated to the MSCAL5 calibration mixture (details in chapter 5.1.1, page 79). The ion source conditions were as follow: spray voltage 4 kV, capillary voltage 44 V, tube lens 120 V, capillary temperature 275 ºC, sheath gas (N_2) flow rate 60 arbitrary units, auxiliary gas (N_2) flow rate 3 arbitrary units, and sweep gas (N_2) flow rate 6 arbitrary units. The LIT ion optics conditions include multipole 00 offset -3 V, lens 0 voltage -4 V, multipole 0 offset -5.75, Lens 1 voltage -10 V, gate lens voltage -66 V, multipole 1 offset -6.5 V, multipole RF amplitude 400 Vpp, and front lens -6.5 V. The FT ion optics conditions were as follow: FT multipole 1 offset -25 V, FT intermultipole lens -55 V, FT multipole 2 offset -43 V, FT intermultipole lens 2 -85 V, FT multipole 3 offset -56 V, FT multipole 1 amplitude 408, and FT multipole 2 and 3 amplitude 500.

From all available drug impurities, only 18 were chosen for IRMPD experiments, including: 1839013, 2171003, 2171005, 2171006, 2171007, 2171008, 2171017, 2171023, 6474008, 6474011, 6474012, 6474013, 6474014, 6474015, 6474024, 6474032, 6474034, and 8931006, Appendix 1, page 165.

The IRMPD experiments were performed using the CO_2 fan-cooled laser Synrad Firestar v-series (Chapter 1.3.3, page 32). The protonated molecules of the analytes were exposed with 60, 70 and 80 % of a laser power (100 % flashes energy of photons of 5 kHz) with a 50 msec. of the irradiation time. Compounds 2171008, 6474011, 6474012, 6474013, 6474014, 6474024, 6474032, and 6474034 were additionally analysed using an increased value of the laser power (80, 90, and 100 %) and the time of irradiation of 150 msec. that allowed a sufficient fragmentation of protonated molecules and the observation of the product ion mass spectra.

5.1.2.4 ESI-QTOF MS

The accurate mass measurement analyses were also performed using micrOTOF-Q mass spectrometer. The positive ion electrospray mass spectra were acquired using the internal enhanced quadratic calibration curve containing: piperazine (*m/z* 87.0917), 4-dimethylaminopyridine (*m/z* 123.0917), diphenhydramine (*m/z* 256.1696, 167.0855), oxybutynin (*m/z* 358.2377), terfenadine (*m/z* 472.3210), reserpine (*m/z* 609.2807) and erythromycin (*m/z* 734.4685).

The samples were injected by loop injection of 5 µL at a flow rate of 2 mL $min.^{-1}$ of 96 % MeOH and 4 % of 25 mM HCOOH, Table 5.1. The ion source conditions were following: end plate offset -500 V, capillary -4500 V, and drying gas temperature 200 °C. Transfer conditions: funnel RF1 150 V_{pp}, funnel RF2 100 V_{pp}, ISCID (in-source CID) energy 10 eV, and a hexapole RF 60 V_{pp}. All mass spectral data were acquired using varied values of the ion activation energy between 10 and 48 eV. The variation of collision energies values allows the observation of the fragmentation stages during the in-space CID experiments of analysed compounds, observation of more favoured product ions, and acquisition of mass spectra with a full decomposition of the precursor ion. Data can be compared with the in-space CID data acquired using ESI-QqQ mass spectrometer. All ESI-QTOF MS data were evaluated using Data Analysis™ v. 4.0 SP1 software from Bruker Daltonics Inc., Bremen, Germany.

5.1.2.5 ESI-QqQ MS

The sample solutions were introduced into the Agilent 6410 Triple Quad LC/MS *via* the loop injection of 3 µL. The isocratic flow at 1 mL $min.^{-1}$ of 60 % of MeOH and 40 % of 0.1 % aqueous solution of HCOOH was delivered using an Agilent G1312B binary HPLC pump. The profile MS data were acquired for 20 msec. scanning the mass range from 50 to 600 *m/z* units using varying collision energy values (from 5 to 40 V). The ion optic conditions were as follow: fragmentor 60 V, skimmer 15 V, octapole 600 V, octapole DC 5 V. The quadrupole 1 conditions included DC 3 V and a positive filter DC 2 V. Collision cell conditions were following: cell RF 400 V, cell DC 0 V, cell enhance 1 V, cell exit -8 V. The quadrupole 3 MS2 DC was -12 V, and pre-filter DC2 -44 V. Data were evaluated using MassHunter Workstation Software Qualitative analysis v. B.02.00 from Agilent Technologies, Inc., Palo Alto, USA.

5.2 Computational methods

5.2.1 Mass Frontier™ 6.0

Product ions of first generation product ion mass spectra of three positional isomers, *i.e.* 2171003, 2171005, and 2171006, were compared to predicted product ions using Mass Frontier™ 6.0.

A maximum of six-step dissociation reaction of protonated molecules was used to limit the product ions generated by Mass Frontier™. The Mass Frontier data can be compared to experimental mass spectral data acquired using different types of mass spectrometers.

5.2.2 Spartan ’02, ’08, and ’10

Three versions of Spartan software were used during the studies. Compounds 2171003, 2171005, 2171006, 6471011, 6474012, 6474013, 6474014, and 6474015 were studied, (Appendix 1, page 165). The compound 2171003 was chosen as a model structure for the validation of the simulation model.

A two-step simulation process was chosen, (Chapter 3.3, page 69), for calculations of the geometry conformers and the internal energies of species with varied sites of protonation. The first part evaluates possible conformers and indicates the most stable molecule’s geometry using MMFF calculations. The second part focuses on the most favourable forms of protonated molecules and product ions by calculations of energies of protonation for different tautomeric species with a varied position of the proton. Single point energies were calculated using B3LYP/6-31G* for CHNO-atom-containing structures (for most molecules in Spartan’02) and cc-pVTZ (using Spartan’10) for halogen-containing molecules.[195] The halogen-substituted compounds demand a more advanced functionals and basis set to ensure the high-accuracy of calculations and hence the protonation energies of 6474011 were calculated using B3LYP/cc-pVTZ starting from the lowest, chosen geometry conformer. The calculations start from the AM1 geometry for most molecules except 6474011, 6474012, 6474013, and 6474014 compounds that were set to start from a lowest MMFF conformer. The Spartan’10 version and upgraded computer allowed to perform computationally more demanding calculations (B3LYP/cc-pVTZ//MMFF) than using Spratan’02 installed on old PC (B3LYP/6-31G*//AM1). Spartan’08 was used to calculate the geometries and protonation energies of compounds from 2171013 to 2171023 analogously to the model B3LYP/6-31G*//AM1 model using in Spartan’02.

Chapter 6 Typical fragmentation mechanisms of protonated quinazolines substituted with non-aromatic functional groups

Quinazolines, also known as benzypyrimidines, have previously been extensively investigated using EI-MS.[86] The characteristic fragmentation of quinazoline ions forms a product ion due to the loss of HCN, which opens the quinazoline ring and is followed by a loss of H$^{\bullet}$ and CO, or HCN and CO, Scheme 6.1. Porter confirmed the successive loss of HCN in quinazoline ion structures that favours a CO loss in the quinazolinones (with a carbonyl group at position 4 of the ring), Scheme 6.2.[196]

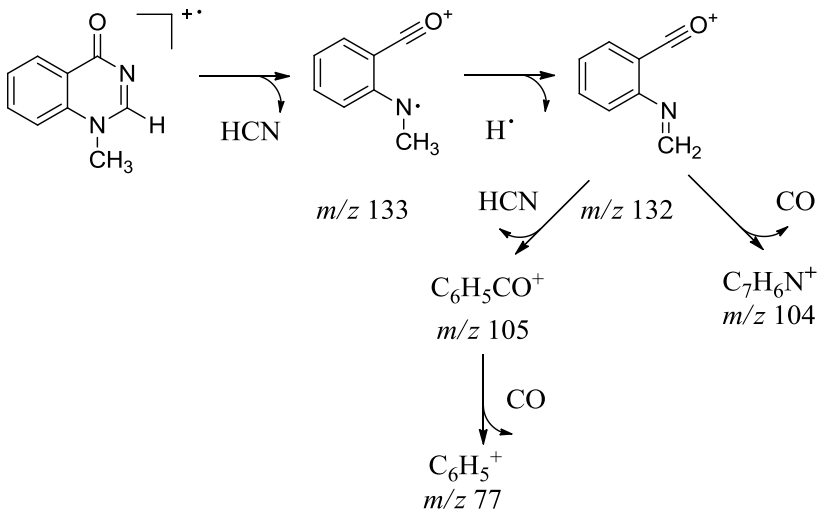

Scheme 6.1 Characteristic fragmentation pathway scheme of quinazoline compounds; page 590.[86]

Studies involving an investigation of mechanistic pathways of protonated quinazolines using soft ionisation methods have not been found in published literature. For example, the use of ESI with tandem mass spectrometry is unexpected to result in a cleavage of the aromatic ring bonds of the quinazoline ring. A soft ionisation technique such as ESI does not transfer sufficient amount

of energy to break an aromatic bond. If the structure is substituted with functional groups, the possible product ions and losses are expected to come from these functional groups.[65] Even a small structural change may affect the fragmentation pathway dramatically.[86] The product ions formed from saturated functional groups of protonated quinazolines should dominate the fragmentation pathways since the saturated bonds are weaker than aromatic bonds.

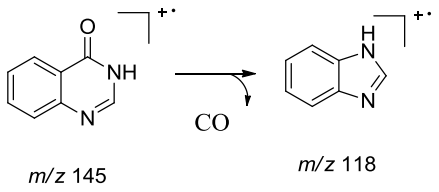

Scheme 6.2 A scheme of typical fragmentation behaviour of quinazolinone using EI-MS showing the preferred loss of a CO; page 740.[196]

It was found that 39 protonated quinazolines substituted with non-aromatic functional groups (*e.g.* piperidin- (*e.g.* 6474001), morpholin- (*e.g.* 6474010), and pyrrolidin- (*e.g.* 2171001) form product ions or losses specific for these functional groups (Appendix 1, page 165). The typical fragmentation behaviour of these compounds was observed for 35 of the 39 compounds studied. The formed product ions and/or losses from these 35 protonated quinazolines are not specific for the quinazoline ions themselves, but are specific for the specific functional group that the quinazoline sub-structures are substituted with. The representative examples of the 35 sub-structures (separated into groups and described below) show that the impurities substituted with a heterocyclic ring cannot always be distinguished from each other, but may help to identify the particular, non-aromatic functional group.

6.1 Fragmentation pathways of protonated 6-(3-morpholinpropoxy)- and 3-pyrrolidin-1-yl-propoxy-substituted quinazolines

Compounds with a 3-morpholinpropoxy- substituent at position 6 in the quinazoline ring (13 compounds studied) form only the product ion at 128 *m/z* units, Figure 6.1.

The only product ion formed in mass spectrum is called the prominent ion.[65] The protonated molecule that forms only one product ion must generally favour only one dissociation pathway.[65] McLafferty states that the formation of the prominent ion is caused by the presence of one, very labile, bond present in the precursor ion compared with the rest of the bonds in the ion and/or the prominent ion must be the most stable product ion hence most favoured to be formed.[65]

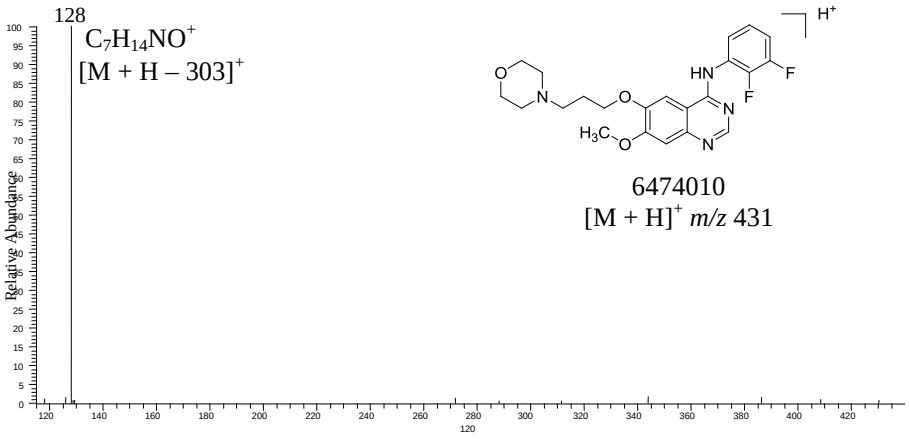

Figure 6.1 Positive ion electrospray first generation product ion mass spectrum of morpholinpropoxy-substituted quinazolines in MeOH; an example displays a mass spectrum of protonated molecule of 6474010, IW = 1 *m/z* unit.

Different substituents on the structure, such as a methoxy- group and/or halogen atoms, do not affect the fragmentation behaviour of these ions. Hence, the large, non-aromatic functional groups may have a stronger influence on the fragmentation behaviour of protonated quinazolines than methoxy- group or

halogen atoms. The morpholinpropoxy- substituent dominates the fragmentation of protonated quinazolines and it often forms the most preferable product ion, *m/z* 128. The proposed mechanism of the formation of the prominent ion indicates that the protonated molecule undergoes the inductive cleavage[78] of the C-O bond followed by the formation of a carbocation, Scheme 6.3. One of the reasons why the *m/z* 128 is the prominent ion may result from the charge stabilisation at the oxygen and nitrogen atoms in the morpholin ring (possibly *via* formation of the new ring), which is most likely the most dominant functional group in the structure, Scheme 6.3. HDX experiments may help to explain the actual dissociation pathway of *m/z* 128. If, in D-labelling experiment, the mass-to-charge of the product ion is shifted to the 129 *m/z* units value, it would indicate that a deuterium atom is involved in the formation of the base peak. If the product ion at 128 *m/z* units is formed when HDX experiment is performed, then the ion must be a carbocation that does not involve the labile hydrogen atom. The first generation product ion mass spectrum acquired in MeOD displays a formation of *m/z* 128 (Appendix 2, Figure A.2.1). Hence, all the deuterium atoms must be retained in the loss part of the molecule and the product ion does not contain any exchangeable hydrogen atoms, which supports formation of a carbocation that may stabilise the charge on oxygen and/or nitrogen atom, Scheme 6.3.

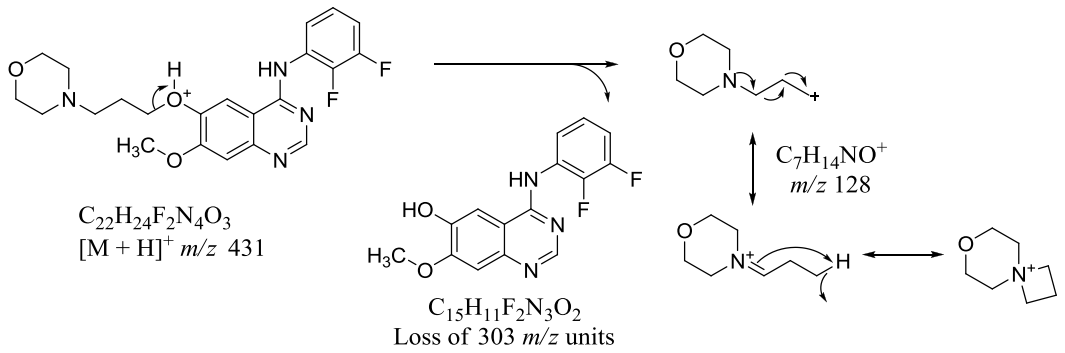

Scheme 6.3 The proposed mechanism pathway of the formation *m/z* 128 ion for compounds substituted with morpholinpropoxy- group; an example displays the fragmentation mechanism of the protonated molecule of 6474010.

The same fragmentation mechanism has been observed for 13 studied protonated quinazolines hence it may be expected that different protonated quinazolines substituted with a 3-morpholinpropoxy- functional group may also form the product ion at 128 *m/z* units *via* a charge-directed fragmentation, Scheme 6.3.

In addition, the density functional calculations have been used to compute the most thermodynamically stable forms of the compound 6474010, (detailed approach explained in Chapter 8.5, page 137). The calculations indicate five forms of the protonated molecule of 6474010, Scheme 6.4. The mechanism displayed in Scheme 6.3 represents the form of the protonated molecule of 6474010 with a charge at the oxygen atom in carbon 6 of the quinazoline ring (Scheme 6.4, a). Two forms of the protonated molecule, b) and c), in Scheme 6.4 represent tautomeric forms of the molecule with the charge placed at the oxygen in the morpholin ring. However, if these forms of the protonated 6474010 ion would exist, the exchangeable proton must be transferred to the quinazoline part of the molecule followed by the hydrogen rearrangement,[78] Scheme 6.5, which is believed to be an energetically demanding and hence unlike fragmentation mechanism of *m/z* 128 formation.

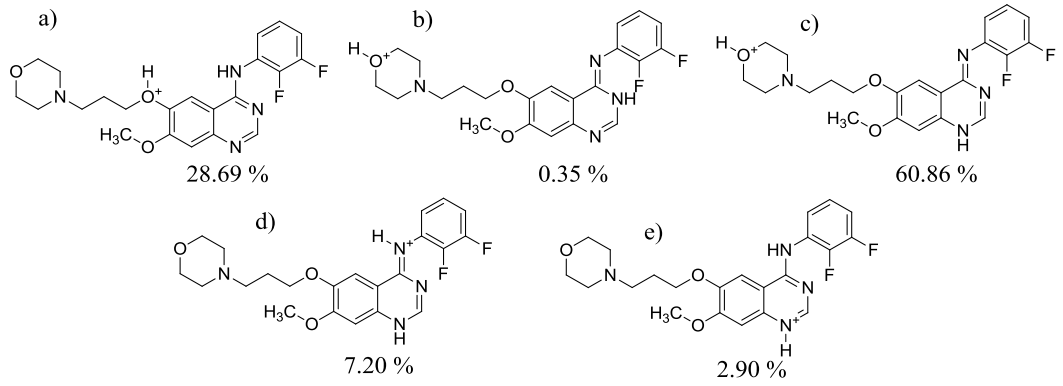

Scheme 6.4 Five forms of the protonated molecule of 6474010 indicated by DFT calculations; the percentage values are equivalent to the probability of the forms formation. (A detailed approach of the use of DFT to indicate and quantify the forms is explained in Chapter 8, page 121).

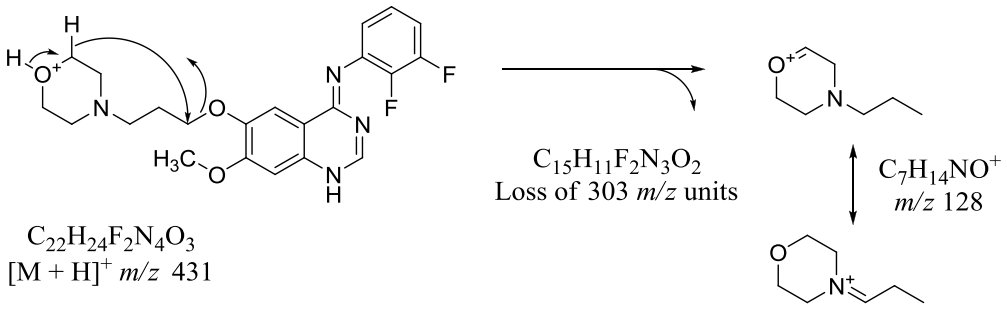

Scheme 6.5 The proposed mechanism for the formation of *m/z* 128 involving a charge migration and a hydrogen rearrangement from forms b) and c) of the protonated molecule of 6474010 displayed in Scheme 6.4.

The forms d) and e) are the species protonated on one of the nitrogen atoms in the quinazoline ring. These two forms of protonated molecule may be also involved in formation of the product ion at 128 *m/z* units, but they must involve a transfer of the charge to the oxygen atom at the 6 carbon of the quinazoline ring. This process would therefore agree with a hypothesis of a charge being mobile in the protonated molecule, which is discussed in chapter 9.2, page 150.

Similarly, a 3-pyrrolidin-1-yl-propoxy- group gives a typical mass spectrum with only one product ion formed, *i.e. m/z* 112 (six compounds studied). A first generation product ion mass spectrum of the lead compound Cediranib (2171001) is presented in Figure 6.2. The *m/z* 112 ion is most probably formed *via* inductive cleavage, similarly to the mechanism of *m/z* 128 formation displayed in Scheme 6.3. It is also believed that different (not studied) compounds substituted with a pyrrolidinpropoxy- functional group will form an ion at 112 *m/z* units.

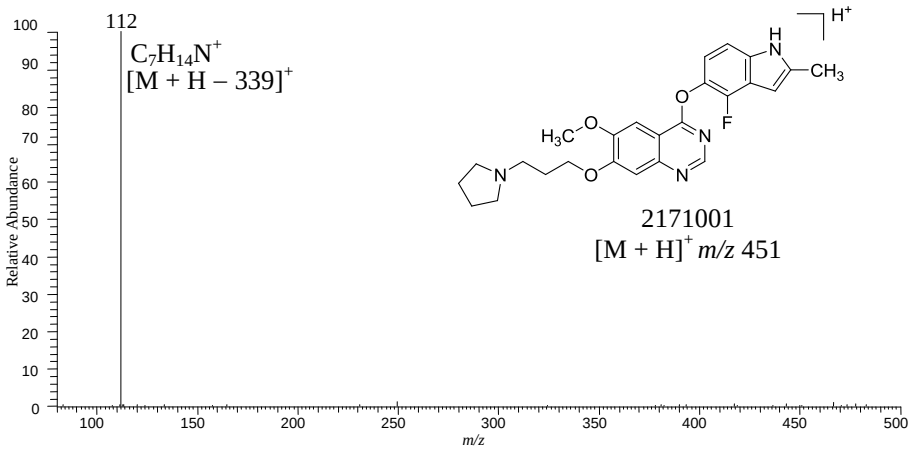

Figure 6.2 Positive ion electrospray first generation product ion mass spectrum of pyrrolidinpropoxy-substituted quinazolines in MeOH; an example displays a mass spectrum of protonated molecule of 2171001, IW = 1 *m/z* unit.

6.2 Fragmentation pathways of protonated piperidin-4-yl-methoxy-substituted quinazolines

Different fragmentation patterns have been observed in the first generation product ion mass spectra of protonated quinazolines substituted with piperidin-4-yl-methoxy- group. The differences are mostly noted between compounds substituted with methyl, *tert*-butyl, and *tert*-butoxycarbonyl groups to the piperidin-4-yl-methoxy- functional group and hence these protonated quinazolines were divided into smaller groups discussed below.

For example, four of the quinazolines substituted with a methyl-piperidinmethoxy- group (*i.e.* 6474001, 6474016, 6474017, and 6474018) result in the formation of only one product ion using ESI CID-MS/MS approaches, Scheme 6.6. The most probable mechanistic pathway involves bond cleavage *via* an inductive cleavage, following protonation on the oxygen atom at carbon 7 in the quinazoline ring, Scheme 6.6, which may result in a possible stabilisation of the charge on the nitrogen atom.

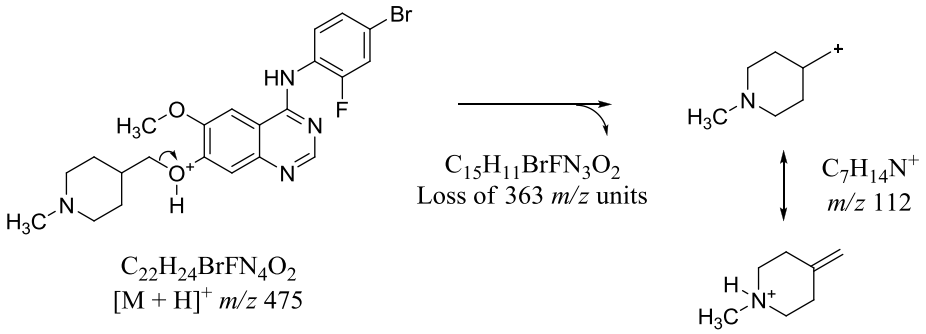

Scheme 6.6 A proposed mechanism for the formation *m/z* 112 for compounds substituted with methylpiperidinmethoxy- group; an example displays the fragmentation mechanism of the protonated molecule of 6474001.

Consequently, an unknown compound that forms a base peak at 112 *m/z* units is likely be a non-aromatic functional group with at least one heteroatom.

All protonated quinazolines substituted with *tert*-butoxycarbonyl-piperidinmethoxy- functional group (nine compounds studied, *e.g.* 6474004) form a product ion due to the elimination of the loss of 56 *m/z* units, Figure 6.3. The formation of this loss, which has been identified as C_4H_8, is most probably formed from the *tert*-butyl substituent *via* a hydrogen transfer. The loss of 56 *m/z* units does not improve a structural identification of the unknown quinazoline ion, Scheme 6.7, nevertheless, it reveals that a 4-carbon-atom alkane is most probably a part of the structure.

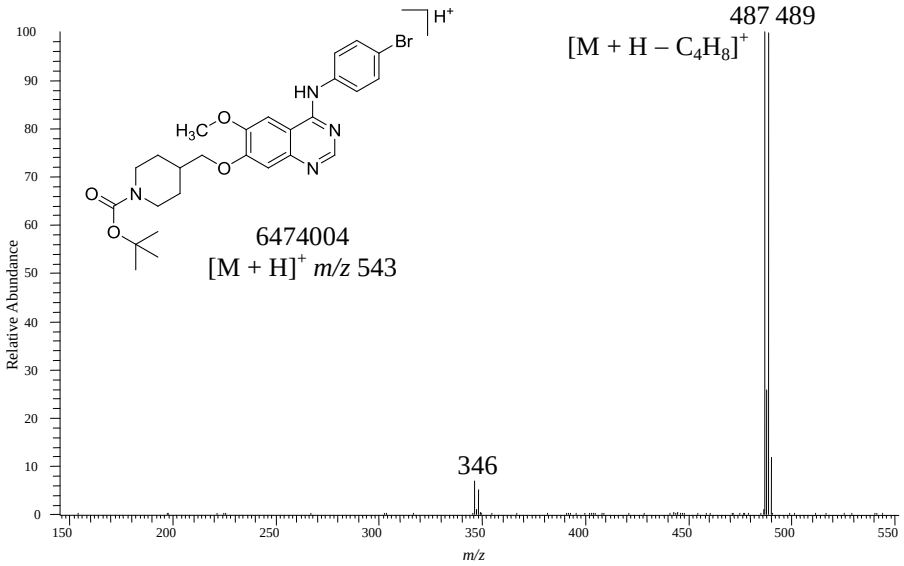

Figure 6.3 Positive ion electrospray first generation product ion mass spectrum of *tert*-butoxycarbonyl-piperidinmethoxy-substituted quinazolines in MeOH; an example displays a mass spectrum of protonated molecule of 6474004, IW = 8 *m/z* units.

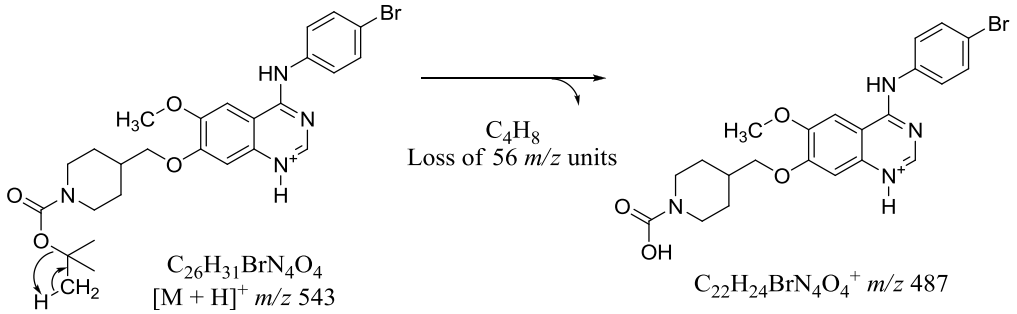

Scheme 6.7 A proposed mechanism for the formation of the product ion due to the loss of *tert*-butyl substituent of compound substituted with *tert*-butoxycarbonyl-piperidinmethoxy- functional group, an example displays the fragmentation mechanism of the protonated molecule of 6474004.

Interestingly, different fragmentation behaviour has been observed for compound 6474007. In its structure, a *tert*-butyl functional group is attached directly to a piperidinmethoxy- group (the ester group is missing), which causes a change in the formed product ions, Figure 6.4. The loss of the *tert*-butyl functional group (56 *m/z* units) is not preferred, but still formed, Figure 6.4. The favoured loss corresponds to a loss of all non-aromatic substituents followed by formation of the

ion containing the quinazoline ring, Scheme 6.8. From the previous example, Figure 6.3 and Scheme 6.7, the expected base peak would be formed due to the loss of 56 *m/z* units therefore it is unexpected that different fragmentation mechanisms are favoured in dissociation of protonated 6474007.

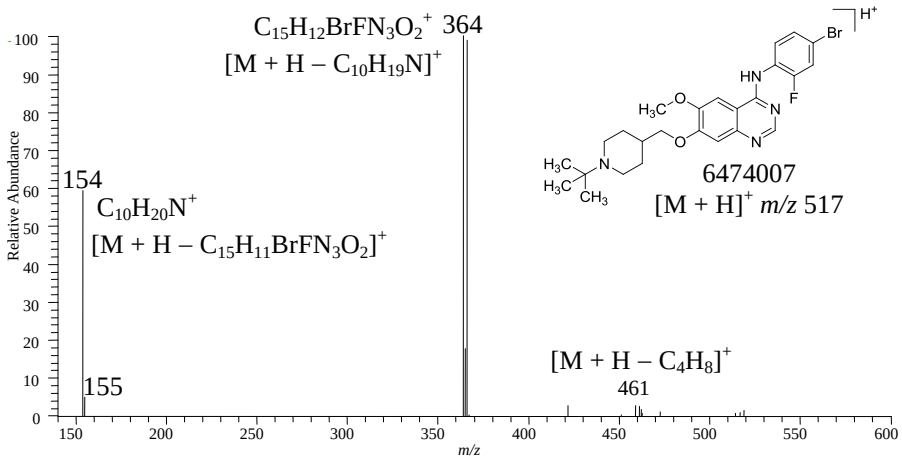

Figure 6.4 Positive ion electrospray first generation product ion mass spectrum of the *tert*-butylpiperidinmethoxy-substituted quinazoline of 6474007 in MeOH; IW = 6 *m/z* units.

It is proposed that the hydrogen-transfer mechanism results in formation of a base peak at 364 *m/z* units, Scheme 6.8. The mechanism of the formation of the ion at 364 *m/z* units should be supported by HDX experiments. If the mechanism in Scheme 6.8 is correct, then exchangeable hydrogen atoms should remain in the product ion containing the quinazoline ring and the loss of 153 *m/z* units must be of constant *m/z* value. The HD exchange experiment supports that the loss does not contain active hydrogen atoms (Appendix 2, Figure A.2.2) hence the formation of the loss must involve the non-labile hydrogen transfer, which confirms the mechanism proposed in Scheme 6.8.

The product ion *m/z* 154 is more likely a loss of the non-aromatic functional group at position 7 in the quinazoline ring (analogous mechanism pathway as displayed in Scheme 6.3 and Scheme 6.6), Figure 6.4.

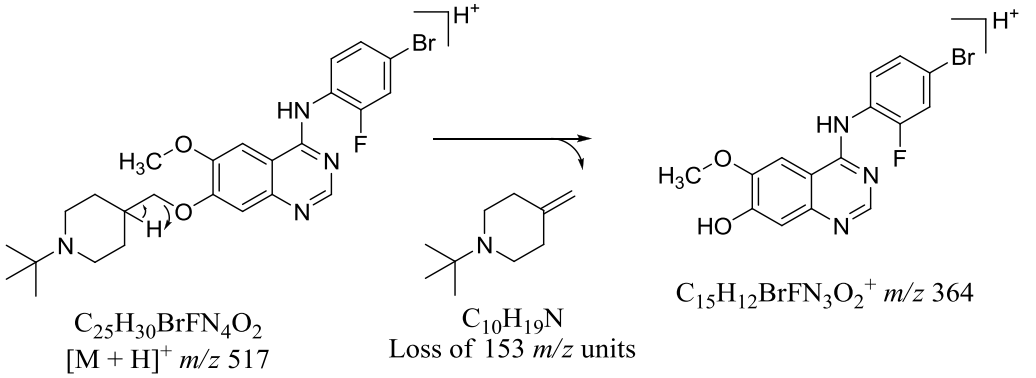

Scheme 6.8 A proposed mechanism for the formation *m/z* 364 of the compound substituted with methylpiperidinmethoxy- functional group, an example displays the fragmentation mechanism of the protonated molecule of 6474007.

In addition, the ions *m/z* 364 and 154 are ions that are formed from the part of the structure at oxygen atom in 7 carbon of the quinazoline ring. Product ion at 154 *m/z* units is probably formed due to an inductive cleavage if the oxygen atom holds the proton (analogous mechanism to Scheme 6.3) and *m/z* 364 is formed if the charge is at the different site of protonation, Scheme 6.8. It is proposed that the ion at 364 *m/z* units is formed due to the charge-remote fragmentation (Scheme 6.8) resulting in formation of a more stable product ion (base peak) than product ion *m/z* 154, which is the most probably formed due to the charge-directed fragmentation, Figure 6.4. Therefore, these two product ions may compete to retain the charge. Stevenson's rule states that the fragment with a lower ionisation energy is more likely to retain a charge,[92] which also relates to proton affinities values of protonated species; the fragment with a higher proton affinity is more likely to retain the charge. Hence the proton affinity of parts of the structure containing i) the quinazoline ring and ii) the saturated ring, must have similar values therefore both parts of the molecule can retain the charge and compete for it to form the product ions at 154 and/or 364 *m/z* units. The *m/z* 364 is however, a more favoured species than *m/z* 154, and hence the fragment of the molecule with the quinazoline ring must prefer (100: 60 of relative abundance) to retain a charge than a tert-butylpiperidinmethoxy- functional group. Therefore,

m/z 364 must have higher proton affinity to attract the proton than the saturated functional group, (Chapter 2.2.2, page 40).

6.3 Summary of the effect of saturated functional groups on the fragmentation pathways of protonated quinazolines

It was found that the fragmentation pathways of protonated quinazolines can be dominated by the presence of the saturated functional group, which results in formation of the typical product ions or losses. Compounds with piperidine substituents such as =N-C-*tert*-butyl (*e.g.* 6474007) and =N-COO-C-*tert*-butyl (*e.g.* 6474004) fragment irrespective of the position of the charge (a charge-remote fragmentation). Compounds substituted with piperidin=N-CH_3 (*e.g.* 6474001), morpholinpropoxy- (*e.g.* 6474010), and pyrrolidinpropoxy- (*e.g.* 2171001) functional groups favour the charge-directed fragmentation with the site of protonation placed at the oxygen atom (Scheme 6.3 and Scheme 6.5). Their PA values of the saturated rings must be higher than the PA values of the quinazoline part of the molecule, therefore the charge remains at the saturated functional groups resulting in formation of the non-aromatic ions, *e.g. m/z* 112 or 128.

The influence of a non-aromatic substituent on the fragmentation behaviour of protonated quinazolines can be compared to the influence of the saturated ring on fragmentation mechanisms of protonated quinolines, Figure 6.5. Two structurally similar quinoline compounds were studied by Bandu and Desaire using a LCQ Advantage QIT mass spectrometer (the ion source and full experimental conditions were not published).[178] It is hypothesised that the bi-cyclic aromatic ring with one nitrogen atom may have similar fragmentation behaviour to a quinazoline ring in the gas-phase. The non-aromatic substituents at the position 7 and 6 of a quinoline ring in compound A and B, respectively, are believed to retain the charge and hence lose the quinoline ring as a neutral, Figure 6.5. However, the presence of a carboxylic group may influence the fragmentation behaviour of the protonated quinolines towards a different mechanistic path.

Bandu and Desaire proposed that a loss of water and CO_2 came from the carboxylic substituent, Figure 6.5. The C-N bond (of the non-aromatic substituent on position 7 or 6 in compound A or B, respectively) is stronger than C-O therefore the carboxylic group needs less energy than the C-N bond to cleave. Hence, the loss containing the oxygen atom is preferred in the fragmentation of protonated quinolines that the loss containing the nitrogen atom.

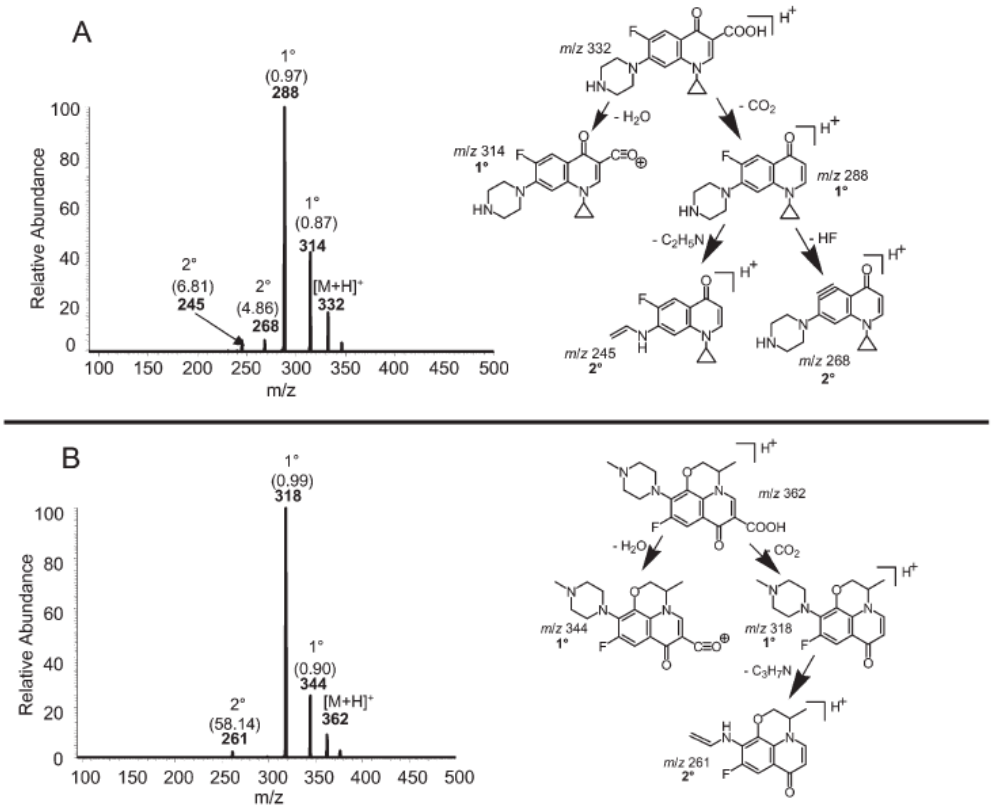

Figure 6.5 Product ion spectra of A) ciprofloxacin and B) ofloxacin acquired using LCQ Advantage QIT mass spectrometer;[178] reprinted with a kind permission of RSC.

The product ion mass spectrum of protonated molecule of compound A favours the loss of CO_2, which is achieved by a charge-remote fragmentation of the –COOH group. The formation of a product ion due to the loss of water is also formed from a carboxylic functional group. The product ion *m/z* 314, must involve an additional proton to allow loss of water, hence it must be formed due to a charge-directed fragmentation. This proves that a loss of water and CO_2 are

competitive processes involving the same –COOH group, but are different types of fragmentation: charge-remote (loss of CO_2) and charge-directed (loss of H_2O). Hence, different forms of precursor ion need to be formed to allow formation of these two product ions. The product ion mass spectrum of protonated molecule of compound B is a proof of concept that a carboxylic group has a dominant influence on the fragmentation behaviour of these two protonated quinolines, Figure 6.5. A charge-remote loss of CO_2 is more favoured than a charge-directed loss of water and hence the favourability of the formation of the product ions depends on the different site of protonation. It is hypothesised that the multiple functional group influence (non-aromatic, carboxylic) may be similar also for protonated quinazoline sub-structures.

Hence, the influence of the functional groups could be placed in the order of their strength and effect on the fragmentation pathways of classes of compounds. It is probable that the –COOH may also dominate the decomposition of protonated quinazolines however, the quinazolines substituted with a carboxylic functional group were not studied. Up to now, the functional groups that have the strongest influence on the fragmentation behaviour of protonated quinazolines are the non-aromatic rings with at least one heteroatom. The presence of –OBn or –OMe has not been found to affect the fragmentation pathways of protonated quinazolines substituted with saturated functional groups more dominant.

In addition, similar fragmentation behaviour of protonated quinazolines substituted with saturated rings was observed when in-space CID experiments were performed using ESI-QTOF and ESI-QqQ mass spectrometers (excluding second generation product ions), for example Figure 6.6, Figure 6.7, Figure 6.8, and Figure 6.9.

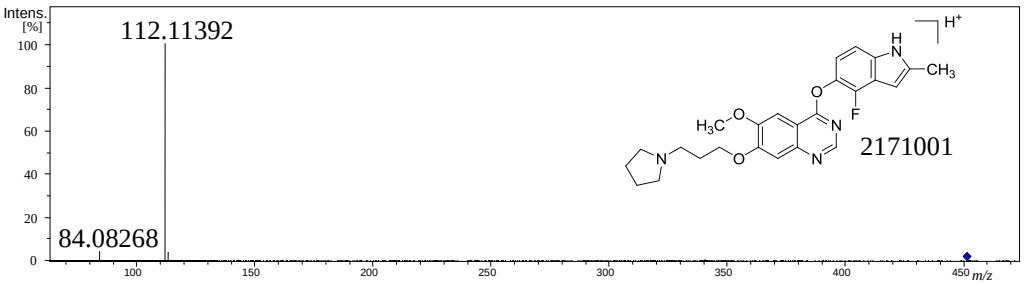

Figure 6.6 Positive ion product ion mass spectrum of 2171001 in MeOH acquired using ESI-QTOF mass spectrometer at 28 eV; IW = 1 *m/z* unit.

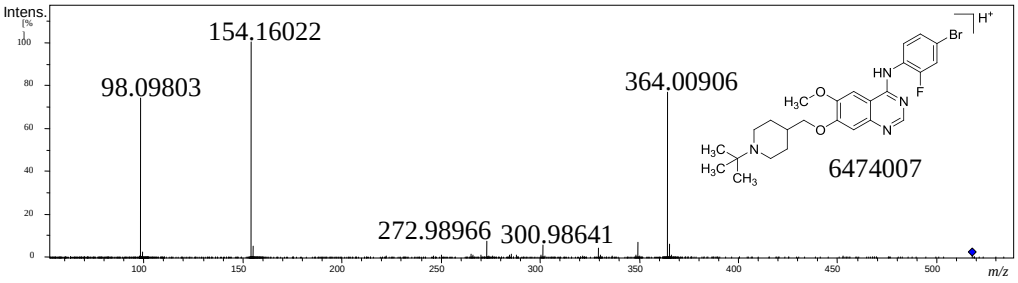

Figure 6.7 Positive ion product ion mass spectrum of 6474007 in MeOH acquired using ESI-QTOF mass spectrometer at 38 eV; IW = 1 *m/z* unit.

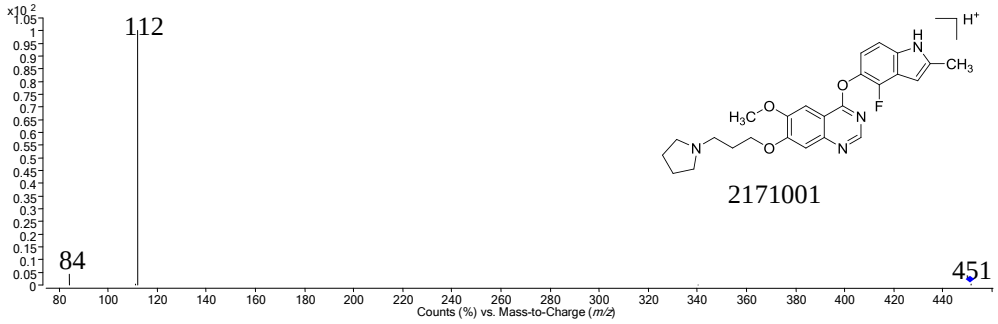

Figure 6.8 Positive ion product ion mass spectrum of 2171001 in MeOH acquired using ESI-QqQ mass spectrometer at 25 eV.

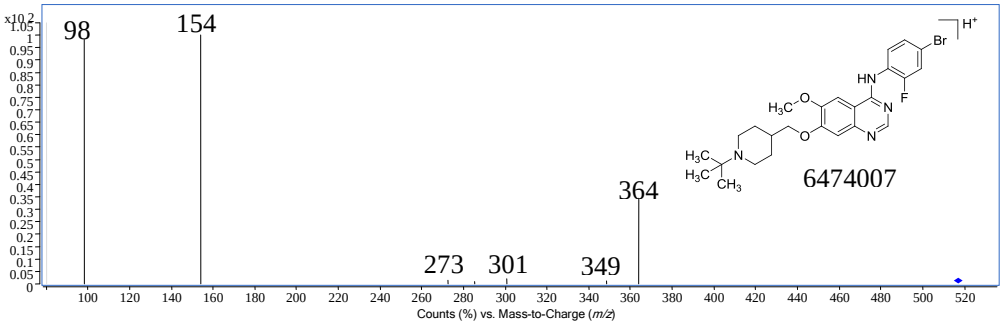

Figure 6.9 Positive ion product ion mass spectrum of 6474007 in MeOH acquired using ESI-QqQ mass spectrometer at 60 eV.

The described typical fragmentation behaviours of protonated quinazolines substituted with a large non-aromatic ring with at least one heteroatom have the similar influence on the mechanism pathways of protonated quinazolines regardless of what type of CID experiment is performed. Hence, the fragmentation behaviour of protonated quinazolines substituted with a saturated ring is structure dependent, and rules for the rapid characterisation of protonated quinazolines substituted with non-aromatic groups may be established regardless of which CID type is used.

Chapter 7 Unusual odd-electron fragmentation mechanisms of protonated quinazolines

The gas-phase ion dissociation of protonated quinazolines was investigated using different mass spectrometers. The comparison of first generation product ion mass spectra may bring to light a pattern of specific fragmentation behaviour of gas-phase quinazoline ions. Evaluation and recognition of the specific fragmentation behaviour for protonated quinazolines can result in a list of general and specific *m/z* ions and losses, which aids the interpretation of mass spectral data of different impurities containing a quinazoline ring.

As previously described in the theoretical chapters, fragmentation behaviour can be structure specific. During fragmentation, quinazoline ions often undergo the homolytic cleavages resulting in formation of odd-electron ions ($OE^{+\bullet}$). The $OE^{+\bullet}$ ions become a general feature of the fragmentation behaviour of protonated quinazolines although they may be treated as specific species formed if a mass spectrum of a quinazoline ion is compared to a mass spectrum of an ion from different class of compounds. This chapter focuses on the unusual odd-electron fragmentation behaviour of protonated quinazolines, which ironically becomes *usual* for quinazoline gas-phase ions. It is hypothesised that the specific odd-electron ions may help to distinguish quinazoline sub-structures and partially identify structures of unknown compounds.

The homolytic bond fission of protonated quinazolines commonly disregards the accepted even-electron rule (chapter 2.2.4, page 44).[78] This chapter describes examples of quinazoline ion fragmentation behaviour and discusses whether the even-electron fragmentation rule helps data interpretation of quinazolines. The chosen examples describe the specific behaviour of protonated quinazolines using CID MS/MS experiments. To follow the specific fragmentation behaviour of

these compounds, the examples are presented according to the pairs of functional groups with which they are substituted.

7.1 The influences of methoxy- and hydroxy- functional groups on fragmentation mechanisms of protonated quinazolines

Nine quinazoline impurities from analysed drugs with $–OCH_3$ and –OH functional groups at position 6 and 7 of a quinazoline ring were studied. Compound 2171008 is one of six impurities that are substituted with hydroxy- and methoxy- functional groups at the 7 and 6 position of the quinazoline ring respectively (Appendix 1, page 165). It is probable that a mass spectrometrist could predict which product ions may be formed by engaging knowledge based on previous interpretations of the mass spectral data and principles of physical-organic chemistry. Thus, by looking at the structure itself (in Figure 7.1), a mass spectrometrist may expect the compounds substituted with –OMe and –OH, *e.g.* 2171008, to possibly form a product ion due to the loss of water (loss of 18 *m/z* units) and/or methanol (loss of 32 *m/z* units). A hydroxyl group induces a higher probability of the protonation at the oxygen atom, which can result in a common loss of water.[146,197] Similarly, protonation at the oxygen atom that bonds the methyl group to the quinazoline ring would afford a loss of methanol.

Figure 7.1 presents a first generation product ion spectrum of 2171008 acquired using an ESI-QIT mass spectrometer. The most favoured species formed – the base peak – is a radical cation and it is mostly the only product ion observed in 2171008 product ion mass spectrum (excluding product ions that abundance is lower than 3 %). The observed loss of 15 *m/z* units (the methyl radical, $CH_3^{\bullet}$) disagrees with the even-electron rule, which states that such fragmentation should not take place as it is energetically less favourable.[79] A radical cation or a radical loss is not stable enough to allow this type of reaction to happen. The observed radical cation however, must have a high internal stability and a preference to be formed compared with the expected even-electron species. The radical cation at

178 *m/z* units must have a higher stability due to the large number of possible resonance forms that it can take; many resonance forms are formed due to the conjugation of the free electron with free electron pairs of the aromatic rings. Scheme 7.1 presents an example of two possible forms of the conjugation of the free electron within the aromatic system of quinazoline rings. It is hypothesised that one of the most stable forms may involve a free electron stabilisation between the oxygen atoms at position 6-(-methoxy-) and 7-(hydroxy-) of the ring. However, many different resonance forms are possible, which additionally enhance the stability of the radical cation.

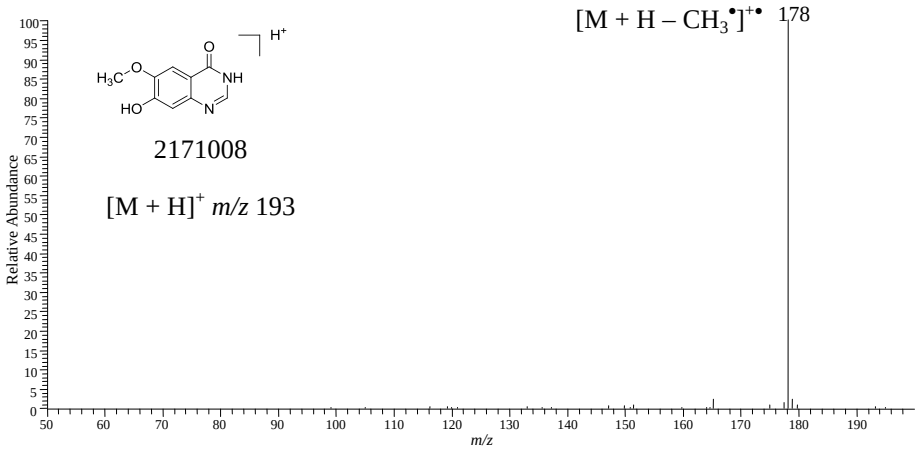

Figure 7.1 Positive ion electrospray first generation product ion mass spectrum of 2171008 in MeOH; IW = 1 *m/z* unit.

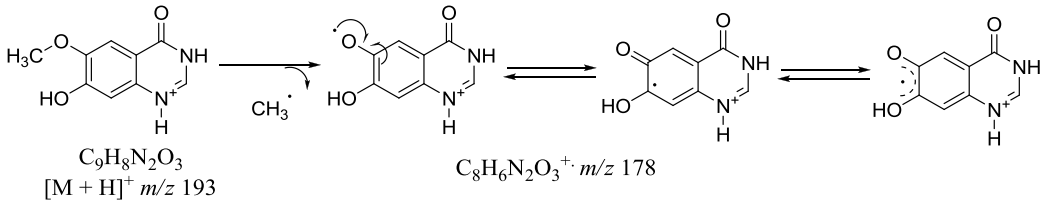

Scheme 7.1 An example of the mechanism resulting in the formation of two resonance forms of the radical cation, *m/z* 178 of 2171008; (many resonance forms are possible).

The radical cation is formed against the even-electron rule since a "radical loss is forbidden".[21,44] Some research groups observed that most compounds substituted

with a methyl or a methoxy- functional group lose $CH_3^{\bullet}$ instead of the expected loss of methanol.[198,199] The thermochemical understanding of formation of the $OE^{+\bullet}$ product ion (loss of methyl radical) instead of the EE^{+} (loss of methanol) using computational studies showed similar values of energy for the two calculated species (the error of calculations was larger than the energy difference between $OE^{+\bullet}$ and EE^{+}).[198] Thus theoretically, the stability of even-electron and odd-electron species is indistinguishable, but higher activation energies relates to the formation of radical cation species.[198] Yet, the stability of the product ion, whichever species it is, controls the fragmentation.[200]

The remaining five compounds with the same position of the –OH and $–OCH_3$ also favour formation of a base peak due to the loss of the methyl radical, *i.e.* 6474012 (Figure 7.7), 2171002 (Appendix 2, Figure A.2.3), 6474013 (Appendix 2, Figure A.2.4), 6474014 (Appendix 2, Figure A.2.5), and 6474027 (Appendix 2, Figure A.2.6). Similarly, sub-structures containing the different position of these functional groups also favour the loss of the methyl radical, *i.e.* 6474024 (Appendix 2, Figure A.2.7) and 8931006 (Appendix 2, Figure A.2.8). The fragmentation behaviour of the remaining compound, *i.e.* 6474011 also favours the loss of the methyl radical, but in a concerted process with loss of HF and CO; its specific fragmentation is described in Chapter 9.1, page 145.

The formation of the base peak due to the loss of a methyl radical takes place despite the presence of different substituents, such as an indole ring or halogens, for protonated quinazolines with hydroxy- and methoxy- functional groups at position 6 and 7 of the quinazoline ring. These observations lead to a possible hypothesis that it is not only characteristic functional groups that influence the fragmentation behaviour (Chapter 2.2.3, page 42), but pairs of the specific substituents at the fixed positions on the quinazoline ring affecting the fragmentation behaviour of protonated quinazolines.

7.2 The influences of methoxy- and benzyloxy- functional groups on fragmentation mechanisms of protonated quinazolines

Protonated quinazolines substituted with $–OCH_3$ and $–OC_7H_7$ groups at the 6 and 7 position of the quinazoline ring form a specific pattern of characteristic ions and losses. The assumption is that an analyst could propose formation of an even-electron product ion $C_7H_7^+$ and/or loss of methanol with regards to these substituents.

The formation of the ion at 91 *m/z* units is the most favoured ion in all compounds substituted with a benzyl functional group[99] and the position of the benzyl ring influences the fragmentation behaviour.[78] It is proposed that the most possible mechanism of *m/z* 91 formation is due to the inductive cleavage of the neighbouring bond, Scheme 7.2.

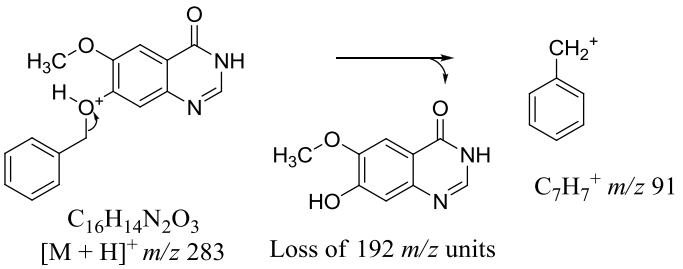

Scheme 7.2 A proposed mechanism for the formation of the *m/z* 91 ion in 2171003 compound.

However, it was found that formation of two product ions (*m/z* 91 and $[M + H –91]^{+\bullet}$) is favoured for compounds with –OMe and –OBn functional groups at the position 6, 7, and 8 of the quinazoline ring (10 impurities studied). There is a competitive process between the formation of $C_7H_7^+$ (*m/z* 91) and a product ion due to the loss of 91 *m/z* units ($C_7H_7^\bullet$). For example, compounds 2171003 (Figure 7.2) favours formation of the *m/z* 91 ion, but compounds 2171023 (Figure 7.3), 2171005 (Figure 7.4) and 6474015 (Appendix 2, Figure

A.2.9) form the $OE^{+\bullet}$ base peak due to the loss of a benzyl radical, *m/z* 192 $[M + H - C_7H_7^{\bullet}]^{+\bullet}$.

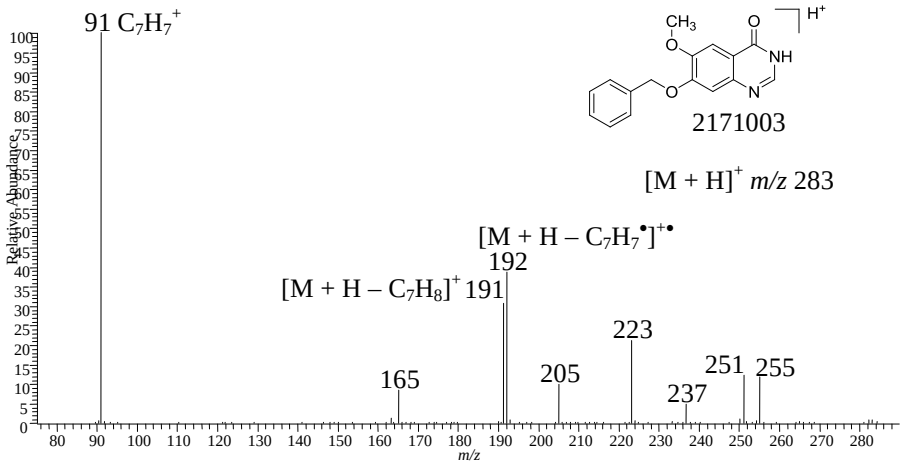

Figure 7.2 Positive ion electrospray first generation product ion mass spectrum of 2171003 in MeOH, IW = 1 *m/z* unit.

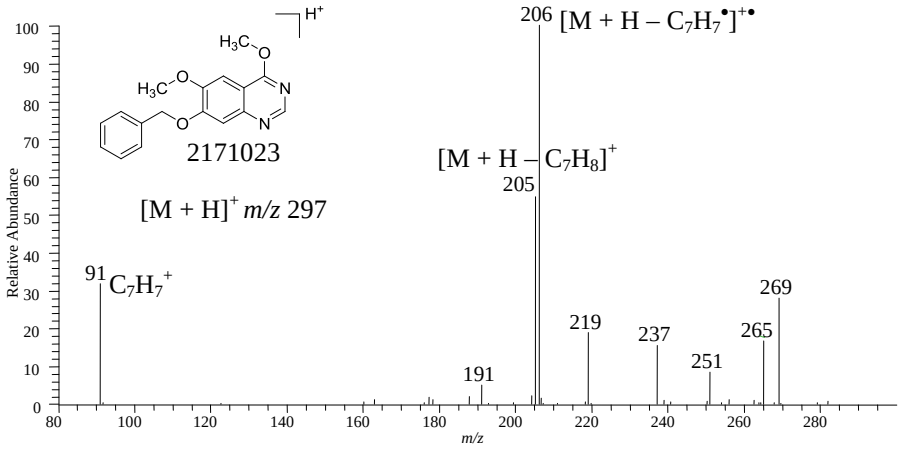

Figure 7.3 Positive ion electrospray first generation product ion mass spectrum of 2171023 in MeOH, IW = 1 *m/z* unit.

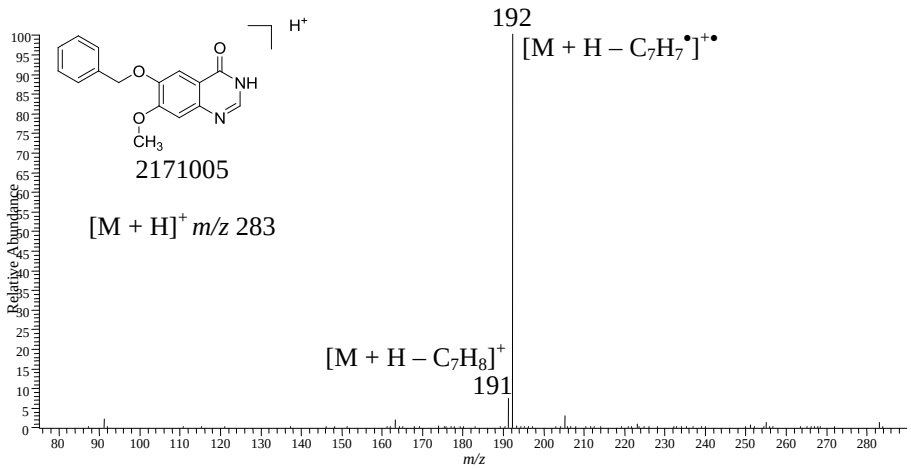

Figure 7.4 Positive ion electrospray first generation product ion mass spectrum of 2171005 in MeOH, IW = 1 *m/z* unit.

Similarly to the presented resonance forms in Scheme 7.1, the stability of the radical cations of the quinazolines substituted with –OBn and –OMe functional groups can be explained by formation of many resonance forms. The radical cation must have a higher stability, thus it is preferentially formed over the hypothetical even-electron product ion. The formation of the odd-electron product ion results from a homolytic cleavage of the C-O bond and can take place independently from the position of the charge.

Many CHNO-containing quinazolines form odd-electron product ions. In these studies, more than half of all the analysed protonated quinazolines (18 of 23 compounds without non-aromatic ring substituents) form one or more odd-electron product ions. However, only a minority of the compounds are prominent ions,[65] *e.g.* 2171005, 2171008.

7.3 The specific pair of ions – the influence of the benzyloxy- functional group on fragmentation mechanisms of protonated quinazolines

Interestingly, the lower abundant product ion due to the loss of 92 *m/z* units always accompanies the radical cation $[M + H - 91]^{+\bullet}$, Figure 7.4. The abundance of the product ion $[M + H - 92]^{+}$ varies from 5 to 70 % for the compounds studied. The AMM experiments confirm that the even-electron species has an analogous formula to the radical cation with less than one hydrogen atom, *i.e.* $C_9H_8N_2O_3^{+\bullet}$ and $C_9H_7N_2O_3^{+}$ at 192.0528 and 191.0456 *m/z* units, respectively. Such specific pairs of ions were also observed for protonated quinazolines substituted with $–OCH_3$ and –OH, however not protonated quinazolines that form a base peak due to the loss of methyl radical form a product ion due to the loss of methane. The accompanied pair of $OE^{+\bullet}$ and (-1 *m/z* unit) EE^{+} may be specific for the loss of a benzyl radical and toluene for quinazoline ions.

The formation of the even-electron product ion due to the loss of C_7H_8 (toluene) involves loss of the additional hydrogen atom. The possible mechanisms may involve the hydrogen atom from the molecule (Scheme 7.3) or the hydrogen atom that protonates the molecule (Scheme 7.4). The mechanism in Scheme 7.3 presents the formation of the *m/z* 191 through a charge-remote fragmentation by involving a hydrogen transfer from the methoxy- group followed by the formation of the new ring. Scheme 7.4 displays the mechanism that involves the additional proton at the oxygen atom followed by a transfer of one of the hydrogen atoms from the methyl group to the oxygen atom that is involved in the formation of the ring.

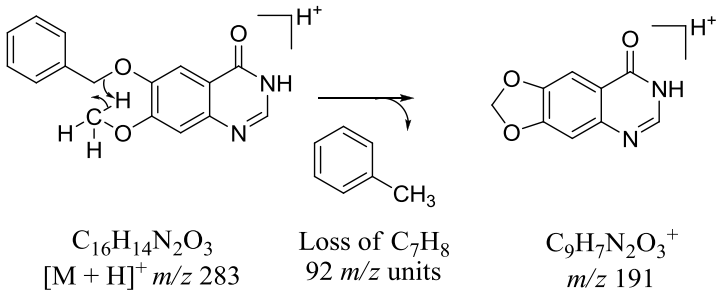

$C_{16}H_{14}N_2O_3$ $[M + H]^+$ *m/z* 283 — Loss of C_7H_8 92 *m/z* units — $C_9H_7N_2O_3^+$ *m/z* 191

Scheme 7.3 The suggested mechanism of charge-remote fragmentation resulting in the formation of *m/z* 191 due to the loss of toluene for compound 2171005.

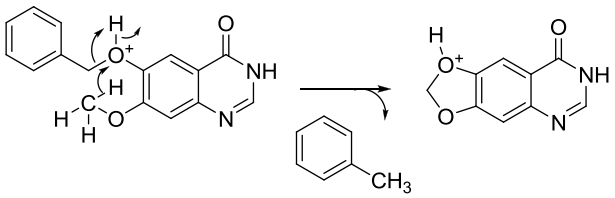

$C_{16}H_{14}N_2O_3$ $[M + H]^+$ *m/z* 283 — Loss of C_7H_8 92 *m/z* units — $C_9H_7N_2O_3^+$ *m/z* 191

Scheme 7.4 The suggested mechanism of a charge-directed fragmentation resulting in the formation of *m/z* 191 due to the loss of toluene for compound 2171005.

Two mechanisms are theoretically possible. The first mechanism involves a labile proton and its presence can consequently differentiate the two proposed mechanisms with the use of HDX experiments. The D-labelling experiment should distinguish the mechanisms in Scheme 7.3 and Scheme 7.4 as the proposed losses would involve a loss of C_7H_8 and C_7H_7D, respectively and hence formation of a product ion at 193 and 192 *m/z* units. Thus, the analogous mass spectrum of protonated 2171005 was acquired in a deuterated solvent, Figure 7.5. It is observed that the product ions due to the loss of 92 and 93 *m/z* units are formed.

The two proposed mechanisms in Scheme 7.3 and Scheme 7.4 are therefore correct, but the product ion formed due to the loss of 92 *m/z* units has a higher abundance. As already stated, the abundance of the ion in a mass spectrum reflects its stability.[65] Thus, a charge-remote mechanism proposed in Scheme 7.3 is more

favoured than formation of the product ion due to the charge-directed mechanism. The charge-remote type of fragmentation has higher activation energy than a charge-directed mechanism.[201] Thus, the mechanism pathway presented in Scheme 7.3 is energetically more demanding than the decomposition reaction presented in Scheme 7.4, but forms a more stable species, which agrees with the Curtin-Hammett principle (Chapter 3.2, page 64) regarding the decomposition pathways of gas-phase ions.[130,163]

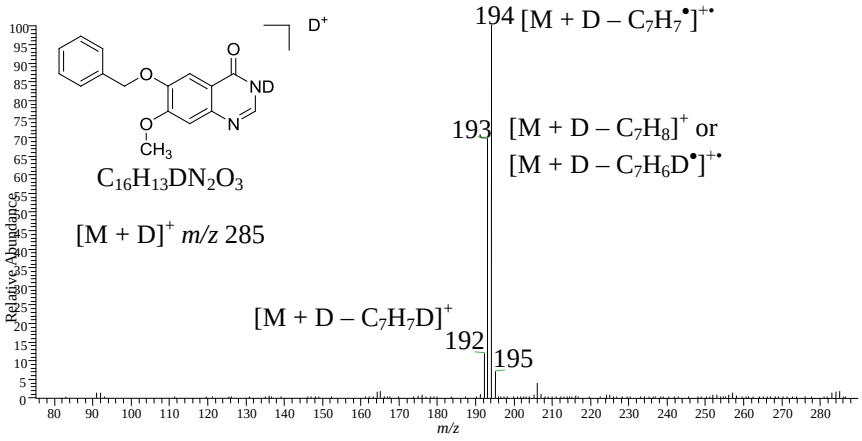

Figure 7.5 Positive ion electrospray first generation product ion mass spectrum of 2171005 in MeOD, IW = 1 *m/z* unit.

In addition, the density functional calculation may indicate the most stable forms of the protonated 2171005 molecule (Chapter 8.5, page 137), which can support or discard the proposed mechanisms. Calculations performed to find the most favoured site of protonation indicated four forms of protonated molecule of 2171005 as the most thermodynamically stable, Scheme 7.5. The scheme displays four structures of 2171005 with the percentage values indicating FPMs with the protonation site place on nitrogen and carbonyl oxygen atoms. The FPMs with the protonation on the oxygen at position 6 or 7 of the quinazoline ring are not indicated, hence this supports the theory that the formation of the product ion at 191 *m/z* units involve a charge-remote fragmentation, Scheme 7.3.

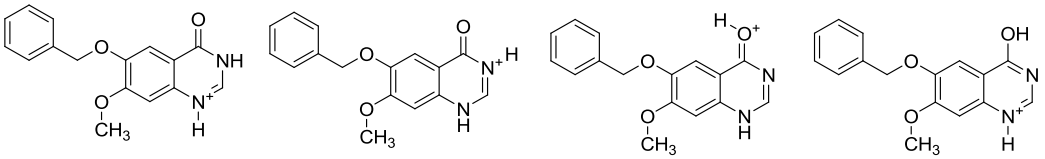

Scheme 7.5 The most thermodynamically favoured forms of protonated molecule of 2171005 in the gas-phase; the percentage values correspond to the probability of species formation, a full description of the DFT use to indicate the percentage values is described in Chapter 8.5, page 137.

7.4 The fragmentation behaviour of the halogen-substituted quinazolines – formation of radical and bi-radical cations

A different phenomenon was observed when analysing compounds substituted with one or more halogen atoms. Figure 7.6 presents a first generation product ion spectrum of a compound 6474032 substituted with two hydroxy functional groups at position 6 and 7 of the quinazoline ring, but containing the phenyl group substituted with halogen atoms at the 4 carbon of the ring. Hydroxyl groups do not influence the fragmentation behaviour of the compound; the mechanism pathways are affected by the specific fragmentation pattern of halogen atoms. A product ion at 320 *m/z* units with 20% abundance is formed due to the specific loss of 20 *m/z* units (a loss of HF). The loss of HF in all F-substituted compounds is expected to be of a low favourability if another substituent (*e.g.* Br atom) is present in one of the neighbouring positions.[80] Here however, bromine atom substitution does not suppress the formation of a product ion formed due to the loss of HF. Product ions at 271, and 270 *m/z* units are formed due to the loss of the bromine radical (loss of 79 *m/z* units) and HBr (loss of 80 *m/z* units), respectively. The product ion at 251 *m/z* units is formed due to a concerted loss of HF and $Br^{\bullet}$. Halogen atoms highly influence the fragmentation behaviour of aromatic ions (Chapter 2.2.3, page 42). The substitution of an aromatic compound with a halogen atom reduces the structure ionisation energy and proton affinity.[202] Thus, the structure preferentially loses the halogen atom as a radical to form a more stable ion (with a higher PA value).[44] The observed radical cations,

m/z 271 and 251, formed due to the loss of $Br^{\bullet}$, and $Br^{\bullet}$ and HF respectively, are therefore expected.

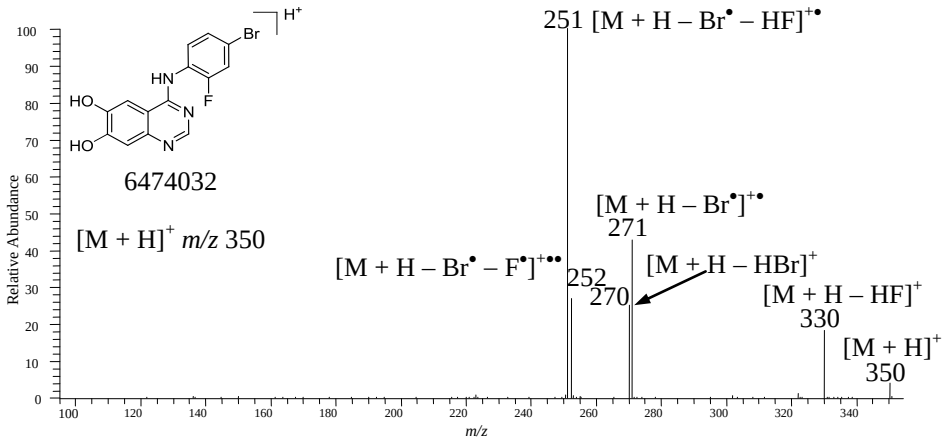

Figure 7.6 Positive ion electrospray first generation product ion mass spectrum of 6474032 in MeOH, IW = 1 *m/z* unit.

The product ion at 252 *m/z* units is formed due to the loss of 98 *m/z* units, which corresponds to the loss of two radicals, $Br^{\bullet}$ and $F^{\bullet}$. The loss of two radicals gives an even-electron product ion. This poses the question is the loss of two radicals to form an even-electron product (or a bi-radical) ion an exception to the even-electron rule?

Theoretically, the fragmentation path of a protonated molecule can be driven by the stability and energetics of the product ion and the formed loss.[101] In this case the loss of two radicals is energetically less demanding and could result in the formation of the *m/z* 252 ion, Figure 7.6. The ion could be: i) a product ion with an additional, new electron pair or ii) a product ion with two free electrons that are separately conjugated to aromatic rings of quinazoline ion. They would then be defined as: i) an even-electron ion, EE^{+} or ii) a bi-radical product ion, $EE^{+\bullet\bullet}$ $[M + H – 98]^{+\bullet\bullet}$, respectively.

It was observed that a halogen substitution induces a cascade of odd-electron fragmentation in many structurally similar compounds to 6474032 (seven impurities studied). They involve a loss of one or two radicals to form an $OE^{+\bullet}$

or EE^+/ $EE^{+\bullet\bullet}$. Extensive studies of radical cations and bi-radical cations by Kenttamaa and co-workers have shown that, using CID as an ion activation method, dibromo-substituted compounds form radical and bi-radical product ions due to the loss of one and two $Br^\bullet$ radicals.[203-205] Multi-iodine-substituted aromatics readily cleave the carbon-iodine bonds to form iodine radicals ($I^\bullet$) and radical and bi-radical cation product ions.[206,207]

Compounds substituted with halogen atoms give recognisable isotope pattern and form characteristic losses that can be readily observed. Mass spectral data of protonated quinazolines substituted with halogen atoms become difficult to interpret for compounds additionally substituted with a methoxy- group, *i.e.* 6474012. The loss of a methyl radical has already been described as dominant in the fragmentation behaviour of protonated quinazolines (chapter 7.1, page 106). The protonated quinazolines that are substituted with halogen atoms and additionally contain a methoxy- group present an enhanced cascade of odd-electron fragmentations, which increases the complexity of mass spectral data interpretation, Figure 7.7. The base peak of 6474012 in the CID-MS/MS mass spectrum is an odd-electron product ion formed due to the loss of the methyl radical.

A loss of $CH_3^\bullet$ is also involved in the formation of product ions *m/z* 329, 301, 273, and 250. If all the product ions formed due to the involvement of a methoxy-substituent, *i.e. m/z* 349, 329, 301, 273, and 250, in Figure 7.7 were eliminated from the spectrum then it would result in a highly similar spectrum to that shown in Figure 7.6 for 6474032. This comparison shows that a methoxy- group and halogen atoms influence the fragmentation pathway of protonated quinazolines and are responsible for the odd-electron fragmentation cascades.

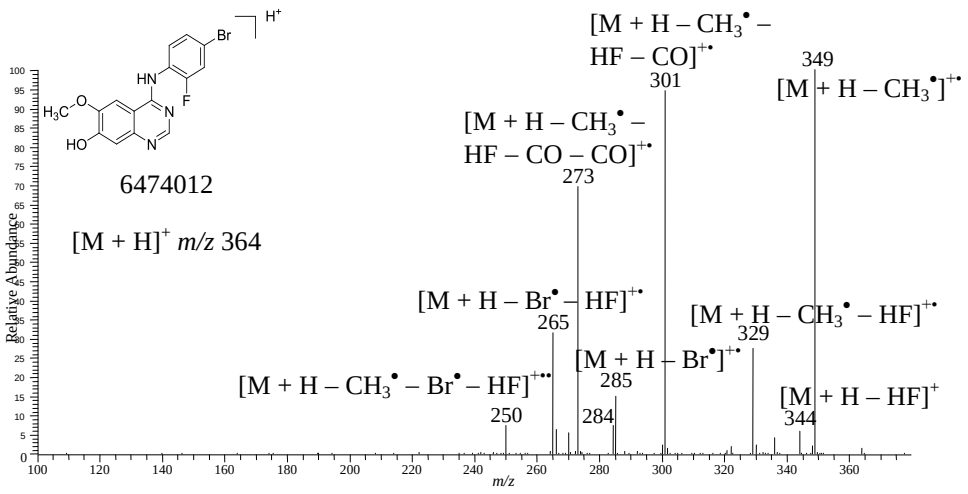

Figure 7.7 Positive ion electrospray first generation product ion mass spectrum of 6474012 in MeOH, IW = 1 *m/z* unit.

7.5 Use of the even-electron rule for the interpretation of mass spectra of quinazolines

A substitution of quinazolines with methoxy-, benzyloxy- groups, and/or halogen atoms, results in the formation of at least one product ion due to the loss of a radical, cascade of radical losses and/or formation of bi-radicals/even-electron product ions. The use of the even-electron rule to interpret mass spectral data would therefore be problematic for the quinazoline class of compounds using ESI-CID mass spectrometry and, when followed without care, could give misleading results or no information towards identifying the structure. Many scientists agree that the even-electron rule should not be treated as a rule but as a guideline only.[104,208] Some classes of compounds are known to disagree with the rule and extensively form odd-electron product ions. Strongly oxidisable compounds such as hydrocarbons and polycyclic aromatic hydrocarbons, preserve a strong ability to stabilise the unpaired radical, which is the reason why these compounds can fragment against the even-electron rule.[209] However, such ability in a quinazoline class of compounds is unknown.

Perhaps, the observations that resulted in the formation of the even-electron rule were over-interpreted. The original statement was focused on even-electron product ions being possibly more stable than odd-electron ions for propane and propylene formation when using EI-MS.[100] Thus, the observations of specific mechanism pathways were formed for analyses using electron ionisation, which forms molecular ions, not protonated molecules.[79] It did not state that odd-electron species are "forbidden to be formed", as is currently regarded by the even-electron rule definition.

There is a suggestion to modify the original even-electron rule schemes (Scheme 2.1, page 45) concerning the reaction types that decompose from the protonated molecule especially for the interpretation of the protonated quinazolines, Scheme 7.6. The Scheme 7.6 represents the observed dissociation reactions of gas-phase quinazoline ions (Chapter 6, page 89 and Chapter 7, page 105). It is possible that reactions a, b, and c in Scheme 7.6 can additionally eliminate a loss of one or more neutral molecules. To ensure that all reaction types are possible in fragmentation pathways using ESI-MS/MS, software packages that aid mass spectrometrists in data interpretation should be set up for the choice of "both" with regards to the number-of-valence-electrons in the product ions. This process will result in a higher probability of correct data interpretation.

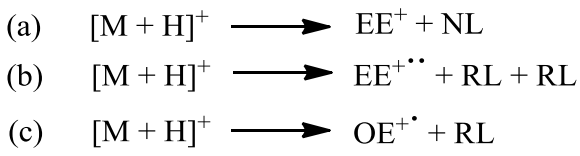

Scheme 7.6 Schematic description of types of reactions that should be allowed when interpreting mass spectra of protonated quinazolines acquired using ESI-CID MS/MS.

Chapter 8 An investigation of the fragmentation mechanisms of protonated positional isomers of quinazolines; an example of a predictive mass spectrometry approach using DFT-MS/MS

This chapter focuses on the analyses of the fragmentation behaviour of protonated positional isomers of quinazolines, *i.e.* 2171003, 2171005, and 2171006, using different ion activation methods, including CID, SORI/CID, and IRMPD. In addition, the comparison of the first generation product ion mass spectra of three protonated positional isomers using ESI, APPI, and APCI is described. These comparison studies should help to confirm or discard the possibility of building a set of rules for the rapid characterisation of protonated quinazolines independent of the type of mass spectrometer used. An attempt to predict which product ions can be formed from protonated quinazolines using Mass Frontier™ and DFT approaches is also discussed.

8.1 The fragmentation mechanisms of protonated positional isomers of quinazolines using ESI CID-QIT MS/MS

The positive ion electrospray CID product ion mass spectra of three protonated impurities, *i.e.* 2171003, 2171005, 2171006, of Cediranib (AZD2171) were acquired using an LCQ Classic QIT mass spectrometer. It was found that the change of the position of methoxy- or benzyloxy- functional groups between carbons 6, 7, and 8 in the quinazoline ring has a profound influence on ESI-CID MS/MS fragmentation pathways of protonated molecules. The product ion mass spectra of protonated positional isomers may differ significantly.[210] The electrospray mass spectra would not distinguish between these three protonated positional isomers; *i.e.* the three mass spectra would show a peak corresponding to the protonated molecule at *m/z* 283. Figure 8.1 displays first generation product

ion mass spectra of three protonated positional isomers acquired using CID MS/MS.

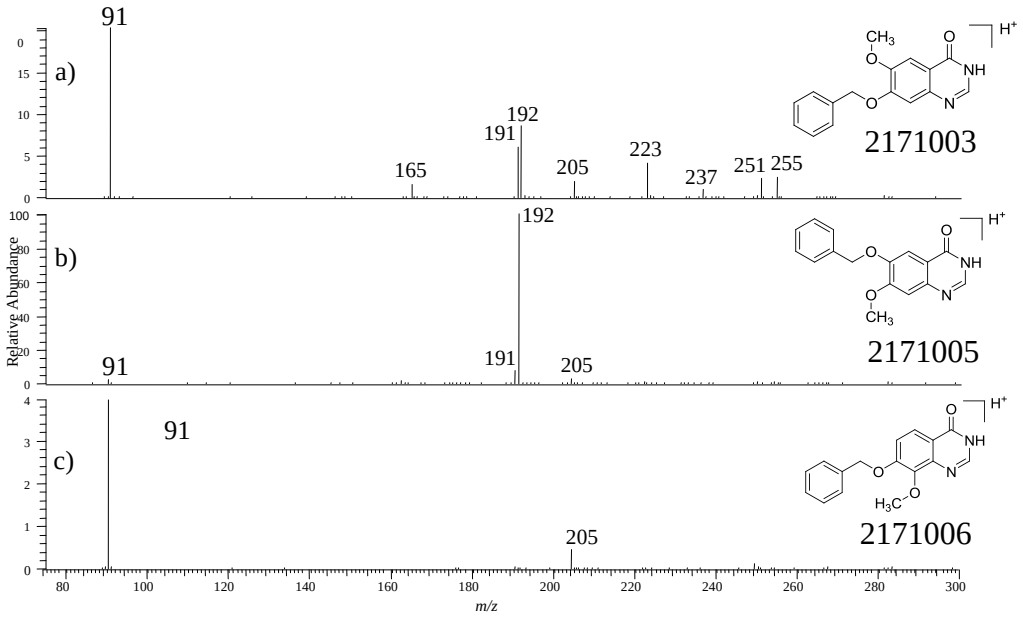

Figure 8.1 Positive ion electrospray first generation CID product ion mass spectra of: (a) 2171003, (b) 2171005, and (c) 2171006 in MeOH; IW = 1 *m/z* unit.

Protonated 2171003 favours even-electron fragmentation and results in the formation of the ion at *m/z* 91, ($C_7H_7^+$, data confirmed by AMM), Figure 8.1 a). The same product ion is the base peak for protonated 2171006, Figure 8.1 c). However, 2171003 forms more product ions in the higher *m/z* units range due to the losses of CO, CH_3OH or concerted loss of CO and CH_3OH from the protonated molecule, *i.e. m/z* 255, 251, 223, respectively. Apart from the base peak, the protonated compound 2171006 forms only one additional product ion due to the loss of benzene. These even-electron losses agree with the even-electron rule, Chapter 2.2.4, page 44.

Conversely, the fragmentation pattern of 2171005 does not show such similarities; it favours odd-electron dissociation. (The *m/z* 91 ion is present but only at less than 3 % abundance.) The base peak (*m/z* 192) has been confirmed as a radical cation product ion formed due to the loss of benzyl radical ($C_7H_7^{\bullet}$), which does

not agree with the even-electron rule, (analogous mechanism pathway is displayed in Scheme 7.1, page 107). The same radical cation product ion is observed in the product ion mass spectrum of compound 2171003, however with a lower relative abundance. (The formation of the ion $[M + H - 91]^{+\bullet}$ and $[M + H - 92]^{+}$ has already been discussed in Chapter 7.3, page 112.) Product ions due to smaller *m/z* units losses from the precursor ion of 2171005 are not observed. The benzyloxy-substituent is involved in two mechanisms: i) formation of the ion at 91 *m/z* units and ii) formation of a radical cation product ion (192 *m/z* units). The formation of one or both of these ions could be considered as a structurally competitive process as it requires the same part of the structure, *i.e.* the benzyloxy- group, but result in a different dissociation mechanism followed by formation of different product ion.

8.2 Comparison of first generation product ion mass spectra acquired using different types of mass spectrometers

This sub-chapter presents product ion mass spectra acquired using different in-time and in-space tandem mass spectrometers. The previous example shows that the fragmentation pathways of protonated quinazolines can be structurally dependent. The examples below are used to discuss whether the use of different ion activation methods may or may not affect the fragmentation pathways of protonated quinazolines.

8.2.1 Comparison of fragmentation pathways of protonated positional isomers of quinazolines using in-time tandem mass spectrometry experiments

8.2.1.1 Use of SORI/CID to investigate the fragmentation behaviour of protonated positional isomers of quinazolines

Figure 8.2 displays first generation product ion mass spectra of the three protonated positional isomers acquired using SORI/CID as an ion activation method. The base peaks of these three mass spectra are the same as when protonated molecules were analysed using CID MS/MS experiments, Figure 8.1.

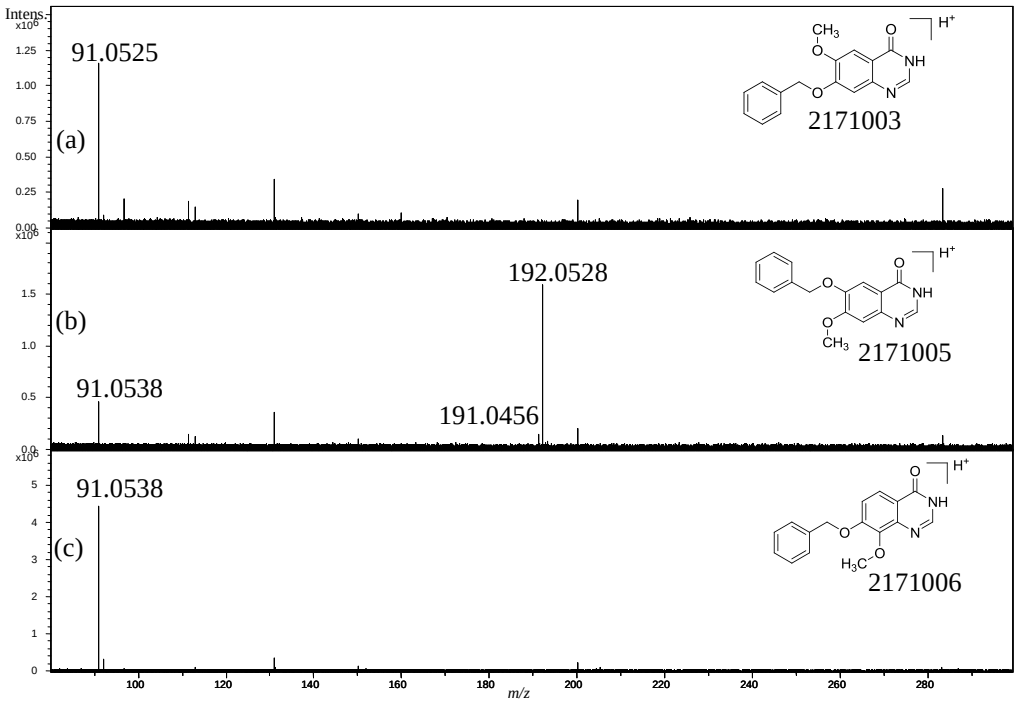

Figure 8.2 Positive ion electrospray first generation SORI/CID product ion mass spectra of: (a) 2171003, (b) 2171005, and (c) 2171006 in MeOH; IW = 1 *m/z* unit.

The formation of the $C_7H_7^+$ product ion from protonated 2171005 is more favoured using SORI/CID than when CID was used as the ion activation method. Thus, the favourability of forming the same species using CID and SORI/CID may be different and/or may relate to different experimental conditions. SORI/CID does not result in formation of any product ions in the higher *m/z* mass range (*m/z* 200-283) due to smaller losses, such as CO or MeOH, *e.g. m/z* 255 or 251, Figure 8.2, a). These losses often include structure rearrangement (*e.g.* ring opening), and therefore may not be favoured. Rearrangement reactions depend on the length of the RF pulse time during activation in SORI/CID processes. The mass spectra presented in Figure 8.2 were acquired using the RF pulse for 250 msec. and an activation time longer than 1 second may cause structure rearrangements.[21] Therefore, the lack of the smaller losses that involve structure rearrangements, *e.g.* an opening of the quinazoline ring, would not be preferred when SORI/CID, in these particular experimental conditions, is used as the ion activation method.

If either CID or SORI/CID was used, the formation of the radical cation at 192 *m/z* units in protonated 2171005 is favoured. Nevertheless, the formation of the odd-electron product ion in protonated 2171003 differs between the two types of CID used, Figure 8.1, a) and Figure 8.2, a). The formation of the $OE^{+\bullet}$ ion from position 6 in the quinazoline ring (*i.e.* 2171005) is more stable than when –OBn is substituted at position 7 in the quinazoline ring (*i.e.* 2171003, 2171006).

The main differences between CID and SORI/CID include: i) the use of a different collision gas (helium and argon, respectively) and ii) the use of different pressures during experiments (10^{-5} in QIT and 10^{-9} Torr in the ICR cell, respectively). The use of different gas and pressure affect changes in experiments, and hence may affect the fragmentation behaviour of the protonated quinazolines. The use of a different collision gas changes the amount of internal energy that the precursor ion receives before its decomposition (Equation 1.12, page 29). The precursor ion dissociates only if it possesses more internal energy than the energetic barrier of the dissociation reaction.[72] In addition, the pressure affects the

kinetic rate of the dissociation reaction; lower pressure increases the kinetic rate of the decomposition reaction, but the internal energy of the precursor ions must still exceed the energy barriers so that dissociation processes can take place (Reaction 3.2, page 65). Thus, observed differences between formed product ions other than the base peaks may originate from the different experimental conditions used in the CID and SORI/CID methods. Nevertheless, the most favoured product ions support the theory that the use of CID or SORI/CID does not affect the fragmentation behaviour of protonated quinazolines.

8.2.1.2 Use of IRMPD to investigate the fragmentation behaviour of protonated positional isomers of quinazolines

In addition, the fragmentation behaviour of three protonated positional isomers of quinazolines was studied using IRMPD MS/MS, Figure 8.3. The main difference affecting the possible fragmentation behaviour of protonated molecules using IRMPD compared to CID or SORI/CID is the lack of the collision gas. The ion/photon interactions in IRMPD may affect the mechanism pathways of protonated molecules of the positional isomers differently to the ion/neutral interactions, because of lack of the collision gas during ion activation process, (Chapter 1.3.3, page 32).[42]

Figure 8.3 displays the first generation product ion mass spectra of 2171003, 2171005, and 2171006. The main difference between these IRMPD mass spectra to previously discussed SORI/CID and CID mass spectra is that the even-electron product ion at 191 *m/z* units is formed in preference to the $OE^{+\bullet}$ at 192 *m/z* units in protonated 2171003 and 2171005, Figure 8.3, a) and b). Thus, the even-electron ions may be favoured in the decomposition pathways of the analysed protonated positional isomers. The formation of the $C_7H_7^+$ reflects a similar pattern to the mass spectra acquired using SORI/CID, Figure 8.3, a) and c), but *m/z* 91 has a higher abundance (is more favoured) in IRMPD than in the SORI/CID mass spectrum of protonated 2171005.

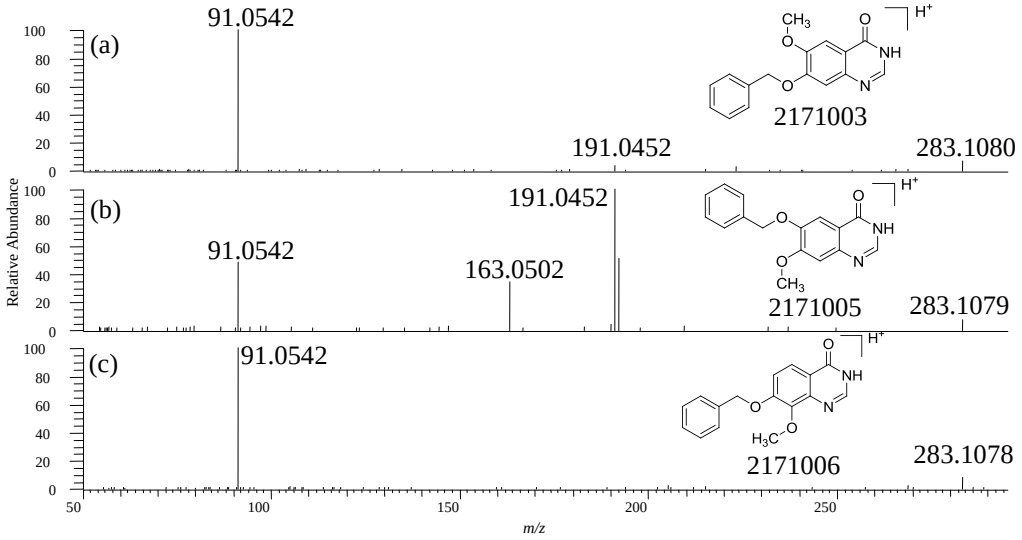

Figure 8.3 Positive ion electrospray first generation IRMPD product ion mass spectra of: (a) 2171003, (b) 2171005, and (c) 2171006 in MeOH with 80, 70, and 80 % of the laser power for 50 msec., respectively; IW = 1 *m/z* unit.

Contrary to previously presented first generation product ion mass spectra of protonated 2171003, 2171005, and 2171006 acquired using CID and SORI/CID, the IRMPD product ion mass spectra show an additional product ion that is not observed in previous mass spectra, *i.e. m/z* 163 from protonated 2171005. The AMM experiments confirm that the product ion at 163.0502 *m/z* units is $C_8H_7N_2O_2^+$ formed due to the loss of C_8H_8O. The loss of 120 *m/z* units (C_8H_8O) as a first generation product ion may be a concerted loss; the loss of one large neutral of 120 Da must involve opening of the quinazoline ring and possible rearrangement reactions, which are energetically less favoured than an elimination of the few smaller *m/z* losses. It is proposed that the *m/z* 163 can be formed due to the concerted loss of i) C_7H_8 and CO and/or ii) $C_7H_7^{\bullet}$ and $HCO^{\bullet}$. Additionally, the IRMPD process can often cause formation of second generation product ions.[21]

The first possibility *i.e.* a concerted loss of two, even-electron losses, has already been partially discussed in chapter 7 (Scheme 7.3, page 113 and Scheme 7.4, page 113). It was concluded that two mechanism pathways might form the product ion due to the loss of 92 *m/z* units. The formation of *m/z* 163 may undergo a different mechanism than initiated from a loss of 92 *m/z* units, but for the simplicity of

following the mechanistic paths, it is assumed that the same two mechanisms are taking place when performing IRMPD experiments (Scheme 7.3, page 113 and Scheme 7.4, page 113). The concerted losses should be presented by one reaction step (*i.e.* using one arrow), however to ease the display of the mechanism pathways, the reactions has been broken into many steps. Scheme 8.1 and Scheme 8.2 present mechanism pathways of the formation of the product ion at 163 *m/z* units from the two most probable mechanisms that form the *m/z* 191 as previously discussed (Scheme 7.3, page 113 and Scheme 7.4, page 113). The loss of CO may come from the carbonyl group in the quinazoline ring in both cases, Scheme 8.1 and Scheme 8.2.

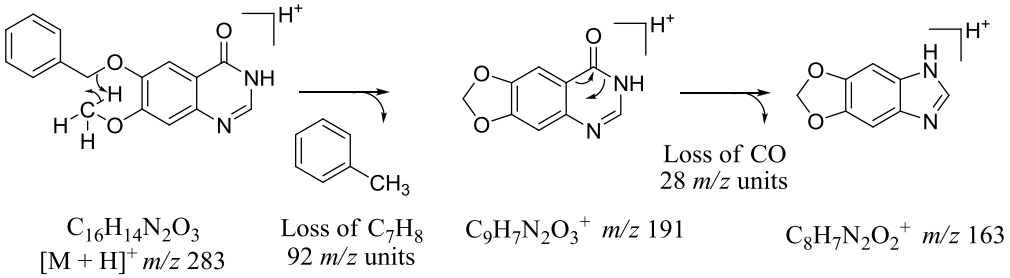

Scheme 8.1 Proposed mechanism of *m/z* 163 formation from protonated molecule of 2171005 *via* a charge-remote and even-electron type fragmentation.

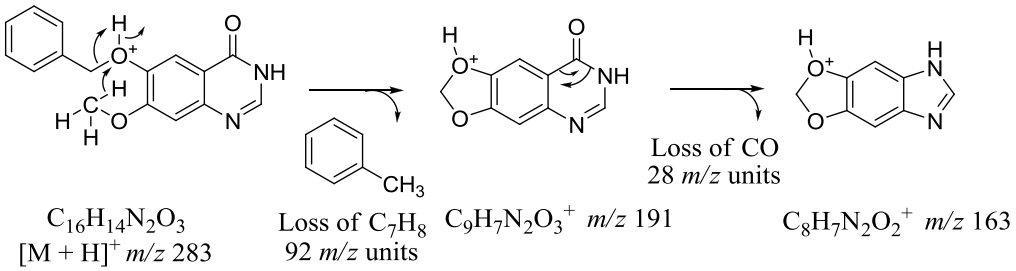

Scheme 8.2 Proposed mechanism of *m/z* 163 formation from protonated molecule of 2171005 *via* a charge-directed and even-electron type fragmentation.

The formation of the *m/z* 163 is also possible *via* a loss of two radicals, Scheme 8.3. The odd-electron fragmentation involves the opening of the quinazoline ring to eliminate $CHO^{\bullet}$, to form the 5-membered ring and a carbocation. The site of

the protonation of the radical cation is indicated by DFT calculations as one of the favoured ones for this product ion (a full discussion of use of DFT approach is in sub-chapter 8.5, page 137).

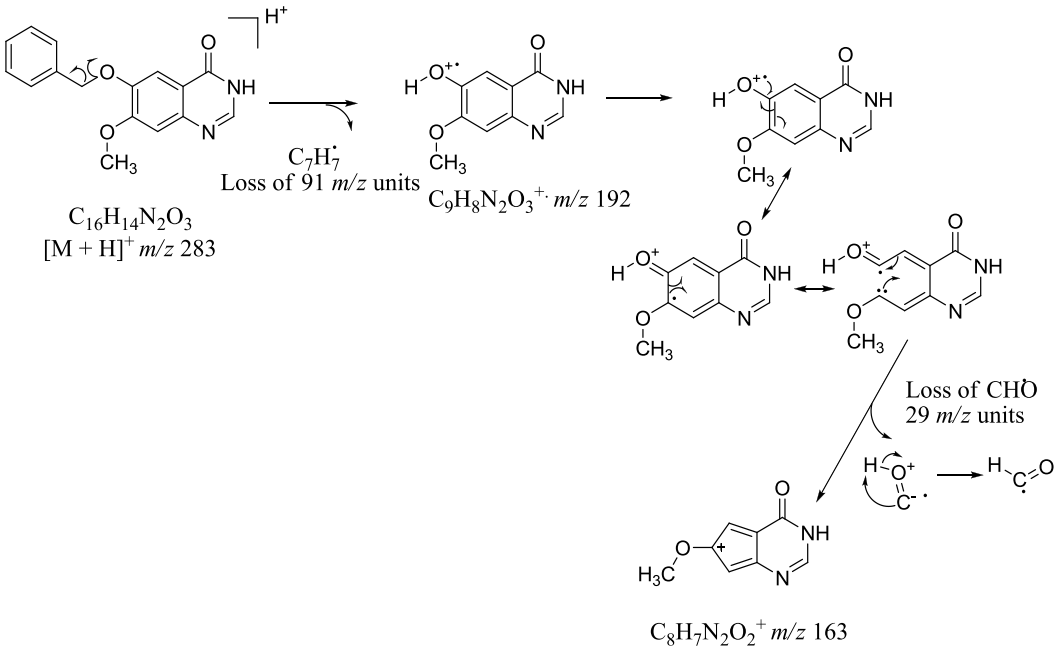

Scheme 8.3 Proposed mechanism of *m/z* 163 formation from protonated molecule of 2171005 *via* a charge-remote and odd-electron type fragmentation.

8.2.2 Comparison of fragmentation pathways of the protonated positional isomers using in-space tandem mass spectrometry

Figure 8.4 presents the product ion mass spectra of the protonated quinazolines acquired using a QTOF mass spectrometer. In the mass spectrum a), the *m/z* 91 and the pair of ions, *m/z* 191 and 192, are formed in a similar way to the mass spectra of 2171003 acquired using in-time MS/MS, Chapter 8.2.1, page 124. The *m/z* 91 is a base peak of protonated 2171003 and 2171006, Figure 8.4, a) and c), but it is the least favoured ion formed in 2171005. The 2171003 compound almost equally favours formation of the product ion at 191 *m/z* units, which is also formed in the mass spectrum for 2171005, Figure 8.4, a) and b). Thus, in-space

CID performed using QTOF mass analyser favours formation of the EE^+ (*m/z* 191) over the $OE^{+\bullet}$ (*m/z* 192) or odd-electron product ions readily dissociate to even-electron product ion *via* a loss of $H^\bullet$. The additional ions, *i.e. m/z* 178, 163, and 146 are most likely second generation product ions, because they are not formed when lower collisional energy values were applied.

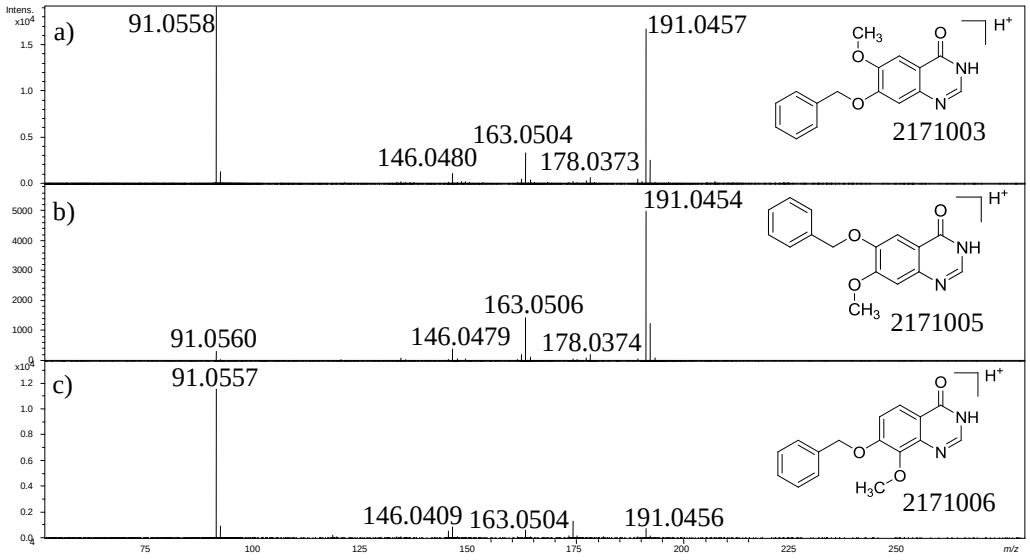

Figure 8.4 Comparison of the positive ion electrospray product ion mass spectra of 2171003, 2171005, and 2171006 in MeOH acquired at 28 eV of cone voltage using ESI-QTOF mass spectrometer; tables of the product ions formulae are available in Appendix 2, Table A.2.1, Table A.2.2, and Table A.2.3.

In contrast to the ESI-QTOF data, the ESI-QqQ MS/MS data show that the fragmentation behaviour of protonated 2171003 is almost identical to 2171006 protonated molecule, Figure 8.5, a) and c). Protonated molecule of 2171003 does not favour formation of the even-electron ion at 191 *m/z* units, nor formation of the radical cation (*m/z* 192) when using QIT MS/MS. Similarly to product ion mass spectra acquired using QTOF mass spectrometer, the radical cation at 192 *m/z* units may formed, but it may be unstable enough to rapidly eliminate the hydrogen radical and form the even-electron ion at 191 *m/z* units, Figure 8.5, b).

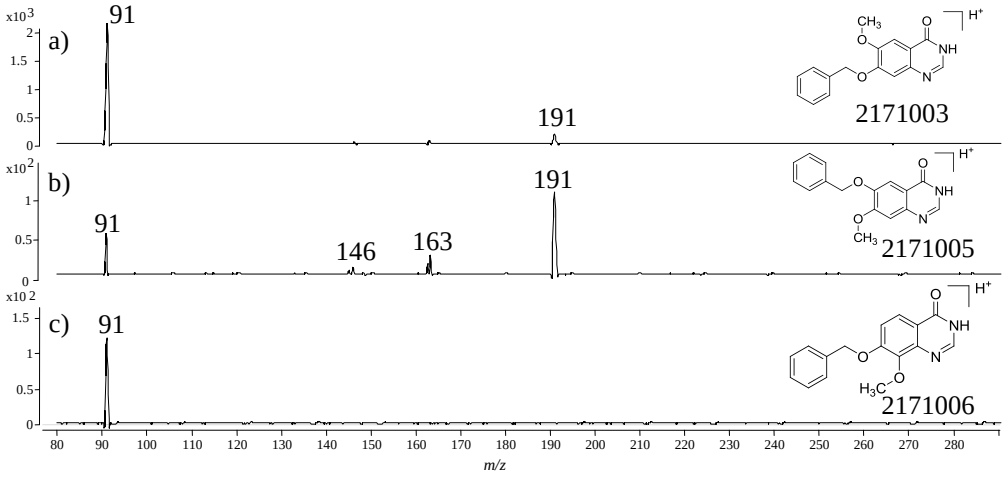

Figure 8.5 Comparison the positive ion electrospray product ion mass spectra of 2171003, 2171005, and 2171006 in MeOH acquired at 40, 40 and 20 eV of cone voltage, respectively, using ESI-QqQ mass spectrometer.

The cross platform differences are not fully understood although it is possible that the individual instrumental conditions affect the fragmentation behaviour of protonated quinazolines.

The fragmentation behaviour of the protonated positional isomers using different types of mass analysers differs in formation of low in abundance product ions and in the formation of the even-electron and odd-electron product ions, *i.e. m/z* 192 and 191, respectively. The formation of even-electron product ion at *m/z* 91 is the same for three protonated positional isomers irrespective of the ion activation technique used. In-time CID and SORI/CID experiments produce similar product ion mass spectra and the lack of low in abundance product ions in SORI-CID mass spectra compared to in-time CID mass spectra most possibly come from different experimental conditions, collision gas, and pressure inside the mass analyser. IRMPD and in-space CID experiments favour the formation of even-electron product ion at 191 *m/z* units, which might be readily formed from odd-electron product ion following the loss of $H^{\bullet}$. The mass spectra of protonated positional isomers acquired using in-space CID and IRMPD are very similar except low abundance product ions formed that may be second generation product

ions; their formation most probably depends on the amount of collision energy applied.

Summarising, the mass spectrometer type comparison experiments support the hypothesis that the fragmentation behaviour of protonated quinazolines depends on the mass spectrometer set up and experimental conditions, but not on the type of mass spectrometer nor ion activation used. The common trends of formation of most abundant product ions can be observed and apply into the rules for rapid characterisation of protonated quinazolines.

8.3 Comparison of first generation product ion mass spectra of protonated positional isomers acquired using different ionisation techniques

Similar discussion was undertaken when the product ion mass spectra of protonated quinazolines were acquired using different ionisation techniques, *i.e.* ESI, APCI and APPI. It is discussed whether the choice of the ionisation technique may or may not affect, to some extent, the fragmentation mechanisms of protonated positional isomers.

It is generally accepted that an APCI product ion mass spectrum mostly reveals the same product ions as when using ESI,[211,212] although ESI is expected to be gentler ionisation technique than APCI.[212] The product ion mass spectra acquired using APCI are similar to ESI product ion mass spectra, because the fragmentation mechanisms depend on the structure of the analyte than on the ion source used.[213] It was found that the positive ion APCI first generation product ion mass spectra of three protonated positional isomers, *i.e.* 2171003, 2171005, and 2171006, are similar to ESI product ion mass spectra shown in Figure 8.1. The ion at 91 *m/z* units is base peak of 2171003 and 2171006, but the protonated compound 2171005 favours the formation of odd-electron product ion at 192 *m/z* units.

The APPI data often differ from an ESI mass spectrum.[27] The APPI process is more kinetically than thermodynamically driven and it is also based on the interactions of the dopant and the analyte (a higher PA of an analyte will attract a proton from a dopant more easily).[27] The formation of the product ions using APPI as an ionisation technique should therefore reveal the ions where formation is driven kinetically. The first generation product ion mass spectra of three protonated isomers acquired using APPI are presented in Figure 8.6. Their analyses support the theory that APPI data often differ from ESI or APCI data.[27] The product ion at 91 *m/z* units is favoured in APPI first generation product ion mass spectra regardless of the position of the –OBn group, whereas in ESI first generation product ion mass spectra, the position of the benzyloxy- group affects the fragmentation mechanisms, Figure 8.1. It is hypothesised that if the *m/z* 91 is formed from each studied protonated positional isomer, it may be a product ion, which formation is driven by the kinetic processes; the base peak may not be the most stable species formed, but it may be the product ion formed first.

Conversely, the electrospray process is strongly endothermic, because the ions in the solution interact with solvent molecules, which form a solvent sphere around the analyte ion.[12] The energy required to transfer, for example, a Na^+ from a liquid to a gas phase is $-\Delta G_{liq.\rightarrow gas}$ = 98 kcal/mol ($-\Delta H_{liq.\rightarrow gas}$ = 106 kcal/mol). The reverse value of Gibbs energy means that the process is favoured in the direction from the gas phase to the liquid phase and hence to allow the desolvation process, the energy is required.[12] The amount of this energy is higher than cleavage of the C-C bond, which supports the theory that an electrospray desolvation process is a gradually thermal, soft ionisation technique,[12] and can often be thermodynamically driven.

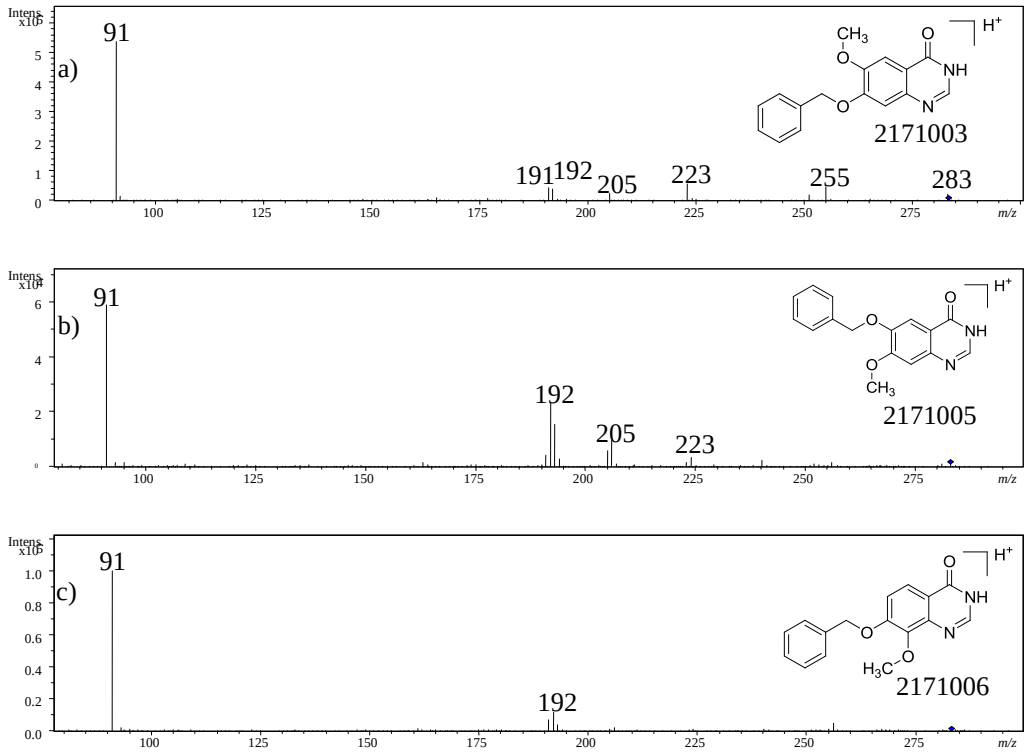

Figure 8.6 Positive ion APPI first generation product ion mass spectra of: a) 2171003, b) 2171005, and c) 2171006 in MeOH; fragmentation amplitude 1.1, IW = 0.5 *m/z* unit.

8.4 Prediction of the fragmentation pathways of protonated quinazolines using Mass Frontier™

The protonated quinazolines were also theoretically studied using the mass spectral predictive software Mass Frontier™. The software is commonly used to predict possible product ions, which helps to characterise the mechanistic pathways of protonated molecules using tandem mass spectrometry approaches. It is hypothesised that the use of Mass Frontier™ can help in rapid characterisation of product ion mass spectra of three positional isomers and therefore its use can be expanded to characterise mass spectral data of whole class of quinazolines.

Mass Frontier™ has been used to predict product ions of protonated 2171003. The software indicated 14 product ions that can be formed from protonated

2171003, including *m/z* 267, 256, 255, 251, 241, 240, 228, 213, 205, 177, 175, 145, 107, and 91. The product ions were compared to experimentally formed first generation product ions displayed in product ion mass spectra acquired using ESI-QIT mass spectrometer, Figure 8.1, a). Only four theoretical product ions have actually been formed in positive ion electrospray product ion mass spectra of protonated 2171003; *i.e. m/z* 255, $[M + H - CO]^+$; 251, $[M + H - MeOH]^+$; 205, $[M + H - C_6H_6]^+$; and 91, $C_7H_7^+$.

It is proposed that the protonated 2171003 may lose CO by the elimination of the carbonyl group, Scheme 8.4 and C_6H_6 by the hydrogen transfer and formation of the new ring, Scheme 8.5. Oppose to these two remote-control fragmentation pathways, the formation of *m/z* 251 and 91 is believed to result from a charge-directed process, Scheme 8.6 and Scheme 8.7.

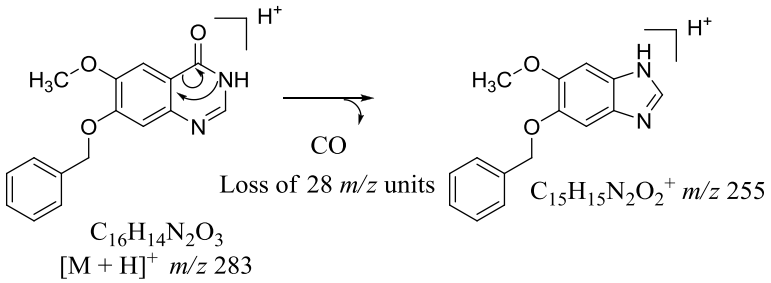

Scheme 8.4 Proposed mechanism of *m/z* 255 formation from protonated molecule of 2171003 *via* a charge-remote type of fragmentation.

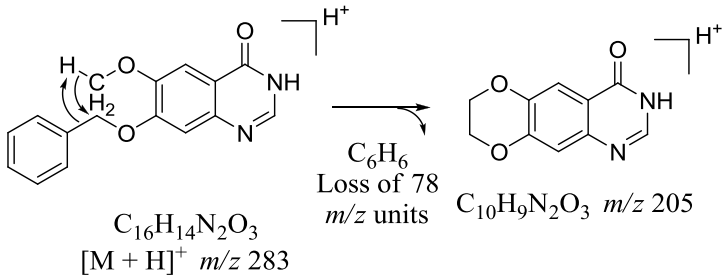

Scheme 8.5 Proposed mechanism of *m/z* 205 formation from protonated molecule of 2171003 *via* a charge-remote type of fragmentation.

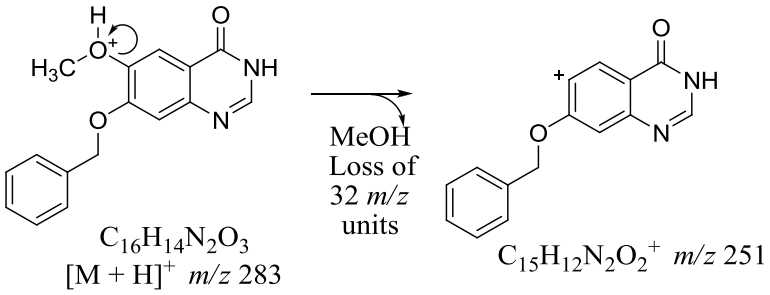

Scheme 8.6 Proposed mechanism of *m/z* 251 formation from protonated molecule of 2171003 *via* a charge-directed type of fragmentation.

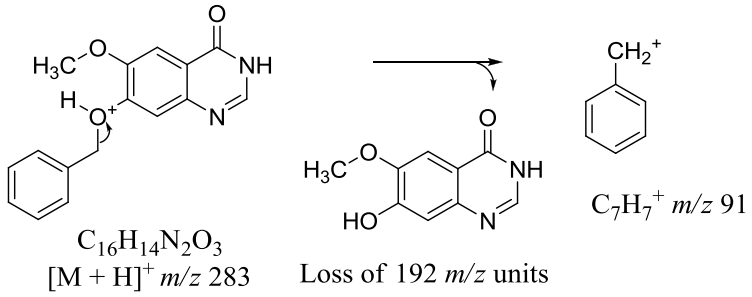

Scheme 8.7 Proposed mechanism of *m/z* 91 formation from protonated molecule of 2171003 *via* a charge-directed type of fragmentation.

The mechanism pathways of the product ions proposed by the software differ from ones proposed in this study (excluding *m/z* 251, Scheme 8.6). The proposed theoretical mechanisms involve a charge placed on one of the aromatic carbon atoms followed by the opening of the quinazoline ring. The only mechanism proposed by Mass Frontier™ that involves a location of the proton on the heteroatom and hence agrees with proposed mechanism is displayed in Scheme 8.6. Remaining mechanisms most probably involve the advance structure rearrangements and ring openings, which are not believed to occur in ESI-CID MS/MS experiments, because they require high-energy activation processes.

No odd-electron product ions have been predicted from the theoretical simulations using Mass Frontier™ hence inclusion of the possibility for odd-electron dissociation types when simulating product ions using ESI MS/MS rules in Mass Frontier™ (*e.g.* loss of benzyl radical as shown in this study) would improve

automated interpretation of protonated quinazolines using prediction software. The theoretical prediction of product ions formed from the protonated 2171003, although based on observations from thousands of reference data, may help to partially interpret the mass spectra excluding formation of odd-electron product ions.

8.5 Predictive approach of specific product ions formation from protonated quinazolines using DFT-MS/MS

The possibility of understanding and recognising the fragmentation patterns of protonated quinazolines may help to build a new approach to predict the formation of specific product ions. The DFT B3LYP/6-31G*//AM1 method was used to help explain the specific fragmentation behaviour of the protonated positional isomers (details of experimental part are in Chapter 5.2.2, page 88).

It is hypothesised that different sites of protonation can influence the fragmentation pathway of protonated molecules,[11,87-89] so the comparison of calculated protonation energies for all possible forms of protonated molecules may help to select the most thermodynamically stable forms of protonated molecule. The enthalpies of protonation of a precursor ion, *m/z* 283, for three positional isomers were calculated. Table 8.1 presents the total minimum energy values for each site of protonation and a tautomeric form of 2171003 (analogous tables for 2171005 and 2171006 are in Appendix 2, Table A.2.4 and Table A.2.5 2, respectively). The protonated molecule can have more than one protonation site and tautomeric form (Chapter 2.2.1, page 39) and in particular, the quinazoline can have three tautomeric sites. Additionally, 2171003, 2171005, and 2171006 have five most probable sites of protonation, which give 15 possible forms of protonated molecule for each compound. These calculations do not represent all possible forms of protonated molecule (FPMs) but the forms of the protonated molecule that are thermodynamically stable; the calculations performed do not indicate any FPMs that can be formed *via* kinetic processes.

Table 8.1 List of total minimum energy values for each tautomeric form of 2171003 with different site of protonation.

Site of protonation	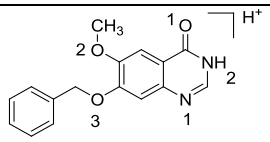	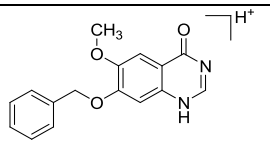	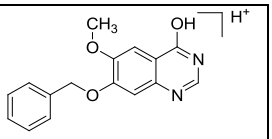
2171003	Energy of protonation [Hartree]*		
N1	-953.676525	-953.59462	-953.676537
N2	-953.612554	-953.676525	-953.660138
O1	-953.657118	-953.676539	-953.579139
O2	-953.629316	-953.606059	-953.614109
O3	-953.631951	-953.616188	-953.617019

* – 1 Hartree is 27.211 eV or 627.51 kcal/mol.[95]

The hypothesis of this approach is as follows. Individual forms of the protonated molecule may dissociate to form specific, analogous FPIs. The most thermodynamically stable forms of product ions can be selected and compared to the indicated FPMs. This comparison may illustrate how the fragmentation mechanisms progress, which may indicate which FPMs fragment to which FPIs. Consequently, the proposed mechanisms of the formation of each product ion can be defined, narrowing the number of possible dissociation mechanisms. Moreover, the population studies of the hypothetical protonated molecules and the product ions could quantify (in the percentage values) the stable forms.

According to the Boltzmann distribution of ion energies, the probability of the forms of protonated molecules and ions can be quantified.[214] The Boltzmann distribution theory represents the theoretical approach of quantifying the ions, which are in equilibrium, according to their internal energies in the quadrupole-ion trap.[215,216] Consequently, the Boltzmann distribution theory has been applied to calculate the most stable forms of protonated molecule and forms of product ion (FPIs), which can be compared to the experimental data acquired using a QIT mass spectrometer. In this study the $\Delta H_{prot.}$ of all 15 possible species were calculated according to the Boltzmann population distribution equation,[214]

Equation 8.1, and all protonated molecule and product ion forms of 2171003, in normalised populations (percentages), are presented in Table 8.2 and Table 8.3. (Tables of all forms of protonated molecule and product ion of 2171005 and 2171006 are presented in Appendix 2, Table A.2.6-Table A.2.9).

Equation 8.1 $$N_i = \frac{Ne^{-E_i/kT}}{\sum_i e^{-E_i/kT}}$$

N_{ion} – number of molecules in the sample of N molecules, k – Boltzmann constant (1.381×10^{-23} J K^{-1}), E_{ion} – energy of the ion, T – temperature (273.15 K)

Table 8.2 Energies of forms of protonated molecule of 2171003 converted into their population probability displayed in percentage values.

2171003	Site of protonation	Energy [Hartree]	Rel. Energy	Rel. Occupancy	Occupation %
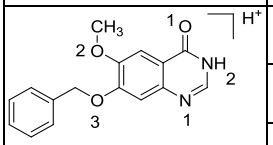	N1	-953.676525	1.40E-05	0.985032721	24.8
	N2	-953.612554	0.063985	1.17E-30	0.0
	O1	-953.657118	0.019421	8.22E-10	0.0
	O2	-953.629316	0.047223	8.10E-23	0.0
	O3	-953.631951	0.044588	1.38E-21	0.0
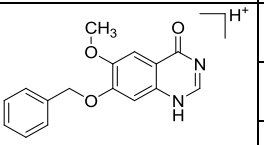	N1	-953.59462	0.081919	4.76E-39	0.0
	N2	-953.676525	1.40E-05	0.985032721	24.8
	O1	-953.676539	0	1	25.2
	O2	-953.606059	0.07048	1.07E-33	0.0
	O3	-953.616188	0.060351	5.85E-29	0.0
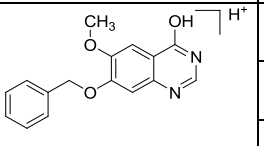	N1	-953.676537	2.00E-06	0.997847973	25.2
	N2	-953.660138	0.016401	2.13E-08	0.0
	O1	-953.579139	0.0974	2.72E-46	0.0
	O2	-953.614109	0.06243	6.23E-30	0.0
	O3	-953.617019	0.05952	1.43E-28	0.0

The calculations performed on positional isomers indicate four favoured forms of the protonated molecules for compounds 2171003 (Table 8.2), four for 2171005

(Appendix 2, Table A.2.6), and three for 2171006 (Appendix 2, Table A.2.7). A detailed explanation of compound 2171003 will be used to explain the population distribution. The schemes representing the distribution mapping of compounds 2171005 and 2171006 are displayed in Appendix 2, Scheme A.2.1, and Scheme A.2.2.

Table 8.3 Energies of forms of product ion at *m/z* 192 of 2171003 converted into their population probability percentage values.

$[M + H - 91]^{+\bullet}$ 2171003	Site of protonation	Energy [Hartree]	Rel. Energy	Rel. Occupancy	Occupation %
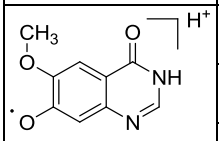	N1	-682.675626	0	1	44.3
	N2	-682.611141	0.064485	6.81E-31	0.0
	O1	-682.649498	0.026128	5.98E-13	0.0
	O2	-682.609508	0.066118	1.17E-31	0.0
	O3	-682.674359	0.001267	2.55E-01	11.3
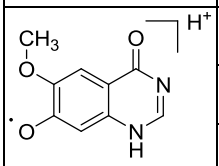	N1	-682.594149	0.081477	7.66E-39	0.0
	N2	-682.675625	1.00E-06	0.99892341	44.2
	O1	-682.669683	0.005943	0.00165884	0.1
	O2	-682.593937	0.081689	6.10E-39	0.0
	O3	-682.654787	0.020839	1.78E-10	0.0
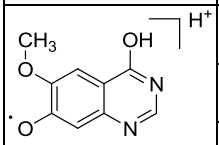	N1	-682.669688	0.005938	0.0016678	0.1
	N2	-682.649487	0.026139	5.91E-13	0.0
	O1	-682.569077	0.106549	1.43E-50	0.0
	O2	-682.604762	0.070864	7.06E-34	0.0
	O3	-682.657977	0.017649	5.54E-09	0.0

The population studies indicated four FPMs for protonated 2171003 (a, b, c, and d) and five forms of product ion at 192 *m/z* units (a', b', c', d', and e', Table 8.3) as the most thermodynamically stable, Scheme 8.8. The four indicated forms of protonated molecule are estimated to be of an equal formation of ca. 25% each. The first two forms of FPI, *i.e.* a' and b', have the highest probability of

formation, estimated at more than 40%. It is also observed that c' and d' analogue FPIs are theoretically less favourable, *i.e.* 0.1 %, but one additional FPI – e' – has a thermodynamically probable formation of 11.3%, Table 8.3, Scheme 8.8.

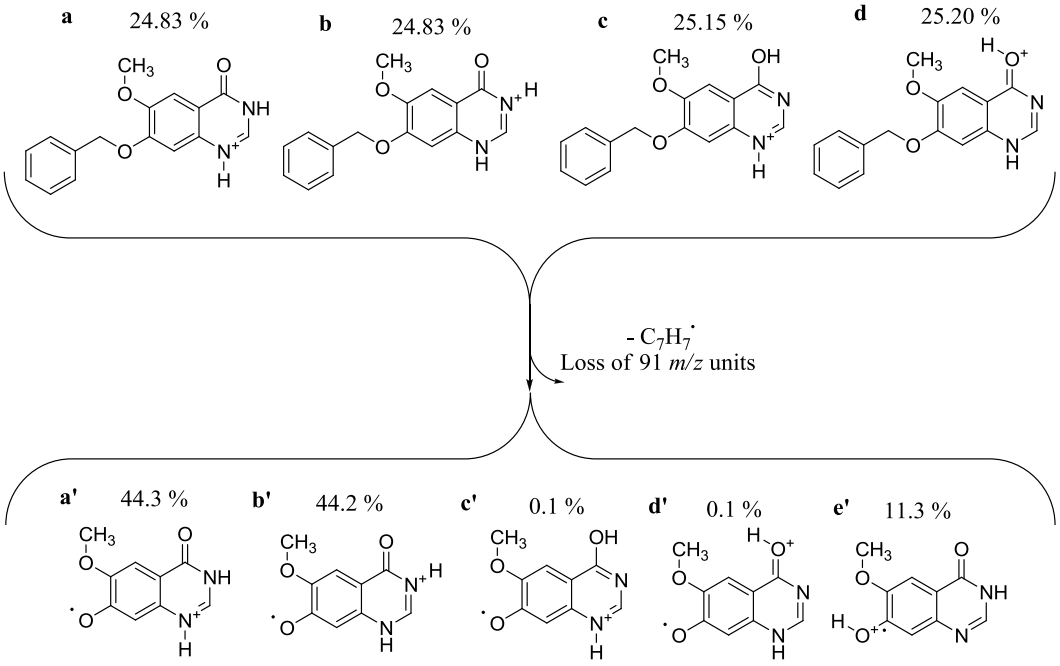

Scheme 8.8. Schematic population distribution (% values) of most thermodynamically favourable forms of protonated molecule (FPM, top row) and forms of product ion (FPI, bottom row, *m/z* 192) of 2171003 indicated from heats of formation calculated by single point energies B3LYP/6-31G*//AM1.

The analogous e' FPI, which does not have an analogous form of protonated molecule (e, in the upper row), has also been indicated in the theoretical calculations of compound 2171005 (Appendix 2, Table A.2.8) and 2171006 (Appendix 2, Table A.2.9). The probability of formation of the equivalent e' form of the product ion for 2171005 and 2171006 is 96.5 % and 1.1 %, respectively, Appendix 2, Scheme A.2.1, and Scheme A.2.2.

Summarising, the normalised intensities of the radical cations at 192 *m/z* units for 2171003, 2171005, and 2171006 in first generation product ion mass spectra are 16, 89, and 0 % respectively, Figure 8.1. Population studied for the specific forms

of the radical cation indicate a probability of formation of 11.3, 96.5, and 1.1 % for 2171003, 2171005, and 2171006, respectively. The theoretical and experimental data shows a good correlation, which means that the calculations support the MS/MS data for formation of the radical cation at 192 *m/z* units.

The hypothetical analogous form (form e) of the protonated molecule would support the suggestion of a simple homolytic cleavage due to the loss of 91 *m/z* units. However, in a scheme such as this, the additional e' form of the product ion must be formed from one of thermodynamically indicated a, b, c, or d forms of the protonated molecule. Therefore, the mechanistic pathway resulting in formation of the e' form has to be more complex than just a simple odd-electron dissociation. It must involve the charge migration to the oxygen atom where the elimination of the benzyl radical has occurred. A movement of a charge to the cleaved bond seems to be thermodynamically favoured and agrees with experimental data. Depending on the possible mechanism of this process, a movement of a hydrogen atom to a different site of protonation is known as a mobile proton, which is discussed in more detail in Chapter 9, page 145.[217] It is interesting, that one of the most stable and favourable forms of radical cation species of the three positional isomers has been indicated as a protonated species with the charge on the radical oxygen atom. It is unlikely that a mass spectrometrist would immediately propose the structure of discussed form of product ion before experimental and theoretical analyses. The interpretation of CID mass spectral data involves consideration of many rules and observations that can be an aid as well as a hindrance during structural elucidation studies, *e.g.* even-electron rule.

8.6 Summary

Comparison of the first generation product ion mass spectra of the protonated positional isomers shows that the product ions may differ (but mostly in abundance) when different ion activation methods and types of mass spectrometer

have been used. The fragmentation mechanisms of protonated quinazolines are mostly structurally dependent. One of the main differences is the formation of even-electron and odd-electron ions. The even-electron product ion is preferentially formed when IRMPD or in-space CID is used as the ion activation method and the formation of the odd-electron product ion is favoured when analyses are performed using in-time CID and SORI/CID experiments. Except that, the rules for rapid characterisation of protonated quinazolines could be established for general use regardless of what type of mass spectrometer is used rather than be mass spectrometer specific.

The choice of the ionisation method may influence the fragmentation behaviour of the compounds. The use of the APPI as the ionisation method, affects the first generation product ion mass spectra despite the position of the specific functional groups. Nevertheless, the use of ESI or APCI have shown no major difference in product ion mass spectra of protonated quinazolines hence these two ionisation technique do not influence the fragmentation behaviour of protonated positional isomers.

The specific product ion, *i.e.* radical cation formed due to the loss of benzyl radical was used as an example for the use of DFT-MS/MS approach. It was found that the intensities of formed radical cations can be predicted using DFT and their correlation to the experimental data is within 10 % error in abundance. It is believed that DFT-MS/MS could form an important role in a predictive science approach to the interpretation of tandem MS data, although further studies are necessary.

Chapter 9 The benefit of the use of hydrogen/deuterium exchange and accurate mass measurement experiments to characterise fragmentation behaviour of protonated quinazolines

This chapter describes the example of the use of H/D exchange and accurate mass measurement experiments to enhance the confidence in elucidating the structures of protonated quinazolines. It also discusses whether the proton in protonated quinazolines can be mobile; the hypothesis is initiated from the results and discussion section in Chapter 7 (page 105) and Chapter 8 (page 121) as well as the theoretical calculations in Chapter 8.5 (page 137).

9.1 Complementary analyses of HDX and AMM in structural elucidation studies of protonated quinazolines

To ensure a correct MS/MS spectra assignment, H/D exchange and AMM experiments are often necessary. They are crucial to guard against data misinterpretation, because the HDX experiments narrow the number of possible species formed by the mass shift in the mass spectrum resulted from the exchange of labile hydrogen atoms to deuterium atoms as well as AMM experiments define the formulae of product ions formed. The measurements of the number of exchangeable hydrogen atoms in the gas-phase ions become a useful technique to support structure elucidation studies.[146,218-221] Many HDX experiments for ESI MS studies involve the preparation of a sample solution in a deuterated solvent[219] or a replacement of the drying gas with ND_3.[218] These two methods were found efficient to fully exchange labile hydrogen atoms to deuterium atoms in small molecules.[218] Yet, the HDX and AMM add extra time to the process of mass spectral interpretation. This sub-chapter presents the example of how easily

a product ion can be misidentified when studying the fragmentation behaviour of protonated quinazolines.

The first generation product ion mass spectrum of protonated 6474008 (see Figure 9.1, a) was acquired using the LCQ Finnigan mass spectrometer. The product ion at *m/z* 363 is base peak of the 6474008 product ion mass spectrum; it contains one bromine atom and it is formed due to the loss of 91 *m/z* units, which is the most probably the loss of a benzyl radical, Figure 9.1, b). (The isolation width of the mass spectrum acquired in deuterated environment was narrowed to 1 *m/z* unit to simplify the assignment of deuterated product ion. This procedure was performed for all HDX presented experiments.) The D-labelling experiments should support whether the proposed product ion $[M + H - C_7H_7^{\bullet}]^{+\bullet}$ is formed. If the loss of 91 *m/z* units is constant when H/D exchange experiment is performed, then the loss of 91 *m/z* units does not contain any labile hydrogen atoms and hence the product ion must contain two exchangeable hydrogen atoms. Figure 9.1 c), displays the first generation product ion mass spectrum of deuterated 6474008 in mass range of *m/z* 360-370 and it confirms that the loss does not contain exchangeable hydrogen atoms thus it can be a loss of benzyl radical. (The loss of the benzyl radical in protonated quinazolines has already been discussed in Chapter 7.2, page 109 and Chapter 7.3, page 112). The protonated 6474008 also forms a product ion due to the loss of 92 *m/z* units, which supports the pattern recognition for the –OBn group in quinazoline ions. Accurate mass measurement experiment is a further experiment that can support the evidence that the ion at 363 *m/z* units is formed due to the loss of benzyl radical. The tandem mass spectrometry experiments performed using a FT-ICR mass spectrometer indicate that the most probable formula for the measured *m/z* 363.0017 is $C_{15}H_{11}BrFN_3O_2^{+\bullet}$ (theoretical *m/z* 363.0013 with error of -0.34 mDa (-0.9 ppm)) due to the loss of $C_7H_7^{\bullet}$. The ion at 363 *m/z* units is most likely formed due to the homolytic cleavage of the C-O bond at carbon 7 in the quinazoline ring (analogous mechanism to Scheme 7.1, page 107).

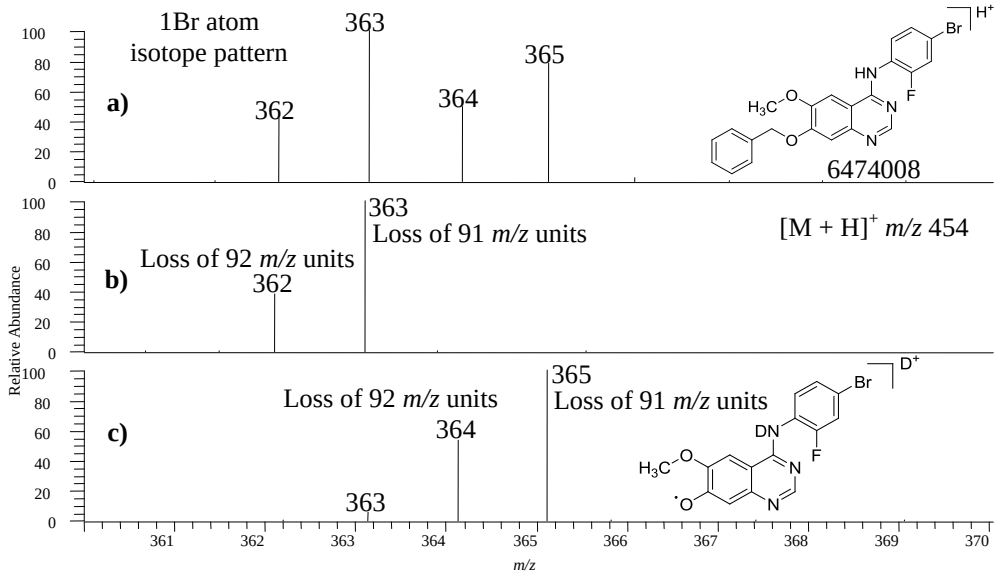

Figure 9.1 Positive ion electrospray first generation product ion mass spectra of protonated 6474008: a) IW = 6 *m/z* units in MeOH, b) IW = 1 *m/z* units in MeOH, and c) IW = 1 *m/z* unit in MeOD.

Interestingly, it was found that protonated quinazolines that are not substituted with –OBn may also form the product ion due to the loss of 91 *m/z* units (three examples studied), Figure 9.2, a). The first generation product ion mass spectrum of protonated 6474012 presents that the *m/z* 273 also contains one Br atom as protonated 6474008 (Figure 9.1, a), and forms the base peak due to the loss of 91 *m/z* units, Figure 9.2, b), but the loss of 92 *m/z* units is absent. The D-labelling experiment could be used to confirm whether the benzyl radical loss take place or not. The loss of $C_7H_7^{\bullet}$ does not contain exchangeable hydrogen atoms therefore all deuterium atoms must remain in the product ion. 6474012 has three exchangeable hydrogen atoms from which, during HDX experiments, two remain in the product ion (*m/z* 275), but one is eliminated within the loss of 92 *m/z* units, Figure 9.1, c). Hence, the loss of 91 *m/z* units in 6474012 must be a different species than a loss of the benzyl radical in 6474008.

Because the structure of 6474012 is known, it can be observed that it does not contain the benzyl group to eliminate benzyl radical easily. However, if the structure of the protonated molecule of 6474012 would be unknown then it could

be assumed that the molecule most likely contains the benzyloxy- substituent, which would cause a false-positive partial identification of the structure.

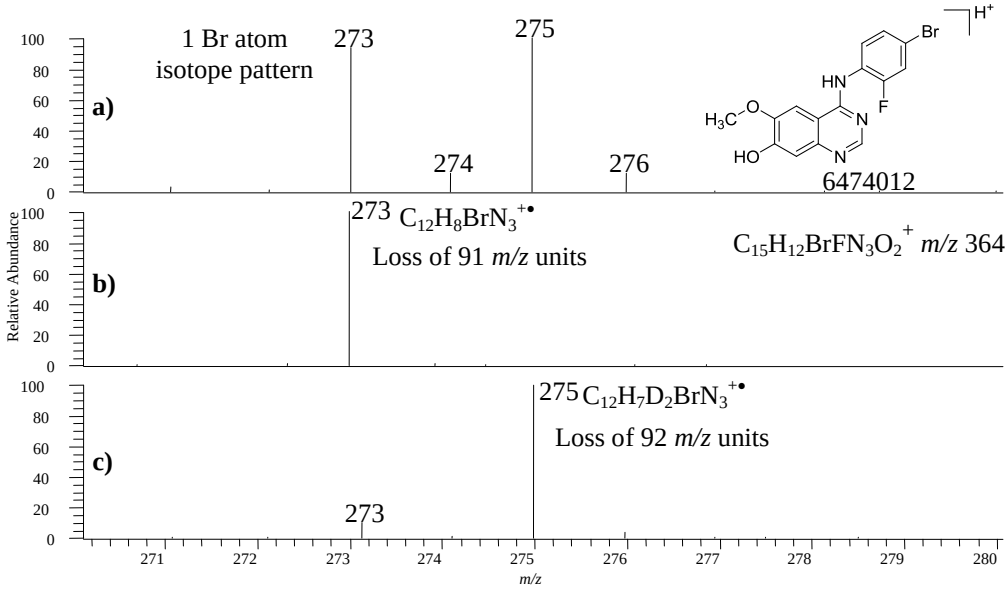

Figure 9.2 First generation electrospray product ion mass spectra of protonated 6474012: a) IW = 6 *m/z* units in MeOH, b) IW = 1 *m/z* units in MeOH, and c) IW = 1 *m/z* unit in MeOD.

The accurate mass measurement experiment supports the theory that a different species is formed. The most probable product ion at 272.9841 *m/z* units is $C_{12}H_8BrN_3^{+\bullet}$ (theoretical *m/z* 272.9896, error of -1.12 mDa (-4.1 ppm)) due to the loss of $C_3H_4FO_2^{\bullet}$. The loss $C_3H_4FO_2^{\bullet}$ as one molecule is rarely possible, because it would involve many structure rearrangements and the opening of the quinazoline rings. It is more probable that the loss of 91 *m/z* units is a concerted loss of $CH_3^{\bullet}$, HF, and two molecules of CO *via* a charge-remote fragmentation involving the formation of a new ring, Scheme 9.1. (The represented fragmentation happens as one reaction, but for the ease of understanding and following it, the fragmentation mechanism was broken to many steps.)

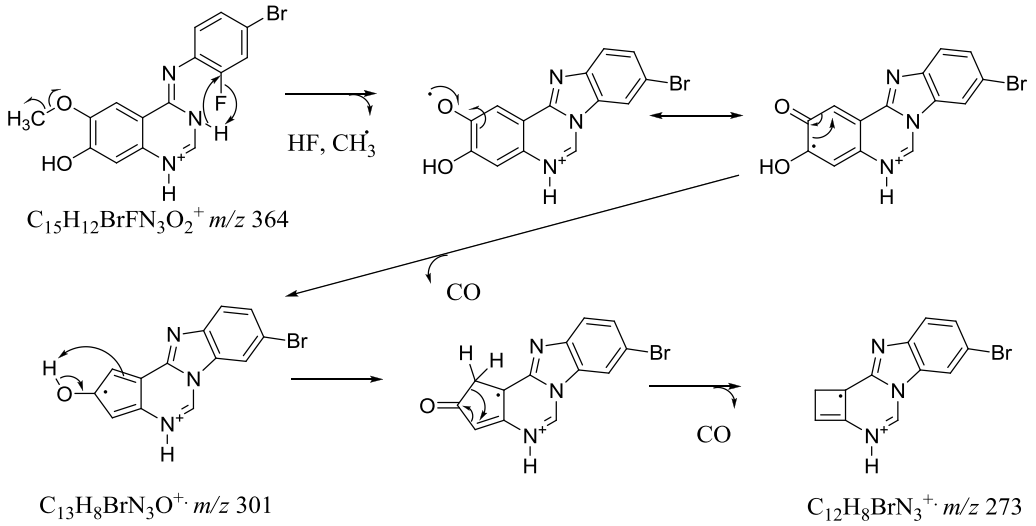

Scheme 9.1 Proposed mechanism pathway of formation of the *m/z* 273 from protonated molecule of 6474012; the loss of 91 *m/z* units is represented in separate reaction steps but the losses are eliminated together.

Comparison of the product ion mass spectra of protonated molecules of 6474008 and 6474012 show how easy the false-positive identification of the structure or its part can be possible. Protonated quinazolines fragment differently and although the benzyl radical is a characteristic loss, it may still cause an incorrect structural identification. The isobaric losses $C_7H_7^{\bullet}$ and $CH_3^{\bullet}$, HF, CO, and CO could cause a wrong characterisation of the structure if studies omit H/D exchange and/or accurate mass measurement experiments. HDX experiments are not commonly performed, but they are very crucial to support mechanistic pathways[221] and they can mark differences between formed product ions, but only if compounds contain different amounts of the exchangeable hydrogen atoms.[44,222] HDX may indicate whether the loss of 91 *m/z* units is coming from the benzyloxy- functional group or not. In addition, the use of accurate mass measurement experiments supports the proposed formulae.

9.2 Understanding intramolecular hydrogen-deuterium exchange in protonated quinazolines: the hydrogen scrambling effect and the mobile proton model

Most of the protonated quinazolines substituted with the benzyloxy- group at carbon 7 of the quinazoline ring form the product ion at 91 *m/z* units. The $C_7H_7^+$ may rearrange to the tropylium ion and different types of H/D exchange experiments can support the theory that the tropylium ion may be formed.[99] The studies of formation of tropylium ion from $C_7H_7^+$ have been mostly performed using EI MS hence it is not proven that tropylium ion can be formed when using ESI MS/MS. However, it is believed that the rearrangement of $C_7H_7^+$ to the tropylium ion can only take place when the carbon and hydrogen atoms bond energies are similar.[146] Moreover, similar values of the bond energies often result in the scrambling of the atoms. The process, when all (or some) hydrogen atoms in the specific substituent do not have a fixed position in the ion, (in this study, *e.g.* a benzyloxy- group in 2171003), is called the hydrogen scrambling effect (or partial hydrogen scrambling)[99,146] and it is only possible when the C-H bond can be broken and re-formed continuously, Scheme 9.2.

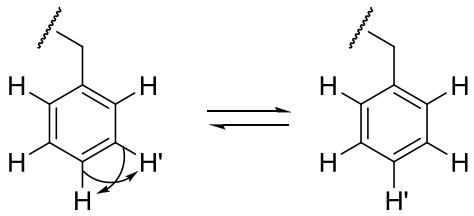

Scheme 9.2 Theoretical illustration of intramolecular hydrogen transfer known as hydrogen scrambling shown on the example of a benzyl substituent.

One of the most useful techniques to recognise the hydrogen transfer is the deuterium labelling experiment. The HDX experiments proven that the hydrogen scrambling effect happens in aromatic, heterocyclic, and methyl substituted ions.[84,99,107,146,223] In addition, the hydrogen scrambling is different for each

benzyl-substituted ions,[99] which may mean that the presence of different atoms affects the rates of rearrangement and the fragmentation reactions that become competitive.[99] Moreover, the hard labelling of the aromatic substituent with 13-C had proven the scrambling effect in many ions.[84]

The first generation product ion mass spectrum of protonated 2171003 (see Figure 9.3) was acquired in MeOD (Figure 9.4 displays analogous mass spectrum but acquired in MeOH). The base peak of product ion mass spectrum of protonated molecule of 2171003 is *m/z* 91, Figure 8.1 a), page 122. The *m/z* 92 contains a deuterium atom therefore during the fragmentation of deuterated molecule, it must rearrange to transfer the deuterium atom to the benzyloxy- substituent. The transfer of the H/D atoms within the −OBn and -OMe supports the theory that the *m/z* 91 in protonated 2171003 undergoes H scrambling or a structure rearrangement, which is believed to result in the formation of a tropylium ion (studied performed using EI MS).[99]

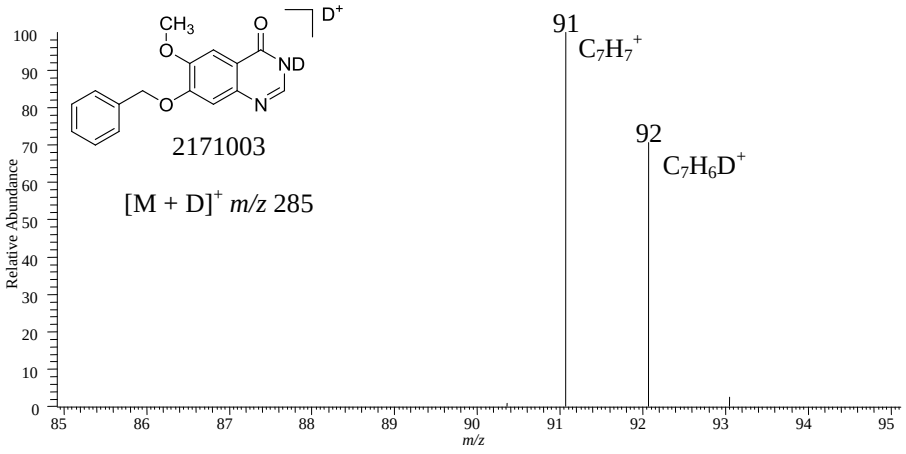

Figure 9.3 Positive ion electrospray first generation product ion mass spectrum of 2171003 in MeOD; IW = 1 *m/z* unit, *m/z* range 85-95.

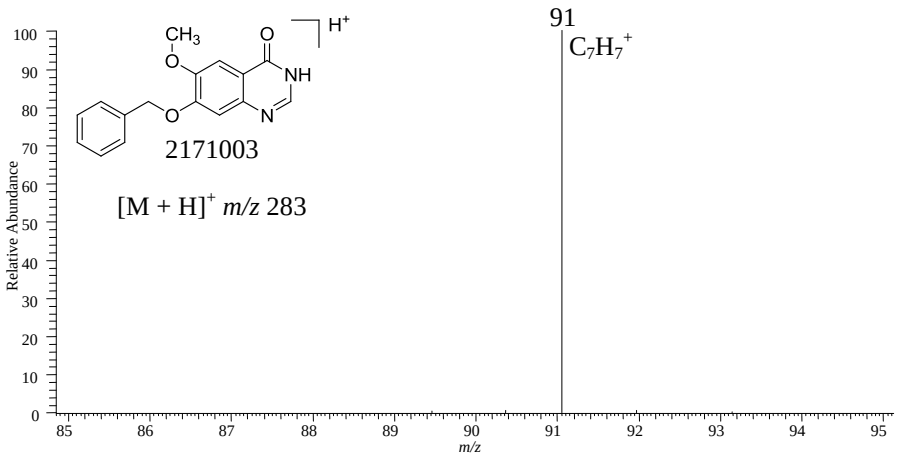

Figure 9.4 Positive ion electrospray first generation product ion mass spectrum of 2171003 in MeOH; IW = 1 *m/z* unit, *m/z* range 85-95.

All protonated quinazolines that form *m/z* 91, also form a product ion at 92 *m/z* units when D-labelling experiments are performed. Therefore, the *m/z* 91 in protonated quinazolines partially rearranges, which proves that hydrogen atoms do not have a fixed position in a benzyloxy- functional group causing the one intramolecular hydrogen transfer, which could be called a partial hydrogen scrambling effect.[84,223] The deuterium atom most probably charges the oxygen atom at carbon 7 of the quinazoline ring resulting in an exchange of deuterium with hydrogen atom of the $=CH_2$ or benzyl group, Reaction 9.1.

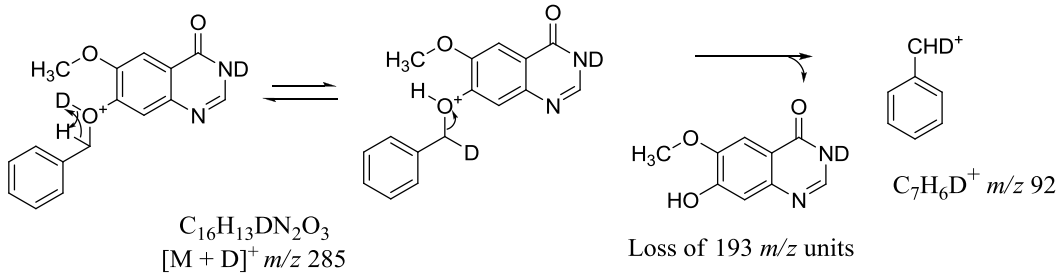

Reaction 9.1 Proposed mechanism of formation *m/z* 92 involving the intramolecular hydrogen/deuterium transfer in protonated 2171003 prior to fragmentation.

Similarly to the benzyloxy- substituent, the presence of methoxy- group supports the hydrogen scrambling effect in protonated quinazolines. The characteristic loss of 15 *m/z* units (mass spectrum acquired from the sample dissolved in methanol) is often accompanied with the peak corresponding to the loss of 16 *m/z* units, $CH_2D^{\bullet}$, when H/D exchange experiments are performed, Figure 9.5 (Figure 9.6 displays the analogous mass spectrum but acquired in MeOH).

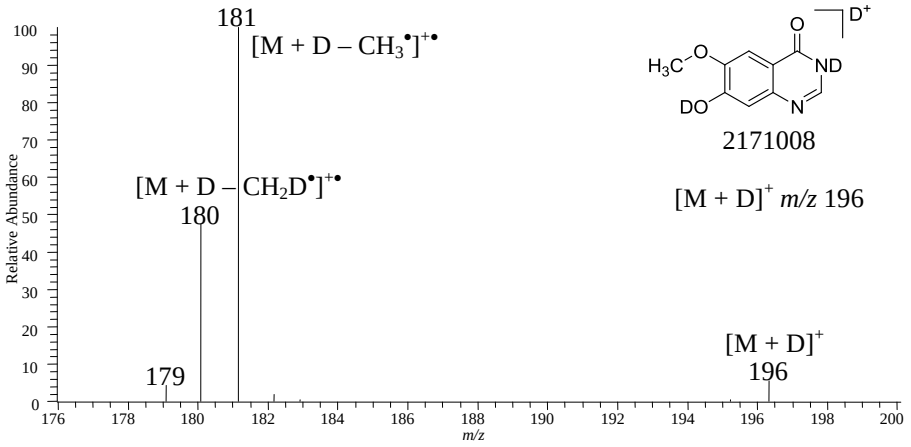

Figure 9.5 Positive ion electrospray first generation product ion mass spectrum of 2171008 in MeOD; IW = 1 *m/z* unit, *m/z* range 176-200.

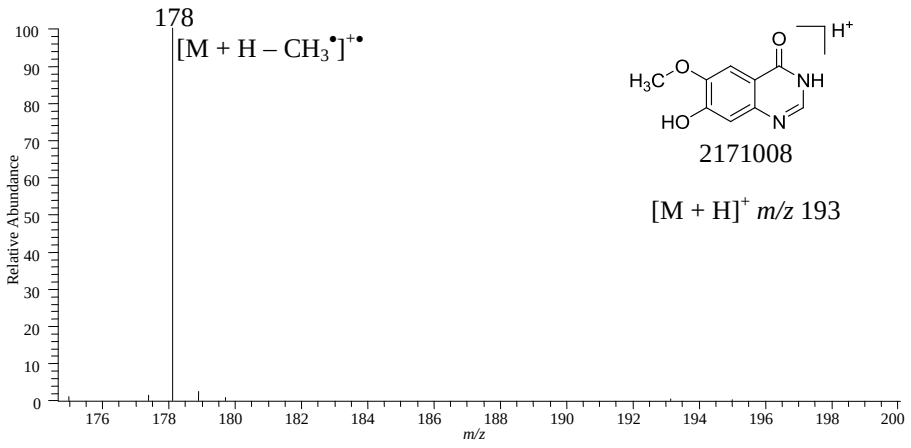

Figure 9.6 Positive ion electrospray first generation product ion mass spectrum of 2171008 in MeOH; IW = 1 *m/z* unit, *m/z* range 176-200.

The analyses of quinoline ions showed that the hydrogen scrambling effect also involves all hydrogen atoms in the quinoline ring,[84,146] therefore it could be expected that the hydrogen atoms in the quinazoline ring may not have a fixed position in the molecule, either. Compound 2171003 has two exchangeable hydrogen atoms and the transfer of two deuterium atoms into the –OBn group happened to approximately 5 % of formed product ion, *m/z* 93, Figure 9.3. One of the labile hydrogen atoms is the result of the hydrogen scrambling in the protonated quinazoline and the other hydrogen atom protonates the molecule and migrates to the benzyloxy- functional group to form a product ion at *m/z* 93. The charge may be positioned on the carbon atom of the methyl group, however it is more probable that it would be placed on one of the heteroatoms in the molecule. Therefore, the charge would have to be transferred to allow the intramolecular H/D exchange within the hydrogen atom from the methyl group. The charge migration from its initial position before the fragmentation is known as the mobile proton model.[224-226]

Compounds with multiple sites of protonation may add the proton to all of the sites, however some of them are more basic and hence they will be preferable sites for the protonation.[224] The protonation at the most basic site results in formation of the most stable ion.[65] It was found that just before fragmentation, the site of protonation changes, because of the decreasing kinetic energy of ions, changes of internal energy, geometry, and formation of different transition states of the ion.[224] In addition, the transfer of the protonation site mostly happens when low-energy dissociation methods are used, such as low-energy CID (as in these studies). The low-energy CID causes the dissociation of the ions mostly *via* a charge-directed fragmentation (the high-energy CID favours a charge-remote fragmentation).[217,227,228]

If it is true that the types of fragmentation depend upon the type of the ion dissociation method, in experiments performed using low-energy CID, the protonated molecules must transfer the proton readily between different sites of protonation resulting in "a heterogeneous population of structures".[217,229,230] The

population of different protonated forms depends on the internal energy and the proton affinities of the different protonation sites of the ions.[228] This hypothesis supports the approach presented in Chapter 8.5 (page 137), where populations of different forms of protonated molecules and product ions are identified. In addition, it helps to explain why the product ion at *m/z* 93 [$C_7H_5D_2^+$] in 2171003 can be actually formed, Figure 9.3.

Despite the mobile proton effect, the structure prior to its fragmentation, can rearrange, which would additionally result in a partial hydrogen scrambling effect. There is no possibility to distinguish, which deuterium atom in the protonated molecule of 2171003 is involved in the formation of product ion at *m/z* 92, Figure 9.3. It may be an effect of the internal hydrogen transfer as well as the mobile proton effect.

Consequently, the analyses using low-energy CID in MeOD can result in formation of product ions with the shifted mass-to-charge ratios, which means that hydrogen atoms lose the fixed, positional identity.[221] In other words, the compounds with active (labile) hydrogen atoms result in a randomisation of the position of every hydrogen atom followed by an equilibrium of all possible species formed before the fragmentation, which, in H/D exchange, is visible by formation of different +1, +2, *etc. m/z* units product ions.[229] So, although the HDX helps to essentially understand gas-phase ion chemistry[221] and it is a powerful technique to distinguish isomeric structures (Chapter 9.1, page 145),[220] it is often not beneficial; it enhances the complexity of mass spectral data interpretation and therefore needs to be supported by other experiments,[84,99] *e.g.* accurate mass measurement.[220] Thus, the interpretation of the mechanistic pathways of protonated molecules where the hydrogen atoms have a fixed position is easier.[44]

9.3 Summary

The isobaric losses of 91 *m/z* units between quinazoline ions are possible and the addition of HDX and AMM experiments to a standard MS/MS experiment improves structural elucidation studies and confidence of mass spectral data assignment. However, the hydrogen atoms of protonated quinazolines can be labile, which results in the hydrogen scrambling (methyl and benzyl group) and mobile proton effects. These effects often improve understanding of the fragmentation behaviour of protonated quinazolines, although may often add complexity to the mass spectral data evaluation.

The mobile proton model theory supports the discussion of performed calculations in Chapter 8.5, page 137. The forms of the radical cation that correlate to the experimental data must be formed due to the charge transfer prior to fragmentation, Scheme 8.8.

Chapter 10 Characteristic interpretation rules for positive ion first generation product ion mass spectra of protonated quinazolines

This chapter presents the summary of observations concerning specific and typical MS/MS fragmentation patterns of protonated quinazolines. The "Standard Interpretation Procedure"[65] should be used as a basis to help interpret the first generation product ion mass spectral data of protonated quinazolines.

Quinazolines substituted with different functional groups on carbon 4, 6, 7, and 8 of the quinazoline ring were studied, therefore the summarised observations may not be applicable to the protonated quinazolines with same functional group on different carbon of the quinazoline ring. It should be noted that the presented rules may not be valid for 100 %; they present the most expected product ions and losses of first generation product ion mass spectra of protonated quinazolines.

It was found when using CID MS/MS that odd-electron product ions are commonly formed from most of the protonated quinazolines. Further, these fragmentation mechanisms are predominantly influenced by the specific functional groups. The descending order of strength of influence of the different functional groups on the fragmentation behaviour of protonated quinazolines is: non-aromatic groups (morpholine, pyrrolidine, piperidine groups) > halogen atoms (Br, F) > –OBn > –OMe > –OH. Interestingly, no specific product ions or losses have been formed from the indole group substituted on the 4 carbon in the quinazoline ring. The indole group may not influence the fragmentation behaviour of protonated quinazolines in a strong way as above functional groups displayed in the descending order.

1. If the product ion formed in the first generation product ion mass spectrum of unknown protonated quinazoline is *m/z* 128 or 112, the quinazoline ion

may be formed from a non-aromatic group with at least one heteroatom, (a heteroatom improves the probability to retain the charge). It was found that protonated 7-non-aromatic-quinazolines including a morpholine ring form a base peak at *m/z* 128 ($C_7H_{14}NO^+$) and the protonated quinazolines substituted with pyrrolidine and piperidine rings form base peaks at *m/z* 112 ($C_7H_{14}N^+$), Chapter 6, page 89.

2. The product ion $[M + H - 56]^+$ suggests that the protonated quinazoline contains a *tert*-butyl group that is eliminated in a form of C_4H_8, Chapter 6, page 89.

3. The loss of 15 *m/z* units indicates the loss of methyl radical, which is probably formed from the methoxy- group in the protonated quinazoline. 6(or 7)-methoxy-quinazoline ions form the product ion (often base peak), $[M + H - 15]^{+\bullet}$, due to the loss of methyl radical, Chapter 7, page 105.

4. Halogen atoms strongly affect the MS/MS fragmentation of protonated quinazolines (although not as strongly as the non-aromatic groups; see the strength order above). The specific losses that indicate the involvement of a halogen atom in the fragmentation mechanisms of protonated quinazolines are:

   i) even-electron losses: loss of 80 *m/z* units (HBr) and loss of 20 *m/z* units (HF),
   ii) odd-electron radical losses: loss of 79 *m/z* units ($Br^\bullet$), loss of 63 *m/z* units ($CH_3^\bullet$, HF, and CO), loss of 91 *m/z* units ($CH_3^\bullet$, HF, CO, and CO),
   iii) bi-radical losses: loss of 98 *m/z* units ($F^\bullet$ and $Br^\bullet$); loss of 114 *m/z* units, ($CH_3^\bullet$, HF, and $Br^\bullet$).

   All of these characteristic losses can be observed in one product ion mass spectrum if the protonated quinazoline contains a Br, F or –OMe group, (Chapter 7, page 105).

5. The observed product ion at 91 *m/z* units, $[M + H - 91^{\bullet}]^{+\bullet}$, or $[M + H - 92]^{+}$ immediately suggests that the protonated quinazoline contains the benzyloxy- group. 6 (or 7)-benzyloxy-quinazolines often form three product ions *i.e.* $C_7H_7^{+}$, product ion due to the loss of benzyl radical, $C_7H_7^{\bullet}$, which is often accompanied with the product ion formed due to the loss of toluene, C_7H_8, Chapter 7, page 105.

   A notable exception to this is the isobaric loss of 91 *m/z* units that can be i) $C_7H_7^{\bullet}$ or ii) $CH_3^{\bullet}$, HF, CO, and CO, Chapter 9, page 145. Obviously, the interpretation of fragmentation behaviour of structurally known protonated quinazolines is easier than an interpretation of mass spectrum of structurally unknown species. For example, the information whether the protonated quinazoline is or is not substituted with a benzyloxy- group would require to perform necessary experiments to support the identification of the loss. The HDX and/or AMM experiments are crucial to ensure a rapid identification of two isobaric losses of 91 *m/z* units, but HD exchange characterises with a lower cost of experiment than accurate mass measurement. It was observed that when loss of 91 *m/z* units is accompanied with the loss of 92 *m/z* units the loss of 91 *m/z* units is the odd-electron loss of $C_7H_7^{\bullet}$ and the loss of 92 *m/z* units is the even-electron loss that may be formed readily from odd-electron product ion by the elimination of $H^{\bullet}$. The loss of $C_7H_7^{\bullet}$ can be confirmed by HDX experiment as no mass shift in the loss would be observed. The shift of mass-to-charge ratio to the loss of 92 *m/z* units indicates that the loss must contain one active hydrogen atom; the loss of $CH_3^{\bullet}$, HF, CO, and CO in D-labelling experiment involves a loss of DF (or $CH_2D^{\bullet}$). This loss is often accompanied with product ions due to the loss of 63 ($CH_3^{\bullet}$, HF, CO), and 15 ($CH_3^{\bullet}$) *m/z* units, which additionally supports the identification of the isobaric loss. However, the observations based on HDX experiments may not be applicable to all protonated quinazolines as they depend on the site of protonation, which possibly may involve different types of fragmentation mechanism. It should be noted that HDX experiments may

be more complex for identification of quinazoline product ions. It was found that the hydrogen atoms of the methyl and benzyl groups of the protonated quinazolines may not have a fixed position hence the partial H-scrambling effect is common, which results in formation of additional product ions as mass-to-charge ratios are shifted to +1 and/or +2 *m/z* units, Chapter 9, page 145.

The use of different ion activation methods, *i.e.* CID, SORI/CID, and IRMPD should not affect the formation of the base peak of the protonated quinazolines, but the other product ions may differ in abundance and (less observed) in *m/z* units value. The first generation CID product ion mass spectra of protonated quinazolines may contain many product ions formed due to small *m/z* units losses (*i.e.* losses up to 70 *m/z* units). Whereas first generation SORI/CID and IRMPD product ion mass spectra of protonated quinazolines often have fewer product ions.

The product ions formed due to the odd-electron fragmentation processes, such as radical cations and bi-radicals, are often observed when using SORI/CID and in-time CID as ion activation methods, and the even-electron fragmentation type dissociations are less common (excluding quinazolines substituted with non-aromatic groups). On the contrary, the even-electron product ions are more common in first generation product ion mass spectra acquired using IRMPD and in-space CID than in in-time tandem mass spectrometry experiments, Chapter 8, page 121.

Concluding remarks

This study has presented analyses of protonated quinazolines using tandem mass spectrometry approaches. The fragmentation mechanisms of the protonated quinazolines are structurally dependent and the investigated functional groups can be placed in the descending order of strength of influence on the fragmentation behaviour of protonated quinazolines, *i.e.* non-aromatic groups (morpholine, pyrrolidine, piperidine groups) > halogen atoms (Br, F) > –OBn > –OMe > –OH.

Protonated non-aromatic quinazolines revealed formation of typical even-electron product ions and/or losses, which agrees with the even-electron rule. Odd-electron processes, which result in the formation of radical cations or bi-radicals, were found to dominate the fragmentation pathways of the majority of protonated quinazoline (without a non-aromatic substituent) and hence disagree with the even-electron rule. The odd-electron base peak was often formed from protonated CHNO quinazolines and a specific cascade of radical losses, which caused formation of radical cations and bi-radicals, was common for protonated quinazolines substituted with halogen atoms.

The H/D exchange and accurate mass measurement experiments have proven to be crucial in structural elucidation studies of protonated quinazolines to distinguish isobaric losses (*i.e.* loss of 91 *m/z* units can be a loss of $C_7H_7^{\bullet}$ or $CH_3^{\bullet}$, HF, CO, and CO). The AMM and H/D exchange experiments help to narrow a number of possible formulae and possible dissociation mechanisms of protonated quinazolines. In addition, the D-labelling experiments have supported the theory that hydrogen atoms in methyl and benzyl group of protonated quinazolines do not have a fixed position and can undergo partial hydrogen scrambling effect.

The fragmentation behaviour of three protonated positional isomers of quinazolines analysed using ESI-CID MS/MS has been compared to the mass spectral data of the positional isomers acquired using different ion sources (*i.e.* ESI, APCI, and APPI) and mass analysers (*i.e.* ICR cell, QqQ, and QTOF). It was

found that the choice of the mass analyser and the ion source may affect the abundances of product ions although further studies, on larger amount of compounds, are necessary.

DFT calculations have been used to calculate enthalpies of protonation of all possible forms of protonated molecule and product ion for the protonated positional isomers, which resulted in a possibility to predict the protonation sites and identify as well as quantify in percentage values the most thermodynamically stable forms of the protonated molecules and product ions. Protonated quinazolines can have many protonation sites resulting in formation of heterogeneous population of forms of protonated molecule and product ion, *e.g.* compound 2171003 has four thermodynamically stable forms of protonated molecule, Scheme 8.8, page 141. However, the dissociation process may cause transfer of the proton and formation of the form of the product ion with a different protonation site than forms of the protonated molecule. For example, *m/z* 192 formed from protonated 2171003 has additional form of product ion, e', which must involve a transfer of a proton from one of the forms of protonated molecule (a, b, c, or d), Scheme 8.8, page 141. The transfer of the proton to a different heteroatom prior the fragmentation agrees with the mobile proton model. Thus, protonated quinazolines form a heterogeneous population of forms of protonated molecules initially, but the proton can be mobile and it can transfer to different sites prior the fragmentation.

In addition, the quantified, theoretical percentage probability values of formation of specific forms of product ions have been compared to the experimental abundances of the radical cation product ions of the positional isomers. It was found that the correlation of product ion intensity to theoretical percentage values is within 10 % error in abundance, which gives a promising approach to predict intensities of product ions formed in tandem mass spectrometry experiments as well as it helps to define specific dissociation pathways of protonated quinazolines. Consequently, the link between mass spectrometry and density functional calculations allows better understanding of dissociation mechanisms of

protonated quinazolines and can aid MS/MS data prediction and structural elucidation of possibly other classes of small molecules.

As for the future aspect of these studies, the combination of rule-based software with a DFT approach may efficiently advance predictive science forward and help to understand the fragmentation behaviour of protonated gas-phase molecules. However, utilisation of HDX and AMM experiments is just as important as understanding physical-organic properties of molecules in a gas phase. If both approaches were used then they could be built into computational rule-based DFT software for structural elucidation.

Appendices

Appendix 1

The first appendix presents structures of analysed compounds with their trivial AZ name. The seven digits represent the numeric code to identify the compounds that are placed in Table A.1.1 in ascending order. First four digits define the project code of the lead compound the impurity comes from, *i.e.* Cediranib 2171, Vandetanib 6474, and Gefitinib 1839. The last three digits complement the code numbers to the unique compound code. The accurate mass measurement and double bond equivalents (DBE) values of protonated molecules help to support the proposed mechanism pathways and structural forms of the product ions.

Table A.1.1 List of analysed compounds from AstraZeneca.

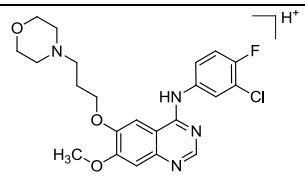 Gefitinib/CRUDE – 1839001 $C_{22}H_{24}ClFN_4O_3$ $[M + H]^+$ *m/z* 447.1594 DBE = 11.5	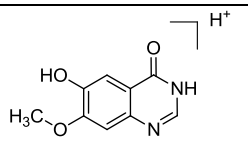 hydroxyone – 1839006 $C_9H_8N_2O_3$ $[M + H]^+$ *m/z* 193.0608 DBE = 6.5
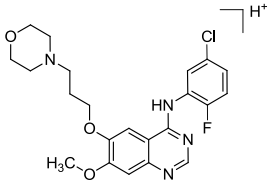 5 Cl 2 F analogue – 1839011 $C_{22}H_{24}ClFN_4O_3$ $[M + H]^+$ *m/z* 447.1594 DBE = 11.5	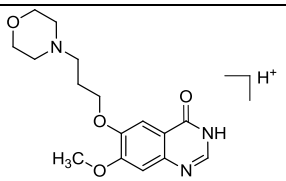 Quinazolone analogue – 1839012 $C_{16}H_{21}N_3O_4$ $[M + H]^+$ *m/z* 320.1605 DBE = 7.5
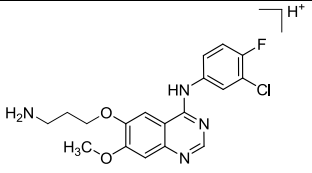 Amino an – 1839013 $C_{18}H_{18}ClFN_4O_2$ $[M + H]^+$ *m/z* 377.1175 DBE = 10.5	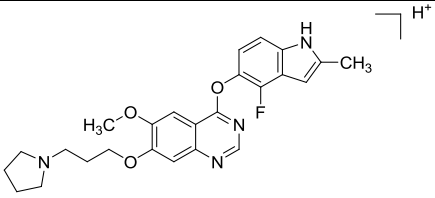 Cediranib/Crude – 2171001 $C_{25}H_{27}FN_4O_3$ $[M + H]^+$ *m/z* 451.2140 DBE = 13.5

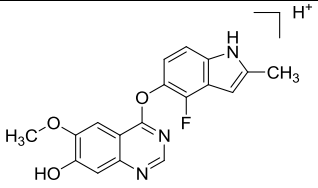 Indole Phenol – 2171002 $C_{18}H_{14}FN_3O_3$ $[M + H]^+$ *m/z* 340.1092 DBE = 12.5	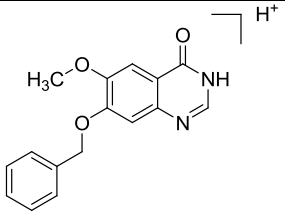 BQ – 2171003 $C_{16}H_{14}N_2O_3$ $[M + H]^+$ *m/z* 283.1077 DBE = 10.5
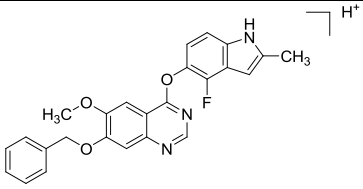 BQ indole – 2171004 $C_{25}H_{20}FN_3O_3$ $[M + H]^+$ *m/z* 430.1561 DBE = 16.5	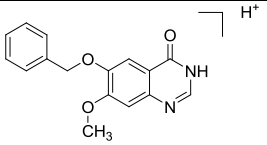 BQ isomer – 2171005 $C_{16}H_{14}N_2O_3$ $[M + H]^+$ *m/z* 283.1077 DBE = 10.5
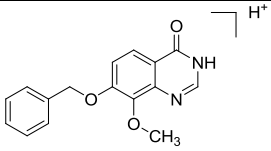 8-methoxy BQ – 2171006 $C_{16}H_{14}N_2O_3$ $[M + H]^+$ *m/z* 283.1077 DBE = 10.5	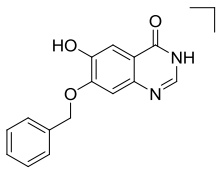 6-hydroxy – 2171007 $C_{15}H_{12}N_2O_3$ $[M + H]^+$ *m/z* 269.0921 DBE = 10.5
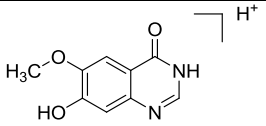 7-hydroxy – 2171008 $C_9H_8N_2O_3$ $[M + H]^+$ *m/z* 193.0608 DBE = 6.5	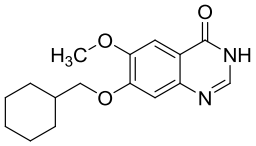 CMQN – 2171011 $C_{16}H_{20}N_2O_3$ $[M + H]^+$ *m/z* 289.1547 DBE = 7.5
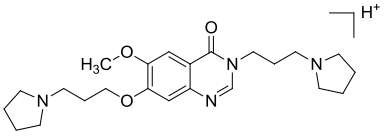 N,O-dialkyl – 2171015 $C_{23}H_{34}N_4O_3$ $[M + H]^+$ *m/z* 415.2704 DBE = 8.5	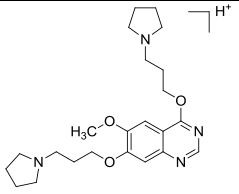 O,O-dialkyl – 2171016 $C_{23}H_{34}N_4O_3$ $[M + H]^+$ *m/z* 415.2704 DBE = 8.5

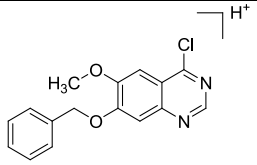

chlorobenzyline – 2171017
$C_{16}H_{13}ClN_2O_2$
$[M + H]^+$ *m/z* 301.0738
DBE = 10.5

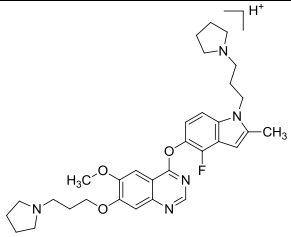

n-alkyl – 2171018
$C_{32}H_{40}FN_5O_3$
$[M + H]^+$ *m/z* 562.3188
DBE = 14.5

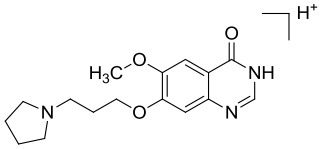

quinazolone – 2171021
$C_{16}H_{21}N_3O_3$
$[M + H]^+$ *m/z* 304.1656
DBE = 7.5

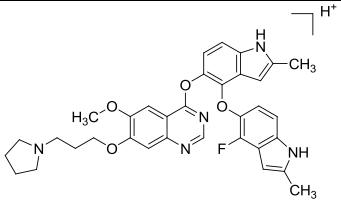

O-dimer – 2171022
$C_{34}H_{34}FN_5O_4$
$[M + H]^+$ *m/z* 596.2668
DBE = 19.5

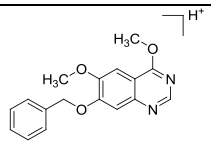

Methoxy BQ – 2171023
$C_{17}H_{16}N_2O_3$
$[M + H]^+$ *m/z* 297.1234
DBE = 10.5

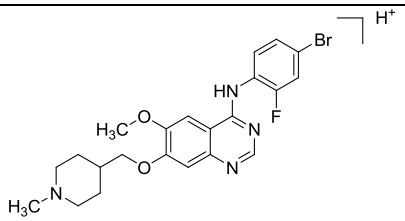

Vandetanib/Crude – 6474001
$C_{22}H_{24}BrFN_4O_2$
$[M + H]^+$ *m/z* 475.1139
DBE = 11.5

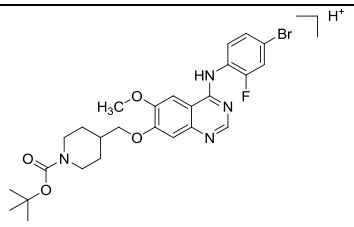

BDC (Boc deriv crude) – 6474002
$C_{26}H_{30}BrFN_4O_4$
$[M + H]^+$ *m/z* 561.1507
DBE = 12.5

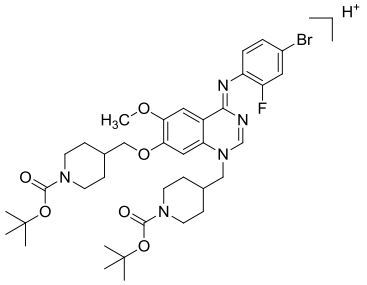

1 alkyl BDC – 6474003a
$C_{37}H_{49}BrFN_5O_6$
$[M + H]^+$ *m/z* 758.2923
DBE = 14.5

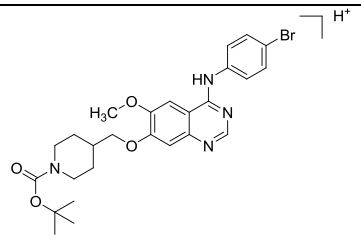 Des fluoro BDC – 6474004 $C_{26}H_{31}BrN_4O_4$ $[M + H]^+$ *m/z* 543.1601 DBE = 12.5	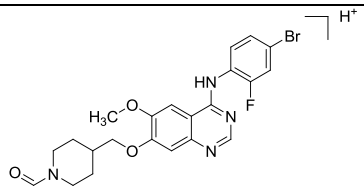 N formyl – 6474006 $C_{22}H_{22}BrFN_4O_3$ $[M + H]^+$ *m/z* 489.0932 DBE = 12.5
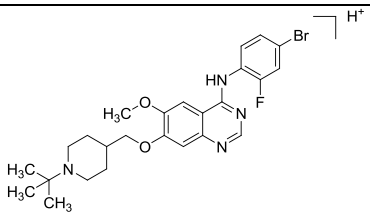 T butyl – 6474007 $C_{25}H_{30}BrFN_4O_2$ $[M + H]^+$ *m/z* 517.1609 DBE = 11.5	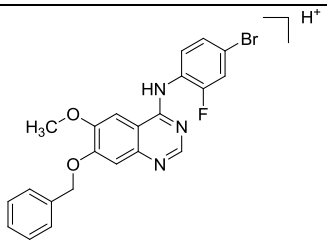 Benzanilide – 6474008 $C_{22}H_{17}BrFN_3O_2$ $[M + H]^+$ *m/z* 454.0561 DBE = 14.5
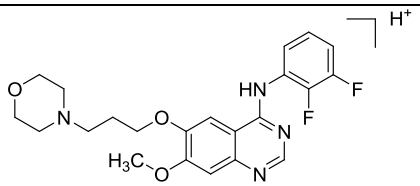 2,3 difluoro analouge – 6474010 $C_{22}H_{24}F_2N_4O_3$ $[M + H]^+$ *m/z* 431.1889 DBE = 11.5	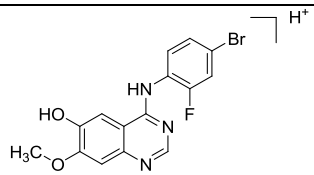 MA isomer – 6474011 $C_{15}H_{11}BrFN_3O_2$ $[M + H]^+$ *m/z* 364.0091 DBE = 10.5
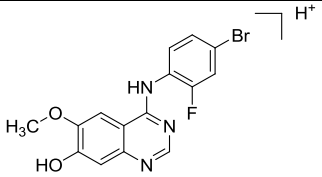 MA – 6474012 $C_{15}H_{11}BrFN_3O_2$ $[M + H]^+$ *m/z* 364.0091 DBE = 10.5	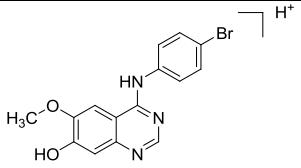 Des fluoro MA – 6474013 $C_{15}H_{12}BrN_3O_2$ $[M + H]^+$ *m/z* 346.0186 DBE = 10.5
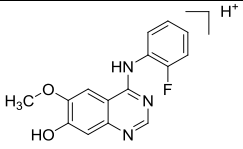 Des bromo MA – 6474014 $C_{15}H_{12}FN_3O_2$ $[M + H]^+$ *m/z* 286.0986 DBE =10.5	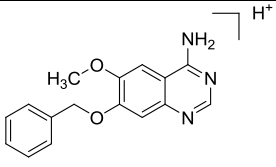 4amino MA – 6474015 $C_{16}H_{15}N_3O_2$ $[M + H]^+$ *m/z* 282.1237 DBE = 10.5

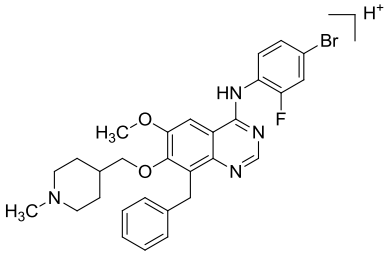

8 benzyl – 6474016
$C_{29}H_{30}BrFN_4O_2$
$[M + H]^+$ *m/z* 565.1609
DBE =15.5

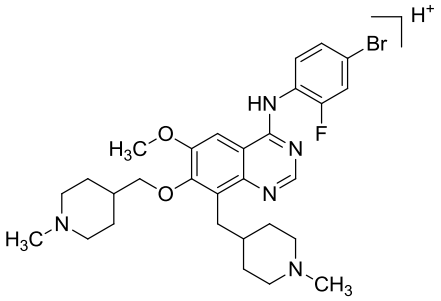

8 alkyl 92b crude – 6474017
$C_{29}H_{37}BrFN_5O_2$
$[M + H]^+$ *m/z* 586.2187
DBE = 12.5

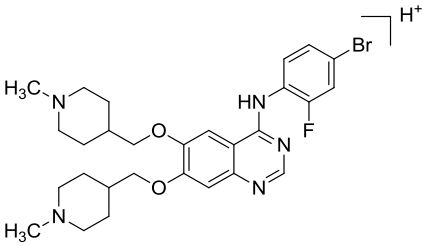

6-alkyl 93b crude – 6474018
$C_{28}H_{35}BrFN_5O_2$
$[M + H]^+$ *m/z* 572.2031
DBE = 12.5

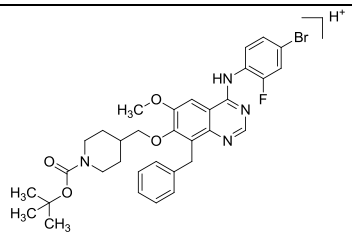

8Bz BDC – 6474019
$C_{33}H_{36}BrFN_4O_4$
$[M + H]^+$ *m/z* 651.1977
DBE = 16.5

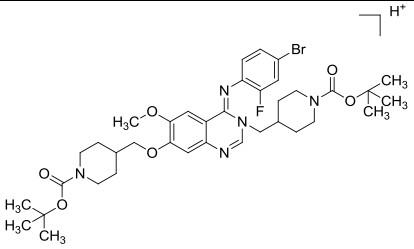

3-alkyl BDC – 6474020
$C_{37}H_{49}BrFN_5O_6$
$[M + H]^+$ *m/z* 758.2923
DBE = 14.5

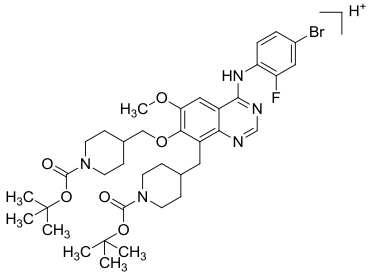

8-alkyl BDC – 6474021
$C_{37}H_{49}BrFN_5O_6$
$[M + H]^+$ *m/z* 758.2923
DBE = 14.5

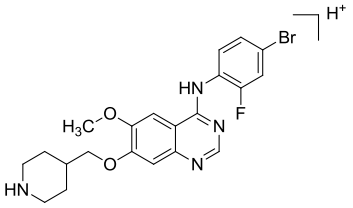

Des methyl – 6474022
$C_{21}H_{22}BrFN_4O_2$
$[M + H]^+$ *m/z* 461.0983
DBE = 11.5

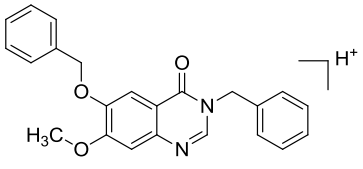

36 diBz 7 methoxy BQ – 6474023
$C_{23}H_{20}N_2O_3$
$[M + H]^+$ *m/z* 373.1547
DBE = 14.5

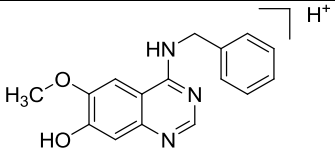

4-benzyloamino – 6474027
$C_{16}H_{15}N_3O_2$
$[M + H]^+$ *m/z* 282.1237
DBE = 10.5

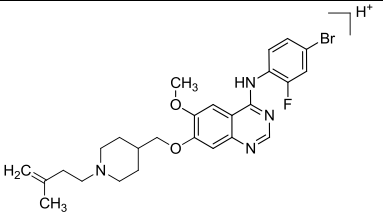

C5 imp – 6474030
$C_{26}H_{30}BrFN_4O_2$
$[M + H]^+$ *m/z* 529.1609
DBE = 12.5

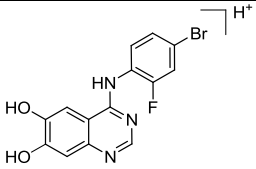

6,7di OH MA – 6474032
$C_{14}H_9BrFN_3O_2$
$[M + H]^+$ *m/z* 349.9935
DBE = 10.5

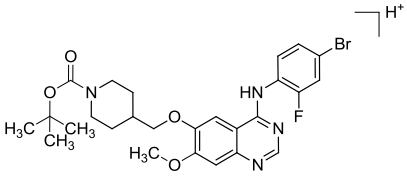

BDC isomer – 6474033
$C_{26}H_{30}BrFN_4O_4$
$[M + H]^+$ *m/z* 561.1507
DBE = 12.5

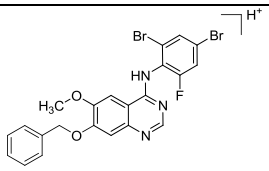

24 di Br 6FA MA – 6474034
$C_{22}H_{16}Br_2FN_3O_2$
$[M + H]^+$ *m/z* 531.9666
DBE = 14.5

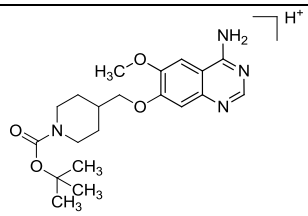

4 amino BDC imp – 6474036
$C_{20}H_{28}N_4O_4$
$[M + H]^+$ *m/z* 389.2173
DBE = 8.5

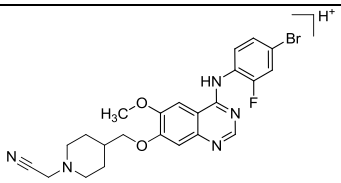

nitryle – 6474038
$C_{23}H_{23}BrFN_5O_2$
$[M + H]^+$ *m/z* 500.1092
DBE = 13.5

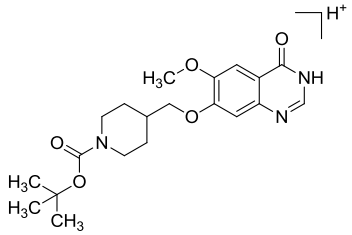

Quinazolone BDC – 6474040
$C_{20}H_{27}N_3O_5$
$[M + H]^+$ *m/z* 390.2023
DBE = 8.5

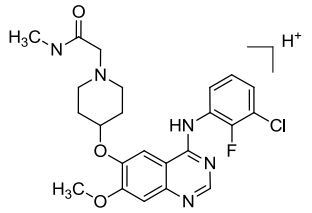 Crude – 8931001 $C_{23}H_{25}ClFN_5O_3$ $[M + H]^+$ *m/z* 474.1703 DBE = 12.5	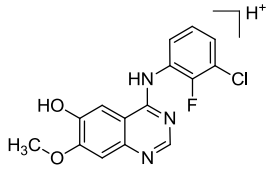 hydroxyanilide – 8931006 $C_{15}H_{11}ClFN_3O_2$ $[M + H]^+$ *m/z* 320.0597 DBE = 10.5

Appendix 2

This appendix consists of first generation product ion mass spectra that support the results and discussion chapters. Figures are ordered from the first to the last R&D chapter to annotate which chapter they belong to.

Supplementary information to Chapter 6, page 89

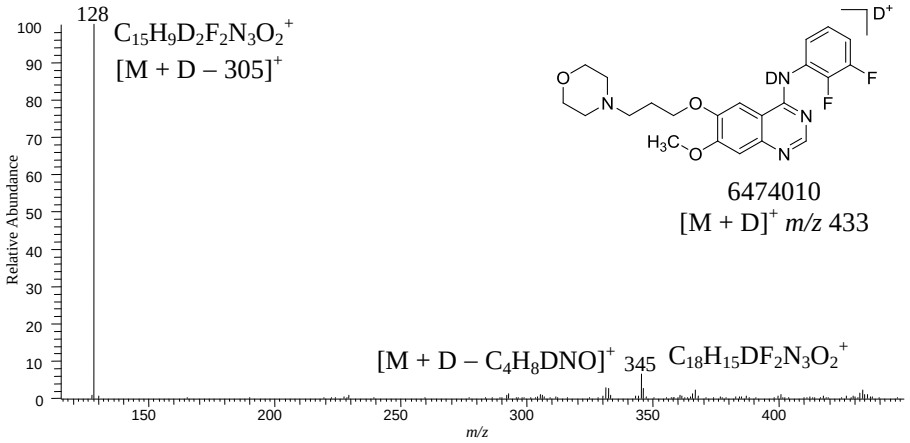

Figure A.2.1 Positive ion electrospray first generation product ion mass spectrum of 6474010 in MeOD, IW = 1 *m/z* unit.

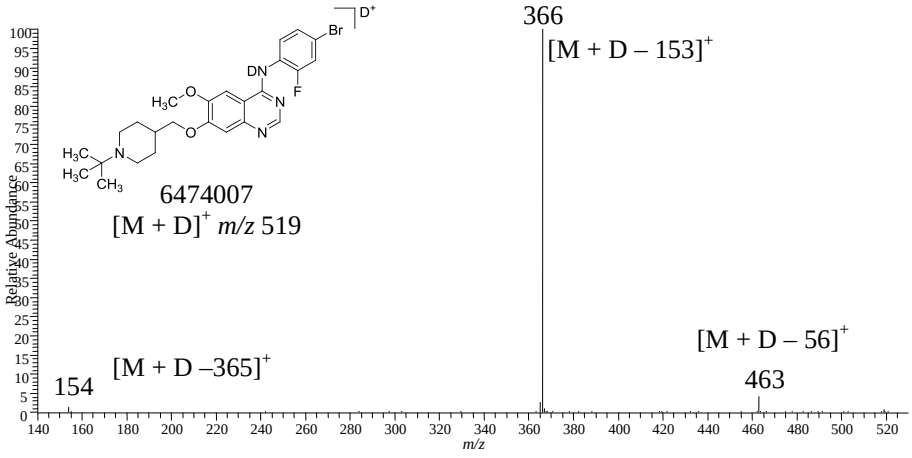

Figure A.2.2 Positive ion electrospray first generation product ion mass spectrum of 6474007 in MeOD, IW = 1 *m/z* unit.

Supplementary information to Chapter 7, page 105

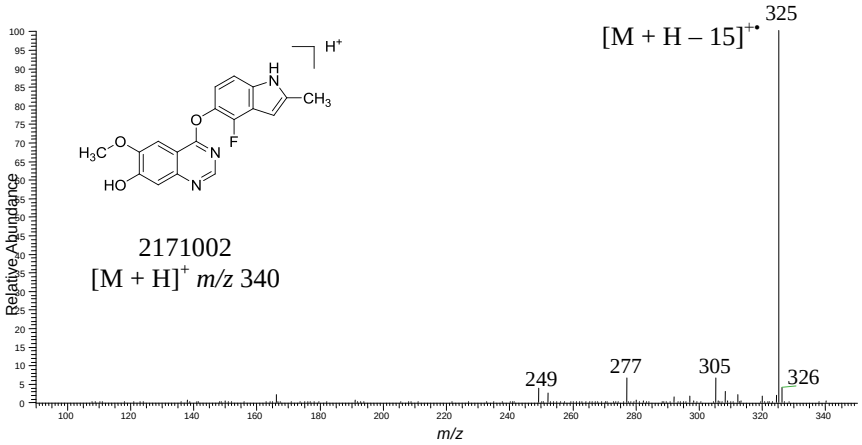

Figure A.2.3 Positive ion electrospray first generation product ion of 2171002 in MeOH, IW = 1 *m/z* unit; loss of 15 *m/z* units (loss of $CH_3^{\bullet}$).

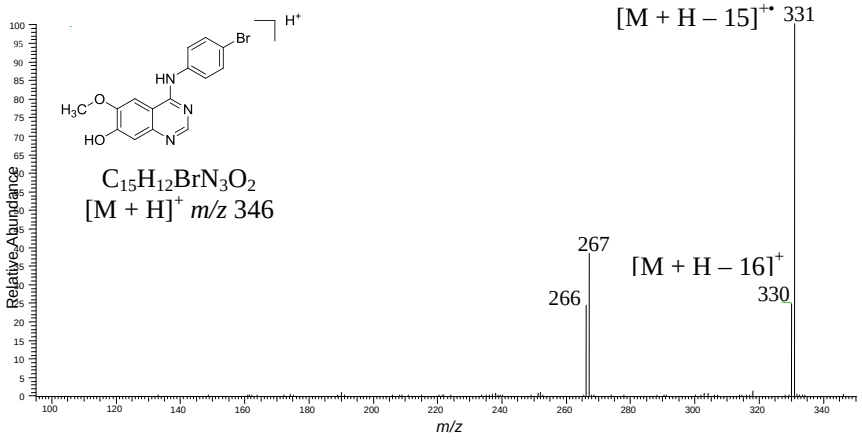

Figure A.2.4 Positive ion electrospray first generation product ion mass spectrum of 6474013 in MeOH, IW = 1 *m/z* unit; loss of 15 and 16 *m/z* units (loss of $CH_3^{\bullet}$ and CH_4, respectively).

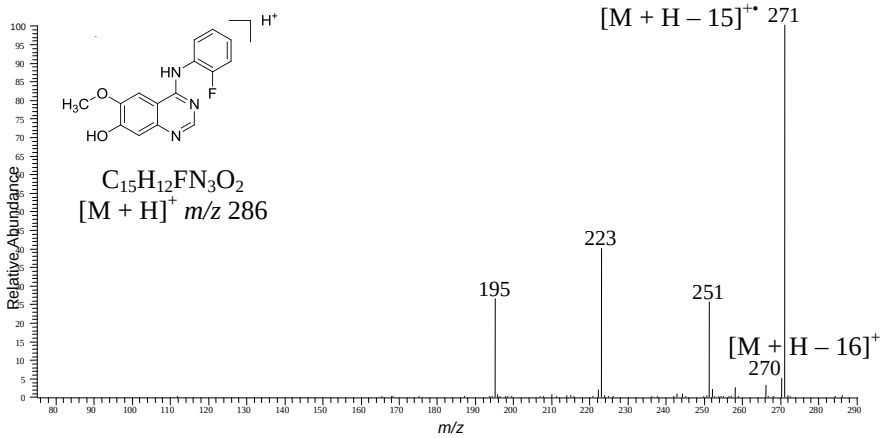

Figure A.2.5 Positive ion electrospray first generation product ion mass spectrum of 6474014 in MeOH, IW = 1 *m/z* unit; loss of 15 and 16 *m/z* units is a loss of $CH_3^{\bullet}$ and CH_4, respectively.

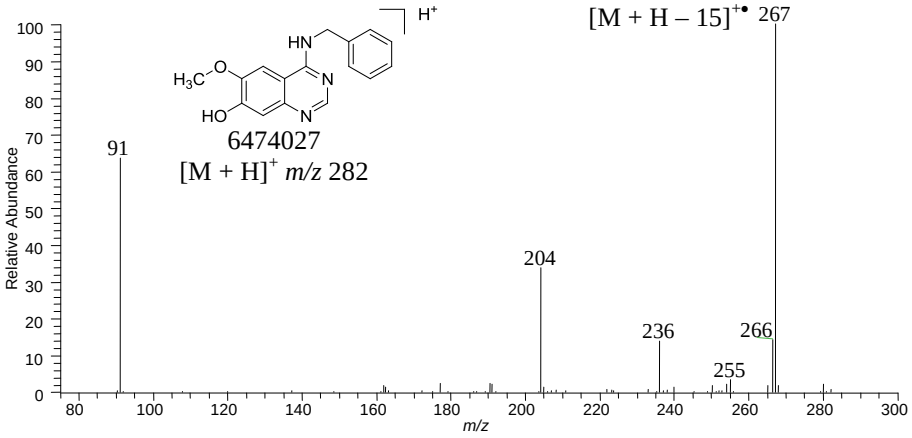

Figure A.2.6 Positive ion electrospray first generation product ion of 6474027 in MeOH, IW = 1 *m/z* unit; loss of 15 *m/z* units is a loss of $CH_3^{\bullet}$.

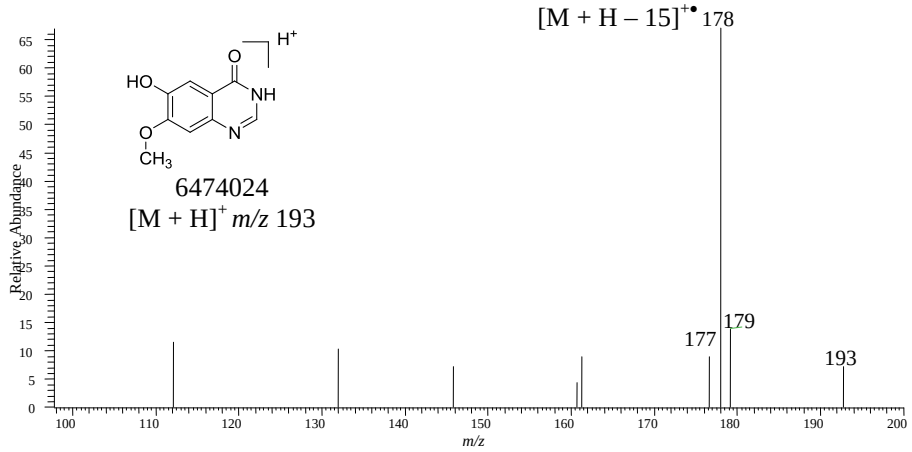

Figure A.2.7 Positive ion electrospray first generation product ion mass spectrum of 6474024 in MeOH, IW = 1 *m/z* unit; loss of 15 *m/z* units is a loss of $CH_3^{\bullet}$.

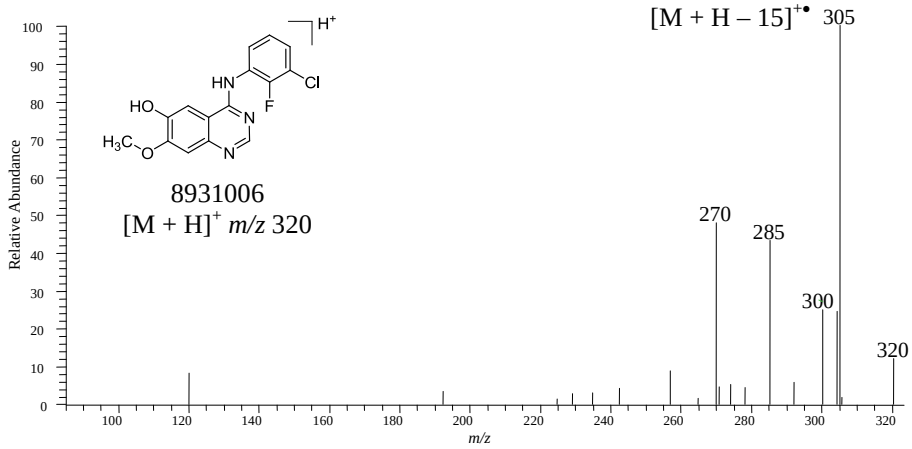

Figure A.2.8 Positive ion electrospray first generation product ion mass spectrum of 8931006 in MeOH, IW = 1 *m/z* unit; loss of 15 *m/z* units is a loss of $CH_3^{\bullet}$.

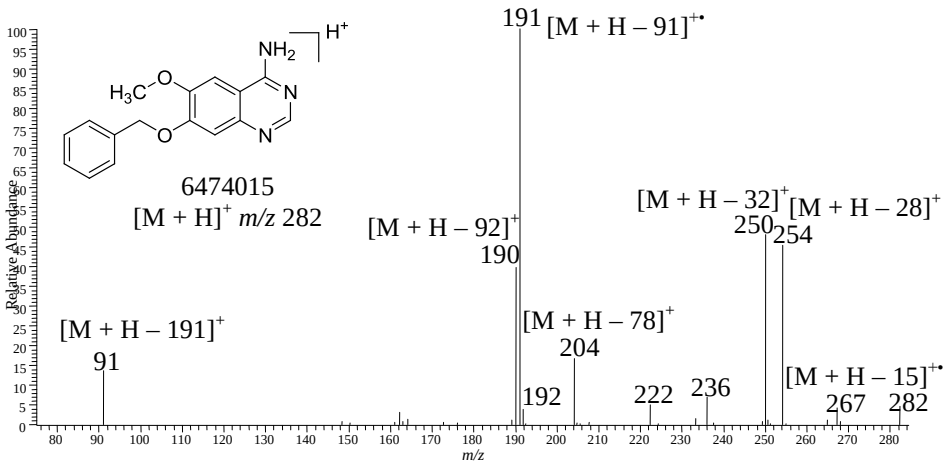

Figure A.2.9 Positive ion electrospray first generation product ion mass spectrum of 6474015 in MeOH, IW = 1 *m/z* unit; loss of 15 is a loss of $CH_3^{\bullet}$, respectively.

Supplementary information to Chapter 8, page 121

Table A.2.1 List of the first generation product ions of compound 2171003, ESI-QTOF MS at 28 eV.

m/z measured	*m/z*	Formula	Error [ppm]	Error [mDa]	DBE	$EE^+/OE^{+\bullet}$ ion
192.0513	192.0529	$C_9H_8N_2O_3^{+\bullet}$	8.5	1.64	7.0	$OE^{+\bullet}$
191.0457	191.0451	$C_9H_7N_2O_3^{+}$	3.0	0.58	7.5	EE^+
178.0373	178.0373	$C_8H_6N_2O_3^{+\bullet}$	0.1	0.02	7.0	$OE^{+\bullet}$
163.0504	163.0502	$C_8H_7N_2O_2^{+\bullet\bullet}$	1.4	0.23	6.5	$EE^+/EE^{+\bullet\bullet}$
146.0480	146.0475	$C_8H_6N_2O^{+\bullet}$	3.8	0.55	7.0	$OE^{+\bullet}$
91.0558	91.0542	$C_7H_7^{+}$	17.0	1.55	4.5	EE^+

Table A.2.2 List of the first generation product ions of compound 2171005, ESI-QTOF MS at 28 eV.

m/z measured	*m/z*	Formula	Error [ppm]	Error [mDa]	DBE	$EE^+/OE^{+\bullet}$ ion
192.0523	192.0529	$C_9H_8N_2O_3^{+\bullet}$	3.4	0.66	7.0	$OE^{+\bullet}$
191.0454	191.0451	$C_9H_7N_2O_3^{+}$	1.5	0.28	7.5	EE^+
178.0374	178.0373	$C_8H_6N_2O_3^{+\bullet}$	0.4	0.07	7.0	$OE^{+\bullet}$
163.0506	163.0502	$C_8H_7N_2O_2^{+}$	2.2	0.35	6.5	EE^+
146.0479	146.0475	$C_8H_6N_2O^{+\bullet}$	2.8	0.4	7.0	$OE^{+\bullet}$
91.0560	91.0542	$C_7H_7^{+}$	19.6	1.78	4.5	EE^+

Table A.2.3 List of the first generation product ions of compound 2171006, ESI-QTOF MS at 28 eV.

m/z measured	*m/z*	Formula	Error [ppm]	Error [mDa]	DBE	$EE^+/OE^{+\bullet}$ ion
191.0456	191.0451	$C_9H_7N_2O_3^{+}$	2.3	0.44	7.5	EE^+
174.0428	174.0424	$C_9H_6N_2O_2^{+\bullet}$	2.3	0.40	8.0	$OE^{+\bullet}$
163.0504	163.0502	$C_8H_7N_2O_2^{+}$	1.5	0.24	6.5	EE^+
146.0486	146.0475	$C_8H_6N_2O^{+\bullet}$	7.7	1.13	7.0	$OE^{+\bullet}$
145.0409	145.0396	$C_8H_5N_2O^{+}$	8.6	1.24	7.5	EE^+
91.0557	91.0542	$C_7H_7^{+}$	16.0	1.46	4.5	EE^+

Table A.2.4 List of total minimum energy values for each tautomeric form of 2171005 and each site of protonation.

Site of protonation	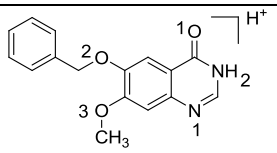	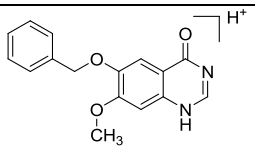	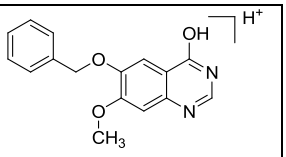
2171005	Total minimum energy [Hartree]*		
N1	-953.672691	-953.595271	-953.673377
N2	-953.610661	-953.677288	-953.656869
O1	-953.661898	-953.67537	-953.577935
O2	-953.635125	-953.621623	-953.618853
O3	-953.626957	-953.605315	-953.611676

Table A.2.5 List of total minimum energy values for each tautomeric form of 2171006 and each site of protonation.

Site of protonation	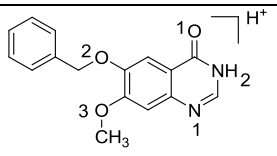	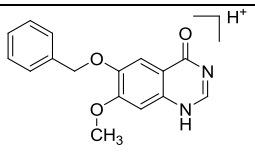	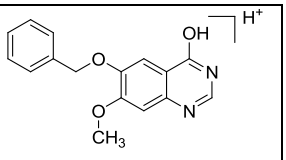
2171005	Total minimum energy [Hartree]*		
N1	-953.672691	-953.595271	-953.673377
N2	-953.610661	-953.677288	-953.656869
O1	-953.661898	-953.67537	-953.577935
O2	-953.635125	-953.621623	-953.618853
O3	-953.626957	-953.605315	-953.611676

* – Unit of energy 1 Hartree corresponds to twice the ionisation energy of H atom 1 Hartree is 27.211 eV or 627.51 kcal/mol.[95]

Table A.2.6 Energies of forms of protonated molecule of 2171005 converted into their population probability displayed in percentage values.

2171005	Site of protonation	Energy [Hartree]	Rel. Energy	Rel. Occupancy	occupation %
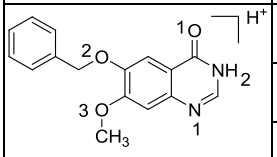	N1	-953.672691	0.004597	0.0070709	0.6
	N2	-953.610661	0.066627	6.78E-32	0.0
	O1	-953.661898	0.01539	6.32E-08	0.0
	O2	-953.635125	0.042163	1.89E-20	0.0
	O3	-953.626957	0.050331	2.85E-24	0.0
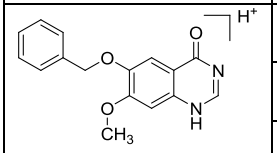	N1	-953.595271	0.082017	4.28E-39	0.0
	N2	-953.677288	0	1	87.1
	O1	-953.67537	0.001918	0.1266893	11.0
	O2	-953.621623	0.055665	9.11E-27	0.0
	O3	-953.605315	0.071973	2.14E-34	0.0
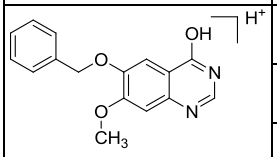	N1	-953.673377	0.003911	0.0148045	1.3
	N2	-953.656869	0.020419	2.80E-10	0.0
	O1	-953.577935	0.099353	3.32E-47	0.0
	O2	-953.618853	0.058435	4.61E-28	0.0
	O3	-953.611676	0.065612	2.02E-31	0.0

Table A.2.7 Energies of forms of protonated molecule of 2171006 converted into their population probability displayed in percentage values.

2171006	Site of protonation	Energy [Hartree]	Rel. Energy	Rel. Occupancy	Occupation %
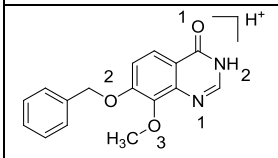	N1	-953.678148	0	1	48.7
	N2	-953.603147	0.075001	8.20E-36	0.0
	O1	-953.648191	0.029957	9.68E-15	0.0
	O2	-953.625807	0.052341	3.27E-25	0.0
	O3	-953.63116	0.046988	1.04E-22	0.0
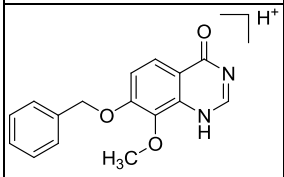	N1	-953.599653	0.078495	1.90E-37	0.0
	N2	-953.678148	0	1	48.7
	O1	-953.675418	0.00273	0.05282971	2.6
	O2	-953.605467	0.072681	9.98E-35	0.0
	O3	-953.59879	0.079358	7.51E-38	0.0
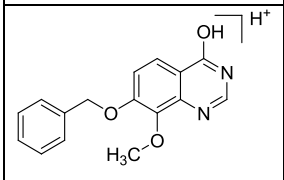	N1	-953.666336	0.011812	2.98E-06	0.0
	N2	-953.653186	0.024962	2.10E-12	0.0
	O1	-953.567953	0.110195	2.82E-52	0.0
	O2	-953.620214	0.057934	7.90E-28	0.0
	O3	-953.607627	0.070521	1.02E-33	0.0

Table A.2.8 Energies of forms of product ion at *m/z* 192 of 2171005 converted into their population probability percentage values.

$[M + H - 91]^{+\bullet}$ 2171005	Site of protonation	Energy [Hartree]	Rel. Energy	Rel. Occupancy	Occupation %
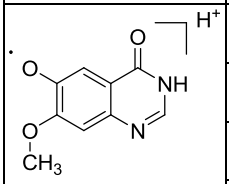	N1	-682.672551	0.005927	0.001687676	0.16
	N2	-682.608719	0.069759	2.32E-33	0.00
	O1	-682.659742	0.018736	1.72E-09	0.00
	O2	-682.678478	0	1.00E+00	96.66
	O3	-682.628383	0.050095	3.67E-24	0.00
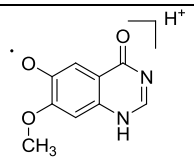	N1	-682.590206	0.088272	5.08E-42	0.00
	N2	-682.675244	0.003234	0.03069742	2.97
	O1	-682.672509	0.005969	0.001613025	0.16
	O2	-682.664259	0.014219	2.23E-07	0.00
	O3	-682.604045	0.074433	1.51E-35	0.00
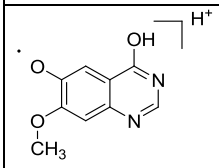	N1	-682.671476	0.007002	0.000530143	0.05
	N2	-682.6547	0.023778	7.52E-12	0.00
	O1	-682.574816	0.103662	3.21E-49	0.00
	O2	-682.656511	0.021967	5.29E-11	0.00
	O3	-682.613744	0.064734	5.21E-31	0.00

Table A.2.9 Energies of forms of product ion at *m/z* 192 of 2171006 converted into their population probability percentage values.

$[M + H - 91]^{+\bullet}$ 2171006	Site of protonation	Energy [Hartree]	Rel. Energy	Rel. Occupancy	Occupation %
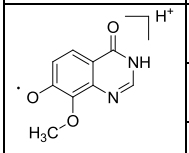	N1	-682.67668	0	1.00E+00	46.7
	N2	-682.602826	0.073854	2.82E-35	0.0
	O1	-682.647445	0.029235	2.11E-14	0.0
	O2	-682.673191	0.003489	2.33E-02	1.1
	O3	-682.62021	0.05647	3.83E-27	0.0
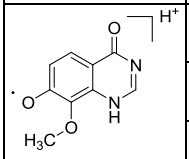	N1	-682.59666	0.08002	3.68E-38	0.0
	N2	-682.676625	5.50E-05	0.942476304	44.0
	O1	-682.675062	0.001618	1.75E-01	8.2
	O2	-682.215285	0.461395	1.43E-216	0.0
	O3	-682.592174	0.084506	2.93E-40	0.0
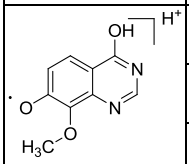	N1	-682.652164	0.024516	3.40E-12	0.0
	N2	-682.652164	0.024516	3.40E-12	0.0
	O1	-682.575333	0.101347	3.88E-48	0.0
	O2	-682.667619	0.009061	5.77E-05	0.0
	O3	-682.593038	0.083642	7.44E-40	0.0

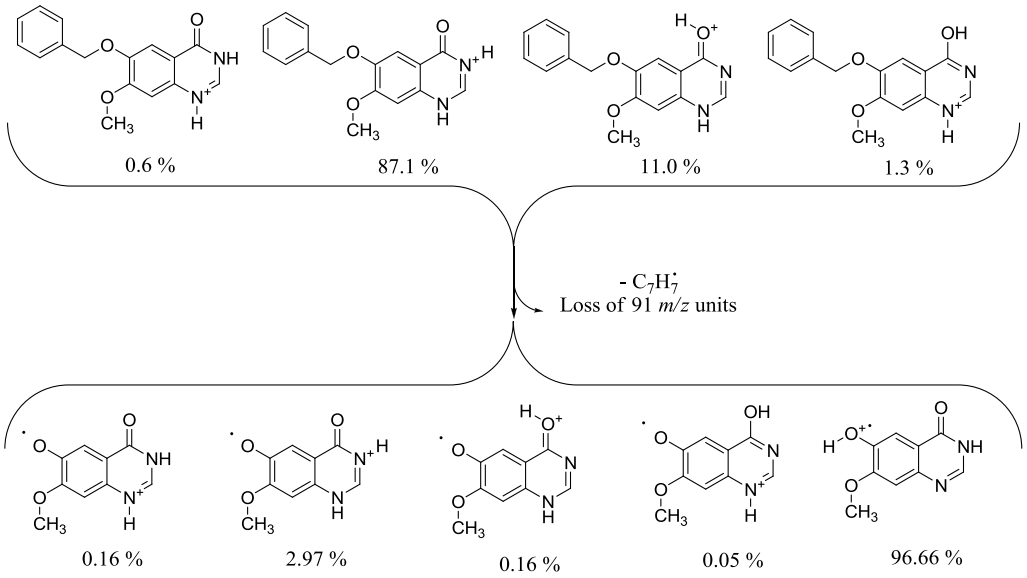

Scheme A.2.1 Schematic population distribution (% values) of most thermodynamically favourable forms of protonated molecule (FPM, top row) and forms of product ion (FPI, bottom row, *m/z* 192) of 2171005 indicated from heats of formation calculated by single point energies B3LYP/6-31G*//AM1.

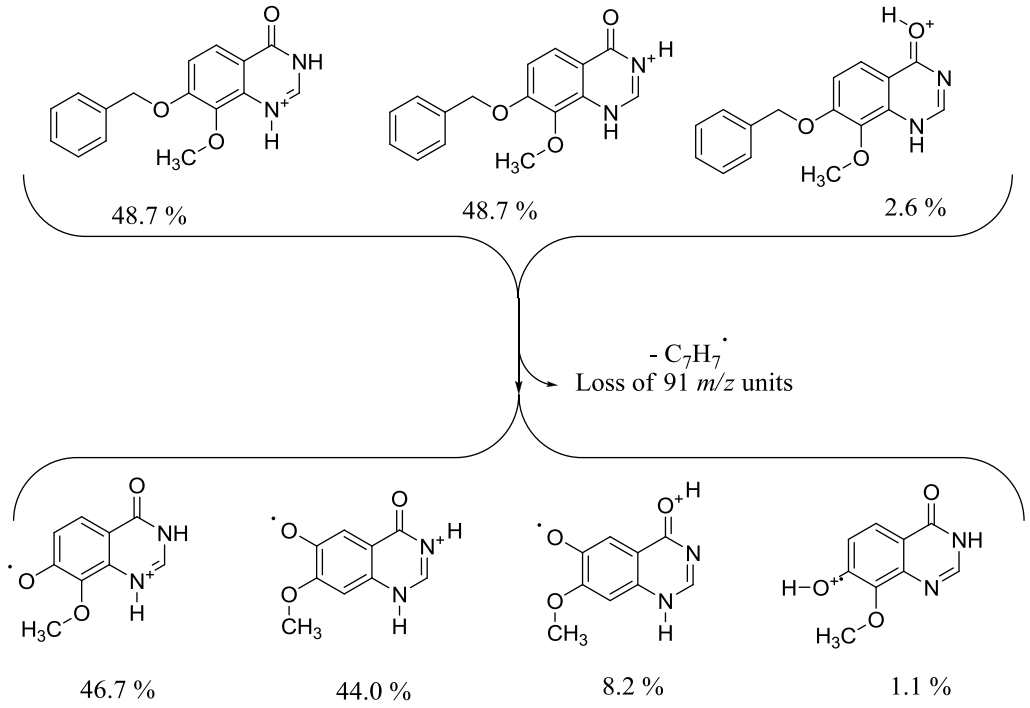

Scheme A.2.2 Schematic population distribution (% values) of most thermodynamically favourable forms of protonated molecule (FPM, top row) and forms of product ion (FPI, bottom row, *m/z* 192) of 2171006 indicated from heats of formation calculated by single point energies B3LYP/6-31G*//AM1.

Appendix 3

List of research presentations; * – the presenting author

G. J. Langley*, A. Galezowska, M. W. Harrison "Structural Elucidation of Quinazolines – a Radical Change of Approach" 59th ASMS Conference on Mass Spectrometry and Allied Topics, 5th-9th June 2011, Denver, USA

A. Galezowska*, M. W. Harrison and G. J. Langley "Good Mass Spectra Interpretation Practise: Complement Analyses of HDX and AMM to ensure correct structure elucidation." Data to Knowledge: The creation, management and application of complex data sets, AstraZeneca, Alderley Park Conference Centre, 29th - 30th March 2011, Alderley Park, UK

A. Galezowska*, M. W. Harrison, G. J. Langley "Approaches towards understanding the specific dissociations of quinazolines using MS/MS and density functional theory (DFT) calculations" 14th PhD Review Meeting, 23rd-24th November 2010, AstraZeneca, Macclesfield, UK

A. Galezowska*, M. W. Harrison, G. J. Langley "Approaches towards understanding the specific dissociations of quinazolines using MS/MS and density functional theory (DFT) calculations" 31st BMSS Annual Meeting 2010, 5th-8th September 2010, Cardiff, UK

A. Galezowska, M. W. Harrison, G. J. Langley "Investigation of fragmentation patterns of quinazolines. A useful tool for structural characterisation in Pharmaceutical Development", AZtech 12 (2), 2010, 101-102

A. Galezowska*, M. W. Harrison, G. J. Langley "The odds are in your favour: an investigation of the unusual fragmentations of quinazolines using ESI-CID QIT-MS and DFT calculations" 58th ASMS Conference on Mass Spectrometry and Allied Topics, 23rd-27th May 2010, Salt Lake City, USA

A. Galezowska*, M. W. Harrison, G. J. Langley "Fragmentation of quinazolines using ESI-CID MS/MS: Unusual formation of radical cation product ions", Structure2010, 24th-25th February 2010, Hinckley, UK

A. Galezowska*, M. W. Harrison, G. J. Langley "Fragmentation of quinazolines using ESI-CID MS/MS: Unusual formation of radical cation product ions", LCMS Meeting, 14th-17th December 2009, Cambridge, UK

A. Galezowska*, M. W. Harrison, G. J. Langley "Investigations of the fragmentation of novel compounds from the synthetic pathway of AstraZeneca compounds to facilitate rapid characterisation using ESI-QIT MS" 57th ASMS Conference on Mass Spectrometry and Allied Topics, 31st May- 4th June 2009, Philadelphia, USA

References

1. De Hoffmann, E. *Mass Spectrometry: Principles and Applications*; John Wiley & Sons Ltd., Chichester, UK, 2002.

2. Covey, T. R.; Thomson, B. A.; Schneider, B. B. *Mass Spectrom. Rev.* 2009, *28*, 870.

3. Siuzdak, G. *Mass Spectrometry for Biotechnology*; Academic Press, San Diego, USA, 1996.

4. Huang, E. C.; Wachs, T.; Conboy, J. J.; Henion, J. D. *Anal. Chem.* 1990, *62*, 713A.

5. Gaskell, S. J. *J. Mass Spectrom.* 1997, *32*, 677.

6. Fenn, J. B.; Mann, M.; Meng, C. K.; Wong, S. F.; Whitehouse, C. M. *Mass Spectrom. Rev.* 1990, *9*, 37.

7. Kebarle, P.; Verkerk, U. H. *Mass Spectrom. Rev.* 2009, *28*, 898.

8. Vestal, M. L. *Chem. Rev.* 2001, *101*, 361.

9. Taylor, G. *Proceedings of the Royal Society of London. Series A. Mathematical and Physical Sciences* 1964, *280*, 383.

10. Cole, R. B. *J. Mass Spectrom.* 2000, *35*, 763.

11. Smith, R. D.; Light-Wahl, K. J.; Winger, B. E.; Goodlett, D. R. In *Biological Mass Spectrometry. Present and Future*; Matsuo, T., Caprioli, R. M., Gross, M. L., Seyama, Y.; John Wiley & Sons Ltd, Chichester, UK, 1995, p. 41.

12. Kebarle, P.; Ho, Y. In *Electrospray Ionisation Mass Spectrometry*; Cole, R. B.; John Wiley & Sons, Inc., New York, USA, 1997, p. 3.

13. Dole, M.; Mack, L. L.; Hines, R. L.; Mobley, R. C.; Ferguson, L. D.; Alice, M. B. *J. Chem. Phys.* 1968, *49*, 2240.

14. Nohmi, T.; Fenn, J. B. *J. Am. Chem. Soc.* 1992, *114*, 3241.

15. Iribarne, J. V.; Thomson, B. A. *J. Chem. Phys.* 1976, *64*, 2287.

16. Klagkou, K.; Pullen, F.; Harrison, M.; Organ, A.; Firth, A.; Langley, G. J. *Rapid Commun. Mass Spectrom.* 2003, *17*, 1163.

17. Klagkou, K.; Pullen, F.; Harrison, M.; Organ, A.; Firth, A.; Langley, G. J. *Rapid Commun. Mass Spectrom.* 2003, *17*, 2373.

18. King, R.; Bonfiglio, R.; Fernandez-Metzler, C.; Miller-Stein, C.; Olah, T. *J. Am. Soc. Mass Spectrom.* 2000, *11*, 942.

19. Siuzdak, G. *The Expanding Role of Mass Spectrometry in Biotechnology*; 2nd Ed.; MCC Press, San Diego, USA, 2006.

20. Zhou, S.; Cook, K. D. *J. Am. Soc. Mass Spectrom.* 2000, *11*, 961.

21. Gross, J. H. *Mass Spectrometry. A Textbook*; Springer, Berlin Heidelberg, 2004.

22. Watson, J. T.; Sparkman, O. D. *Introduction to Mass Spectrometry. Instrumentation, Applications, and Strategies for Data Interpretation*; 4th Ed.; John Wiley & Sons, Ltd, Chichester, UK, 2007.

23. Bruins, A. P. *Mass Spectrom. Rev.* 1991, *10*, 53.

24. Marchi, I.; Rudaz, S.; Veuthey, J.-L. *Talanta* 2009, *78*, 1.

25. Hanold, K. A.; Fischer, S. M.; Cormia, P. H.; Miller, C. E.; Syage, J. A. *Anal. Chem.* 2004, *76*, 2842.

26. Raffaelli, A.; Saba, A. *Mass Spectrom. Rev.* 2003, *22*, 318.
27. Bos, S.; van Leeuwen, S.; Karst, U. *Anal. Bioanal. Chem.* 2006, *384*, 85.
28. Marshall, A. G.; Hendrickson, C. L.; Jackson, G. S. *Mass Spectrom. Rev.* 1998, *17*, 1.
29. McLafferty, F. W.; Beu, S. C.; Quinn, J. P.; Senko, M. W.; Shi, Y.; Suckau, D.; Wampler, F. M.; Zhang, M.-Y. In *Biological Mass Spectrometry. Present and Future*; Matsuo, T., Caprioli, R. M., Gross, M. L., Seyama, Y.; John Wiley & Sons Ltd, Chichester, UK, 1995, p. 199.
30. Matsuo, T.; Seyama, Y. In *Biological Mass Spectrometry. Present and Future*; Matsuo, T., Caprioli, R. M., Gross, M. L., Seyama, Y.; John Wiley & Sons Ltd, Chichester, UK, 1995, p. 3.
31. Despeyroux, D.; Jennings, K. R. In *Biological Mass Spectrometry. Present and Future*; Matsuo, T., Caprioli, R. M., Gross, M. L., Seyama, Y.; John Wiley & Sons Ltd, Chichester, UK, 1995, p. 227.
32. Mallet, A. I.; Down, S. *Dictionary of Mass Spectrometry*; John Wiley & Sons, Ltd., Chichester, UK, 2009.
33. Stafford Jr, G. C.; Kelley, P. E.; Syka, J. E. P.; Reynolds, W. E.; Todd, J. F. J. *Int. J. Mass Spectrom. Ion Proc.* 1984, *60*, 85.
34. Paul, W. *Rev. Modern Phys.* 1990, *62*, 531.
35. March, R. E. *Int. J. Mass Spectrom.* 2000, *200*, 285.
36. Yoshinari, K. *Rapid Commun. Mass Spectrom.* 2000, *14*, 215.
37. Downard, K. *Mass Spectrometry. A Foundation Course*; RSC, Cambridge, UK, 2004.
38. Stafford, G. *J. Am. Soc. Mass Spectrom.* 2002, *13*, 589.
39. March, R. E. *Mass Spectrom. Rev.* 2009, *28*, 961.
40. Cooks, R. G.; Cox, K. A. In *Biological Mass Spectrometry. Present and Future*; Matsuo, T., Caprioli, R. M., Gross, M. L., Seyama, Y.; John Wiley & Sons Ltd, Chichester, UK, 1995, p. 179.
41. Jonscher, K. R.; Yates Iii, J. R. *Anal. Biochem.* 1997, *244*, 1.
42. McLuckey, S.; Mentinova, M. *J. Am. Soc. Mass Spectrom.* 2011, *22*, 3.
43. Louris, J. N.; Cooks, R. G.; Syka, J. E. P.; Kelley, P. E.; Stafford, G. C.; Todd, J. F. J. *Anal. Chem.* 1987, *59*, 1677.
44. Rose, M. E.; Johnstone, R. A. W. *Mass spectrometry for Chemists and Biochemists*; Cambridge University Press, London, UK, 1982.
45. Louris, J. N.; Brodbelt-Lustig, J. S.; Graham Cooks, R.; Glish, G. L.; van Berkel, G. J.; McLuckey, S. A. *Int. J. Mass Spectrom. Ion Proc.* 1990, *96*, 117.
46. Cooks, R. G.; Kaiser, R. E. *Acc. Chem. Res.* 1990, *23*, 213.
47. March, R. E. *J. Mass Spectrom.* 1997, *32*, 351.
48. McLuckey, S. *J. Am. Soc. Mass Spectrom.* 1992, *3*, 599.
49. Lopez, L. L.; Tiller, P. R.; Senko, M. W.; Schwartz, J. C. *Rapid Commun. Mass Spectrom.* 1999, *13*, 663.
50. Papac, D. I.; Shahrokh, Z. *Pharm. Res.* 2001, *18*, 131.
51. Comisarow, M. B.; Marshall, A. G. *Chem. Phys. Lett.* 1974, *25*, 282.
52. Amster, I. J. *J. Mass Spectrom.* 1996, *31*, 1325.
53. *Finnigan LTQ FT Hardware Manual*, 2004.
54. Gauthier, J. W.; Trautman, T. R.; Jacobson, D. B. *Anal. Chim. Acta* 1991, *246*, 211.

55. Gaskell, S. J. In *Biological Mass Spectrometry. Present and Future*; Matsuo, T., Caprioli, R. M., Gross, M. L., Seyama, Y.; John Wiley & Sons Ltd, Chichester, UK, 1995, p. 165.

56. Chernushevich, I. V.; Loboda, A. V.; Thomson, B. A. *J. Mass Spectrom.* 2001, *36*, 849.

57. Campana, J. E. *Int. J. Mass Spectrom. Ion Phys.* 1980, *33*, 101.

58. *Agilent 6410 Triple Quad LC/MS Concepts Guide. The Big Picture.*, 2007.

59. *MicrOTOF-Q User Manual, Version 1.1*, 2007.

60. Herbert, C. G.; Johnstone, R. A. W. *Mass Spectrometry Basics*; CRC Press LLC, Boca Raton, USA, 2003.

61. Yost, R. A.; Enke, C. G. *Anal. Chem.* 1979, *51*, 1251.

62. Morris, H. R.; Paxton, T.; Dell, A.; Langhorne, J.; Berg, M.; Bordoli, R. S.; Hoyes, J.; Bateman, R. H. *Rapid Commun. Mass Spectrom.* 1996, *10*, 889.

63. Yost, R. A.; Enke, C. G. *J. Am. Chem. Soc.* 1978, *100*, 2274.

64. Jennings, K. R. *Int. J. Mass Spectrom. Ion Phys.* 1968, *1*, 227.

65. McLafferty, F. W. *Interpretation of Mass Spectra: An Introduction*; W. A. Benjamin, Inc., New York, 1967.

66. Kenttamaa, H. I.; Cooks, R. G. *J. Am. Chem. Soc.* 1985, *107*, 1881.

67. Laskin, J.; Futrell, J. H. *Mass Spectrom. Rev.* 2005, *24*, 135.

68. Sleno, L.; Volmer, D. A. *J. Mass Spectrom.* 2004, *39*, 1091.

69. Kenttämaa, H. I.; Cooks, R. G. *Int. J. Mass Spectrom. Ion Proc.* 1985, *64*, 79.

70. Guo, X.; Duursma, M. C.; Al-Khalili, A.; Heeren, R. M. A. *Int. J. Mass Spectrom.* 2003, *225*, 71.

71. Cody, R. B.; Burnier, R. C.; Freiser, B. S. *Anal. Chem.* 1982, *54*, 96.

72. Hammes, G. G. *Principles of Chemical Kinetics*; Academic Press, Inc., New York, USA, 1978.

73. Håkansson, K.; Cooper, H. J.; Emmett, M. R.; Costello, C. E.; Marshall, A. G.; Nilsson, C. L. *Anal. Chem.* 2001, *73*, 4530.

74. McLafferty, F. W. *Mass Spectral Correlations*; American Chemical Society, Washington, D. C., USA, 1963.

75. Ardrey, R. E.; Allan, A. R.; Bal, T. S.; Joyce, J. R.; Moffat, A. C. *Pharmaceutical Mass Spectra*; The Pharmaceutical Press, London, UK, 1985.

76. Pellegrin, V. *J. Chem. Educ.* 1983, *60*, 626.

77. Badertscher, M.; Bischofberger, K.; Munk, M. E.; Pretsch, E. *J. Chem. Inf. Comput. Sci.* 2001, *41*, 889.

78. McLafferty, F. W.; Tureček, F. *Interpretation of Mass Spectra*; 4th Ed.; University Science Books, Sausalito, USA, 1993.

79. McLafferty, F. W. *Mass Spectrometry of Organic Ions*; Academic Press Inc., New York, USA, 1963.

80. Holcapek, M.; Jirásko, R.; Lísa, M. *J. Chromatogr. A* 2010, *1217*, 3908.

81. Weissberg, A.; Dagan, S. *Int. J. Mass Spectrom.* 2011, *299*, 158.

82. Bentley, T. W.; Johnstone, R. A. W. In *Adv. Phys. Org. Chem.*; Gold, V.; Academic Press 1970; Vol. Volume 8, p. 151.

83. Hammond, G. S. *J. Am. Chem. Soc.* 1955, *77*, 334.

84. Howe, I. In *Mass Spectrometry*; Williams, D. H.; The Chemical Society, London, UK, 1968; Vol. 1, p. 31.
85. Johnstone, R. A. W. *Mass Spectrometry for Organic Chemists*; Cambridge University Press, London, UK, 1972.
86. Budzikiewicz, H.; Djerassi, C.; Williams, D. H. *Mass Spectrometry of Organic Compounds*; Holden-Day, Inc., San Francisco, USA, 1967.
87. Smith, R. D.; Loo, J. A.; Loo, R. R. O.; Busman, M.; Udseth, H. R. *Mass Spectrom. Rev.* 1991, *10*, 359.
88. Jørgensen, T. J. D.; Bache, N.; Roepstorff, P.; Gårdsvoll, H.; Ploug, M. *Mol. & Cell. Proteomics* 2005, *4*, 1910.
89. Bulleigh, K.; Howard, A.; Do, T.; Wu, Q.; Anbalagan, V.; Stipdonk, M. V. *Rapid Commun. Mass Spectrom.* 2006, *20*, 227.
90. Beynon, J. H. *Mass Spectrometry and its Applications to Organic Chemistry*; Elsevier Publishing Company, Amsterdam, The Netherlands, 1960.
91. Sparkman, O. D. *Mass Spectrometry Desk Reference*; Global View Publishing, Pittsburgh, USA, 2000.
92. Stevenson, D. P. *Discuss. Faraday Soc.* 1951, *10*, 35.
93. Cooks, R. G.; Wong, P. S. H. *Acc. Chem. Res.* 1998, *31*, 379.
94. Deakyne, C. A. *Int. J. Mass Spectrom.* 2003, *227*, 601.
95. Koch, W.; Holthausen, M. C. *A Chemist's Guide to Density Functional Theory*; 2nd Ed.; Wiley-VCH Verlag GmbH, Weinheim, Germany, 2001.
96. McLafferty, F. W. *Anal. Chem.* 1959, *31*, 82.
97. Barnard, G. P. *Modern Mass Spectrometry*; The Insitute of Physics, London, UK, 1953.
98. Levsen, K.; Schiebel, H.-M.; Terlouw, J. K.; Jobst, K. J.; Elend, M.; Preiß, A.; Thiele, H.; Ingendoh, A. *J. Mass Spectrom.* 2007, *42*, 1024.
99. Bursey, M. M.; Hoffman, M. K. In *Mass Spectrometry: Techniques and Applications*; Milne, G. W.; John Wiley & Sons, Inc., New York, USA, 1971.
100. Delfosse, J.; Bleakney, W. *Phys. Rev.* 1939, *56*, 256.
101. Cummings, C. S.; Bleakney, W. *Phys. Rev.* 1940, *58*, 787.
102. Friedman, L.; Long, L. A. *J. Am. Chem. Soc.* 1953, *75*, 2832.
103. Cooks, R. G. *Org. Mass Spectrom.* 1969, *2*, 481.
104. Karni, M.; Mandelbaum, A. *Org. Mass Spectrom.* 1980, *15*, 53.
105. Venkataraghavan, R. In *Mass Spectrometry: Techniques and Applications*; Milne, G. W.; John Wiley & Sons, Inc., New York, USA, 1971.
106. Fennessey, P. V. In *Mass Spectrometry: Techniques and Applications*; Milne, G. W.; John Wiley & Sons, Inc., New York, USA, 1971.
107. Chapman, J. R. In *Mass Spectrometry*; Rose, M. E.; The Chemical Society, London, UK, 1985; Vol. 8, p. 123.
108. Mellon, F. A. In *Mass Spectrometry*; Johnstone, R. A. W.; The Chemical Society, London, UK, 1975; Vol. 3, p. 117.
109. Alcamí, M.; Mó, O.; Yáñez, M. *Mass Spectrom. Rev.* 2001, *20*, 195.
110. Radom, L. *Org. Mass Spectrom.* 1991, *26*, 359.
111. Ting, K.-L. H.; Lee, R. C. T.; Milne, G. W. A.; Shapiro, M.; Guarino, A. M. *Science* 1973, *180*, 417.
112. Mathews, R. J. *Aus. J. Chem.* 1973, *26*, 1955.

113. Bandu, M. L.; Watkins, K. R.; Bretthauer, M. L.; Moore, C. A.; Desaire, H. *Anal. Chem.* 2004, *76*, 1746.
114. Buchanan, B. G.; Duffield, A. M.; Robertson, A. V. In *Mass Spectrometry: Techniques and Applications*; Milne, G. W.; John Wiley & Sons, Inc., New York, USA, 1971.
115. Smith, D. H.; Buchanan, B. G.; Engelmore, R. S.; Duffield, A. M.; Yeo, A.; Feigenbaum, E. A.; Lederberg, J.; Djerassi, C. *J. Am. Chem. Soc.* 1972, *94*, 5962.
116. Sasaki, S.; Kudo, Y. *J. Chem. Inf. Comput. Sci.* 1985, *25*, 252.
117. Lipkus, A. H.; Munk, M. E. *J. Chem. Inf. Comput. Sci.* 1988, *28*, 9.
118. Gasteiger, J.; Hanebeck, W.; Schulz, K. P. *J. Chem. Inf. Comput. Sci.* 1992, *32*, 264.
119. Funatsu, K.; Miyabayashi, N.; Sasaki, S. *J. Chem. Inf. Comput. Sci.* 1988, *28*, 18.
120. Fan, B.; Chen, H.; Petitjean, M.; Panaye, A.; Doucet, J.-P.; Xia, H.; Yuan, S. *Spectrosc. Lett.* 2005, *38*, 145.
121. McLafferty, F. W.; Stauffer, D. B. *J. Chem. Inf. Comput. Sci.* 1985, *25*, 245.
122. Biemann, K.; Cone, C.; Webster, B. R.; Arsenault, G. P. *J. Am. Chem. Soc.* 1966, *88*, 5598.
123. Mistrik, R. In *United States Patent*; Highchem, Ltd.: United States, 2007.
124. Neumann, S.; Bocker, S. *Anal. Bioanal. Chem.* 2010, *398*, 2779.
125. Lam, A. K. Y.; O'Hair, R. A. J. *Rapid Commun. Mass Spectrom.* 2010, *24*, 1779.
126. Blanksby, S. J.; Kato, S.; Bierbaum, V.; Ellison, G. B. *Aus. J. Chem.* 2003, *56*, 459.
127. Vessecchi, R.; Galembeck, S. E. *J. Phys. Chem. A* 2008, *112*, 4060.
128. Vessecchi, R.; Nascimento, P.; Lopes, J. N. C.; Lopes, N. P. *J. Mass Spectrom.* 2006, *41*, 1219.
129. Mercero, J. M.; Matxain, J. M.; Lopez, X.; York, D. M.; Largo, A.; Eriksson, L. A.; Ugalde, J. M. *Int. J. Mass Spectrom.* 2005, *240*, 37.
130. Haupert, L. J.; Poutsma, J. C.; Wenthold, P. G. *Acc. Chem. Res.* 2009, *42*, 1480.
131. Vessecchi, R.; Carollo, C. A.; Lopes, J. N. C.; Crotti, A. E. M.; Lopes, N. P.; Galembeck, S. E. *J. Mass Spectrom.* 2009, *44*, 1224.
132. Wright, P.; Alex, A.; Nyaruwata, T.; Parsons, T.; Pullen, F. *Rapid Commun. Mass Spectrom.* 2010, *24*, 1025.
133. Alex, A.; Harvey, S.; Parsons, T.; Pullen, F. S.; Wright, P.; Riley, J.-A. *Rapid Commun. Mass Spectrom.* 2009, *23*, 2619.
134. Luo, Y.-R. *Comprehensive Handbook of Chemical Bond Energies*; CRC Press Taylor & Francis Group, Boca Raton, USA, 2007.
135. Heinonen, M.; Rantanen, A.; Mielikainen, T.; Kokkonen, J.; Kiuru, J.; Ketola, R. A.; Rousu, J. *Rapid Commun. Mass Spectrom.* 2008, *22*, 3043.
136. Hill, A. W.; Mortishire-Smith, R. J. *Rapid Commun. Mass Spectrom.* 2005, *19*, 3111.
137. Patrick, G. L. *An Introduction to Medicinal Chemistry*; Oxford University Press, Oxford, UK, 2001.

138. Jensen, F. *Introduction to Computational Chemistry*; John Wiley & Sons, Ltd, Chichester, UK, 1999.
139. Simons, J. *An Introduction to Theoretical Chemistry*; Cambridge University Press, Cambridge, UK, 2003.
140. Lewars, E. *Computational Chemistry. Introduction to the Theory and applications of Molecular and Quantum Mechanics*; Kluwer Academic Publishers, Boston, USA, 2003.
141. Cramer, C. J. *Essentials of Computational Chemistry. Theories and Models*; 2nd Ed.; John Wiley & Sons, Ltd., Chichester, UK, 2004.
142. Davidson, E. R.; Feller, D. *Chem. Rev.* 1986, *86*, 681.
143. McMaster, B. N. In *Mass Spectrometry*; Johnstone, R. A. W.; The Chemical Society, London, UK, 1977; Vol. 4, p. 1.
144. Baldwin, M. A. In *Mass Spectrometry*; Rose, M. E.; The Chemical Society, London, UK, 1987; Vol. 9, p. 59.
145. Hehre, W. J. *A Guide to Molecular Mechanics and Quantum Chemical Calculations*; Wavefunction, Inc., Irvine, 2003.
146. Bursey, J. T.; Bursey, M. M.; Kingston, D. G. I. *Chem. Rev.* 1973, *73*, 191.
147. Young, D. C. *Computational Chemistry: A Practical Guide for Applying Techniques to Real-World Problems*; John Wiley & Sons, Inc., New York, USA, 2001.
148. *Spartan'02*; Wavefunction, Inc., Irvine, USA.
149. Gundertofte, K.; Liljefors, T.; Norrby, P.-o.; Pettersson, I. *J. Comput. Chem.* 1996, *17*, 429.
150. Lorquet, J. C. In *Mass Spectrometry*; Johnstone, R. A. W.; The Chemical Society, London, UK, 1984; Vol. 7, p. 1.
151. McMaster, B. N. In *Mass Spectrometry*; Johnstone, R. A. W.; The Chemical Society, London, UK, 1975; Vol. 3, p. 1.
152. Bentley, T. W. In *Mass Spectrometry*; Johnstone, R. A. W.; The Chemical Society, London, UK, 1975; Vol. 3, p. 59.
153. *Density Functional Theory: A Bridge between Chemistry and Physics*; Geerlings, P.; De Proft, F.; Langenaeker, W.; VUBPRESS, Brussels, Belgium, 1999.
154. Springborg, M. In *Density Functional Theory: A Bridge between Chemistry and Physics*; Geerlings, P., De Proft, F., Langenaeker, W.; VUBPRESS, Brussels, Belgium, 1999, p. 15.
155. Perdew, J. P. In *Density Functional Theory: A Bridge between Chemistry and Physics*; Geerlings, P., De Proft, F., Langenaeker, W.; VUBPRESS, Brussels, Belgium, 1999, p. 87.
156. Geerlings, P. In *Density Functional Theory: A Bridge between Chemistry and Physics*; Geerlings, P., De Proft, F., Langenaeker, W.; VUBPRESS, Brussels, Belgium, 1999, p. 7.
157. Parr, R. G.; Yang, W. *Density-Functional theory of Atoms and Molecules*; Oxford University Press, New York, USA, 1989.
158. Skylaris, C.-K.; Haynes, P. D.; Mostofi, A. A.; Payne, M. C. *J. Chem. Phys.* 2005, *122*, 084119.
159. Cooks, R. G.; Koskinen, J. T.; Thomas, P. D. *J. Mass Spectrom.* 1999, *34*, 85.

160. Johnstone, R. A. W. In *Mass Spectrometry*; Johnstone, R. A. W.; The Chemical Society, London, UK, 1979; Vol. 5, p. 1.
161. Baer, T. In *Mass Spectrometry*; Johnstone, R. A. W.; The Chemical Society, London, UK, 1981; Vol. 6, p. 1.
162. Constantin, E.; Schnell, A. *Mass Spectrometry*; Ellis Horwood Ltd, Chichester, 1990.
163. Anslyn, E. V.; Dougherty, D. A. *Modern physical organic chemistry*; University Science Books, Sausalito, USA.
164. Guner, V.; Khuong, K. S.; Leach, A. G.; Lee, P. S.; Bartberger, M. D.; Houk, K. N. *J. Phys. Chem. A* 2003, *107*, 11445.
165. Pokon, E. K.; Liptak, M. D.; Feldgus, S.; Shields, G. C. *J. Phys. Chem. A* 2001, *105*, 10483.
166. Smyth, W. F.; Rodriguez, V. *J. Chromatogr. A* 2007, *1159*, 159.
167. Henchoz, Y.; Bard, B.; Guillarme, D.; Carrupt, P.-A.; Veuthey, J.-L.; Martel, S. *Anal. Bioanal. Chem.* 2009, *394*, 707.
168. *Medicinal Chemistry: Principles and Practice*; King, F. D.; Royal Society of Chemistry, Cambridge, UK, 1994.
169. Kassel, D. B. *Chem. Rev.* 2001, *101*, 255.
170. Poon, G. K. In *Electrospray Ionisation Mass Spectrometry*; Cole, R. B.; John Wiley & Sons, Inc., New York, USA, 1997.
171. Gillespie, T. A.; Winger, B. E. *Mass Spectrom. Rev.* 2011, *30*, 479.
172. Lee, M. S.; Kerns, E. H. *Mass Spectrom. Rev.* 1999, *18*, 187.
173. Obach, R. S.; Baxter, J. G.; Liston, T. E.; Silber, B. M.; Jones, B. C.; Macintyre, F.; Rance, D. J.; Wastall, P. *J. Pharmacol. Exp. Ther.* 1997, *283*, 46.
174. Fang, A. S.; Miao, X.; Tidswell, P. W.; Towle, M. H.; Goetzinger, W. K.; Kyranos, J. N. *Mass Spectrom. Rev.* 2008, *27*, 20.
175. Rang, H. P. In *Drug Discovery and Development*; Rang, H. P.; Elsevier Ltd, London, UK, 2006, p. 221.
176. Brewer, E.; Henion, J. *J. Pharm. Sci.* 1998, *87*, 395.
177. Milne, G. W. In *Mass Spectrometry: Techniques and Applications*; Milne, G. W.; John Wiley & Sons, Inc., New York, USA, 1971.
178. Bandu, M. L.; Desaire, H. *Analyst* 2006, *131*, 268.
179. Rang, H. P. In *Drug Discovery and Development*; Rang, H. P.; Elsevier Ltd, London, UK, 2006, p. 243.
180. Rang, H. P. In *Drug Discovery and Development*; Rang, H. P.; Elsevier Ltd, London, UK, 2006, p. 229.
181. Easdale, C.; Vose, C. W. In *Drug Discovery and Development*; Rang, H. P.; Elsevier Ltd, London, UK, 2006, p. 255.
182. *ICH Guideline: Impurities in New Drug Products*, CPMP/ICH/2738/99, EMEA, London, UK, 2006.
183. Gorog, S. In *Identification and Determination of Impurities in Drugs. Progress in Pharmaceutical and Biomedical Analysis 4*; Gorog, S.; Elsevier, Amsterdam, The Netherlands, 2000, p. 67.
184. Gorog, S. In *Identification and Determination of Impurities in Drugs. Progress in Pharmaceutical and Biomedical Analysis 4*; Gorog, S.; Elsevier, Amsterdam, The Netherlands, 2000, p. 1.

185. IUPAC *Nomenclature of Organic Chemistry*, http://old.iupac.org/reports/provisional/abstract04/favre_310305.html, (accessed 8th December 2011).

186. Sorbera, L. A.; Serradell, N.; Rosa, E.; Bolos, J.; Bayes, M. *Drugs of the Future* 2007, *32*, 577.

187. Dietrich, J.; Wang, D.; Batchelor, T. T. *Expert Opinion on Investigational Drugs* 2009, *18*, 1549.

188. *AstraZeneca Announces results of Recentin HORIZON II Phase III Trail in Metastatic Colorectal Cancer.*, 28th May 2010, http://www.astrazeneca.com/Media/Press-releases/Article/20100528--AstraZeneca-Announces-Results-of-Recentin-HORIZON-II-, (accessed 1st June 2011).

189. Zareba, G.; Castaner, J.; Bozzo, J. *Drugs of the Future* 2005, *30*, 138.

190. Herbst, R. S.; Heymach, J. V.; O'Reilly, M. S.; Onn, A.; Ryan, A. J. *Expert Opinion on Investigational Drugs* 2007, *16*, 239.

191. *FDA approves orphan drug vandetanib.*, 7th April 2011, http://www.astrazeneca.com/Media/Press-releases/Article/20100407-fda-approves-orphan-drug-vandetanib, (accessed 1st June 2011).

192. *Gefitinib*, http://www.gefitinib.org/, (accessed 17th June 2011).

193. Tamura, K.; Fukuoka, M. *Expert Opinion on Pharmacotherapy* 2005, *6*, 985.

194. Campbell, L.; Blackhall, F.; Thatcher, N. *Expert Opinion on Pharmacotherapy* 2010, *11*, 1343.

195. *Basis Set Exchange*, 15th January 2007, https://bse.pnl.gov/bse/portal, (accessed 10th February 2011).

196. Porter, Q. N. *Mass Spectrometry of Heterocyclic Compounds*; 2nd Ed.; John Wiley & Sons, Inc., New York, USA, 1985.

197. Kingston, D. G. I.; Hobrock, B. W.; Bursey, M. M.; Bursey, J. T. *Chem. Rev.* 1975, *75*, 693.

198. Chen, K.; Rannulu, N. S.; Cai, Y.; Lane, P.; Liebl, A. L.; Rees, B. B.; Corre, C.; Challis, G. L.; Cole, R. B. *J. Am. Soc. Mass Spectrom.* 2008, *19*, 1856.

199. Stévigny, C.; Jiwan, J.-L. H.; Rozenberg, R.; de Hoffmann, E.; Quetin-Leclercq, J. *Rapid Commun. Mass Spectrom.* 2004, *18*, 523.

200. Sigsby, M. L.; Day, R. J.; Cooks, R. G. *Org. Mass Spectrom.* 1979, *14*, 273.

201. Adams, J.; Gross, M. L. *J. Am. Chem. Soc.* 1986, *108*, 6915.

202. Flammang, R.; Barbieux-Flammang, M.; Le, H. T.; Nguyen, M. T.; Berthelot, J.; Tortajada, J. *Int. J. Mass Spectrom.* 2000, *199*, 221.

203. Thoen, K. K.; Kenttämaa, H. I. *J. Am. Chem. Soc.* 1997, *119*, 3832.

204. Nelson, E. D.; Thoen, K. K.; Kenttämaa, H. I. *J. Am. Chem. Soc.* 1998, *120*, 3792.

205. Tichy, S. E.; Nelson, E. D.; Amegayibor, F. S.; Kenttämaa, H. I. *J. Am. Chem. Soc.* 2004, *126*, 12957.

206. Adeuya, A.; Price, J. M.; Jankiewicz, B. J.; Nash, J. J.; Kenttämaa, H. I. *J. Phys. Chem. A* 2009, *113*, 13663.

207. Williams, D. H.; Howe, I. *Principles of Organic Mass Spectrometry*; McGraw-Hill Book Company, Ltd, London, UK, 1972.

208. Thurman, E. M.; Ferrer, I.; Pozo, O. J.; Sancho, J. V.; Hernandez, F. *Rapid Commun. Mass Spectrom.* 2007, *21*, 3855.
209. Schäfer, M.; Drayß, M.; Springer, A.; Zacharias, P.; Meerholz, K. *Eur. J. Org. Chem.* 2007, *2007*, 5162.
210. Amundson, L.; Owen, B.; Gallardo, V.; Habicht, S.; Fu, M.; Shea, R.; Mossman, A.; Kenttämaa, H. *J. Am. Soc. Mass Spectrom.* 2011, *22*, 670.
211. Gallagher, R. T.; Balogh, M. P.; Davey, P.; Jackson, M. R.; Sinclair, I.; Southern, L. J. *Anal. Chem.* 2003, *75*, 973.
212. Pihlainen, K.; Sippola, E.; Kostiainen, R. *J. Chromatogr. A* 2003, *994*, 93.
213. Slobodník, J.; Hogenboom, A. C.; Vreuls, J. J.; Rontree, J. A.; van Baar, B. L. M.; Niessen, W. M. A.; Brinkman, U. A. T. *J. Chromatogr. A* 1996, *741*, 59.
214. Atkins, P.; De Paula, J. *Atkins' Physical Chemistry*; 8th Ed.; Oxford University Press, Oxford, UK, 2006.
215. Goeringer, D. E.; McLuckey, S. A. *J. Chem. Phys.* 1996, *104*, 2214.
216. Guan, S.; Marshall, A. *J. Am. Soc. Mass Spectrom.* 1994, *5*, 64.
217. Dongré, A. R.; Jones, J. L.; Somogyi, Á.; Wysocki, V. H. *J. Am. Chem. Soc.* 1996, *118*, 8365.
218. Hemling, M. E.; Conboy, J. J.; Bean, M. F.; Mentzer, M.; Carr, S. A. *J. Am. Soc. Mass Spectrom.* 1994, *5*, 434.
219. Katta, V.; Chait, B. T. *J. Am. Chem. Soc.* 1993, *115*, 6317.
220. Liu, D. Q.; Wu, L.; Sun, M.; MacGregor, P. A. *J. Pharm. Biomed. Anal.* 2007, *44*, 320.
221. Holmes, J. L.; Jobst, K. J.; Terlouw, J. K. *J. Labelled Compd. Radiopharmaceut.* 2007, *50*, 1115.
222. Grostic, M. F.; Rinehart Jr., K. L. In *Mass Spectrometry: Techniques and Applications*; Milne, G. W.; John Wiley & Sons, Inc., New York, USA, 1971.
223. Howe, I. In *Mass Spectrometry*; Williams, D. H.; The Chemical Society, London, UK, 1973; Vol. 2, p. 33.
224. Csonka, I. P.; Paizs, B.; Lendvay, G.; Suhai, S. *Rapid Commun. Mass Spectrom.* 2000, *14*, 417.
225. Summerfield, S. G.; Cox, K. A.; Gaskell, S. J. *J. Am. Soc. Mass Spectrom.* 1997, *8*, 25.
226. Cox, K. A.; Gaskell, S. J.; Morris, M.; Whiting, A. *J. Am. Soc. Mass Spectrom.* 1996, *7*, 522.
227. Johnson, R. S.; Martin, S. A.; Biemann, K. *Int. J. Mass Spectrom. Ion Proc.* 1988, *86*, 137.
228. Wysocki, V. H.; Tsaprailis, G.; Smith, L. L.; Breci, L. A. *J. Mass Spectrom.* 2000, *35*, 1399.
229. Harrison, A. G.; Yalcin, T. *Int. J. Mass Spectrom. Ion Proc.* 1997, *165-166*, 339.
230. Chipuk, J. E.; Brodbelt, J. S. *Int. J. Mass Spectrom.* 2007, *267*, 98.